Functional and Structural Analysis of the Activation Mechanism of Caspase-8

Dissertation

Zur Erlangung der Naturwissenschaftlichen Doktorwürde

(Dr. Sc. Nat.)

vorgelegt der

Mathematisch-Naturwissenschaftlichen Fakultät

der

Universität Zürich

von

Nadine Keller

aus

Deutschland

Promotionskomitee:

Prof. Dr. Markus G. Grütter (Vorsitz)

Prof. Dr. Michael Hengartner

Dr. Elena Conti

Zürich, June 2009

Abstract

Human caspase-8 is an enzyme involved in apoptosis, a process essential to remove unwanted or diseased cells throughout the life of multicellular organisms. Initially caspase-8 is produced in the cell as the monomeric latent precursor procaspase-8 comprising an N-terminal prodomain with two death effector domains followed by a catalytic domain that contains two subunits connected by a 40 amino acid linker. The catalytic domain harbors the substrate binding pocket and the active site residue cysteine. Activation of the enzyme occurs upon binding of the zymogen to the macromolecular death inducing signaling complex, DISC. This binding is facilitated by homotypic death effector domain interactions between the prodomain of procaspase-8 and the adapter protein FADD. Bound to the DISC procaspase-8 becomes activated by dimerization and subsequent proteolytic processing.

This thesis analyzes the activation mechanism of caspase-8 in more detail using biochemical and biophysical as well as structural methods. Thereby, chapter 2 focuses on the prodomain and its binding to FADD whereas chapters 3 and 4 analyze the structural changes occurring within the catalytic domain of caspase-8.

The determinants for binding of procaspase-8 prodomain to FADD were analyzed using pull-down experiments. It was shown that FADD binding depends on the complete prodomain since individual death effector domains were not able to bind FADD. During purification and pull-down experiments an additional oligomerization of the prodomains was evident. An initial hypothesis stated that this oligomerization is cysteine dependent. However, mutation of two cysteins in the second death effector domain of the prodomain of caspase-8 could not confirm this, neither with pull-down ex-

periments nor in cell biological assays.
Preliminary studies using fusion tagged caspase-8 prodomain and FADD were conducted to form a complex between FADD and the caspase-8 prodomain for biochemical and structural studies. However, current problems include a high aggregation tendency of the proteins and the presence of large fusion tags, which might hamper structure determination. Therefore, a discussion in chapter 2.3 includes several strategies to circumvent these problems in future experiments.
Whereas structure determination of the prodomain proved to be difficult the structure of the catalytic domain of the caspase-8 zymogen, procaspase-8 was determined by solution NMR. Whereas the secondary structure elements of procaspase-8 resemble the ones of active caspase-8 significant differences were observed in the loops surrounding the substrate binding pocket and the linker connecting the two subunits. Biochemical and biophysical analyses on a set of various dimerization and processing mutants were performed to elucidate the transition from monomeric procaspase-8 to active dimeric caspase-8 and the influence of inhibitor binding. These studies clearly confirm the requirement of dimerization for caspase-8 activity in unprocessed but also processed form by inducing structural changes around the active site. In addition, it was shown that dimerization is important for activation of the enzyme by relocating the intersubunit linker, which in procaspase-8 covers part of the substrate binding region, into close proximity of the active site of the associated protomer thus allowing intermolecular cleavage within the dimer. Processing has to occur at both cleavage sites within the linker to achieve full caspase-8 activity. After processing structural rearrangements in the active site forming loops and the cleaved linker fragments occur resulting in a preformed active site. Upon substrate binding this region then undergoes additional changes to accommodate the substrate.
This work clearly confirms the importance of dimerization for activation and activity of caspase-8. Furthermore, it highlights the additional importance of proteolytic processing for the activation process. Thus the here described data allow a refinement of the previous model for caspase-8 activation and most likely provides insights into the activation mechanism of other caspases.

Zusammenfassung

Das Enzym Caspase-8 spielt eine ausschlaggebende Rolle in der Apoptose, einem Prozess welcher für die Eliminierung von kranken oder überschüssigen Zellen in mehrzelligen Organismen verantwortlich ist. In der Zelle wird Caspase-8 zunächst als inaktives Zymogen, sogenannte Procaspase-8, produziert. In dieser Form besteht das Enzym aus einer N-terminalen Prodomäne mit zwei Todeseffektordomänen und einer C-terminalen katalytischen Domäne, welche in zwei Untereinheiten unterteilt ist und die Substratbingungsstelle und das katalytische Cystein enthält. Die Aktivierung von Caspase-8 erfolgt durch Bindung der Prodomäne an das Adapterprotein FADD welches Teil eines hochmolekularen Komplexes genannt DISC (death inducing signaling complex) ist. Dort wird durch Dimerisierung und proteolytische Spaltung das aktive Enzym gebildet.

Diese Doktorarbeit beschreibt biochemische, biophysikalische und strukturelle Experimente zur Untersuchung des detailierten Aktivierungsmechanismus der Caspase-8. Im Wesentlichen enthält diese Arbeit zwei Hauptteile: Im Kapitel 2 wird die Interaktion zwischen der Prodomäne und FADD genauer analysiert, während in den Kapiteln 3 und 4 die strukturellen Änderungen in der katalytischen Domäne während des Aktiverungsprozesses genauer untersucht werden.

Die Bindung zwischen der Prodomäne der Caspase-8 und FADD wurde durch biochemische Interaktionsstudien analysiert. Darin wurde gezeigt, dass beide Todeseffektordomänen der Prodomäne benötig werden um FADD zu binden, da keine Bindung durch individuelle Todeseffektordomänen erfolgte. Während der Proteinreinigung und der Interaktionsstudien wurde wiederholt eine Oligomerisation der Prodomäne beobachtet, welche ursprüng-

lich auf die Ausbildung von Disulfidbrücken zwischen den Prodomänen zurückgeführt wurde. Mutation von zwei Cysteinen in der zweiten Todeseffektordomäne zeigte allerdings, dass dieses Phenomän nicht cysteinabhängig und höchstwahrscheinlich biologisch nicht relevant ist.
Erste Versuche zur Expression und Reinigung eines Komplexes bestehend aus Prodomäne und FADD für biochemische und strukturelle Charakterisierungen wurden durchgeführt. Allerdings wurden diese Experimente durch eine hohe Tendenz der Prodomäne zur Aggregation und das Vorhandensein von grossen Fusionsdomänen an der Prodomäne und am FADD erschwert. Eine ausführliche Diskussion im Kapitel 2.3 beschreibt verschiedene Strategien, diese Probleme in zukünftigen Experimenten zu bewältigen.
Während die Strukturbestimmung der Prodomäne bis jetzt nicht erfolgreich war, wurde die Struktur der katalytischen Domäne der inaktiven Procaspase-8 mittels Kernresonanzspektroskopie bestimmt. Diese Struktur zeigt, dass die Sekundärstrukturelemente der Procaspase-8 im Vergleich zur Caspase-8 konserviert sind. Unterschiede zwischen den beiden Strukturen sind in den Loops um die Substratbindungsstelle und dem Linker zwischen den Untereinheiten der katalytischen Domäne zu finden. Biochemische und biophysikalische Analysen an verschiedenen Dimerisierungs- und Prozessierungsmutanten erlauben Einblicke in den strukturellen Übergang von der Procaspase-8 zur Caspase-8 und die Substatbindung an das Enzym. Diese Experimente deuten darauf hin, dass Dimerisierung eine Umlagerung des Linkers herbeiführt. In monomerer Procaspase-8 bedeckt ein Teil des Linkers die Stelle, an welcher die Substratbindungstasche in der aktiven Caspase-8 gebildet wird. Durch die Dimerisierung wird die Position des Linkers so umgelagert, dass dessen Prozessierungsstellen in die Nähe des katalytischen Cysteins des zweiten Caspase-8 Moleküles vom gleichen Dimer rücken und somit intermolekulare Spaltung innerhalb des Dimers ermöglicht wird. Dabei ist es wichtig, dass die Caspase-8 an beiden Prozessierungsstellen gespalten wird, um die volle Aktivität des Enzyms zu erhalten. Nach der Spaltung erfolgen strukturelle Änderungen in den Loops an der Substratbindungsstelle und den gespaltenen Linkerfragmenten. Dadurch wird die Substratbindungstasche teilweise ausgebildet. Weitere Umlagerungen zur vollständigen Bildung der Bindungstasche erfolgen während der Substratbindung.

Diese Arbeit bestätigt den Einfluss der Dimerisierung auf die Aktivierung und Aktivität der Caspase-8. Zusätzlich wird deutlich gemacht, dass proteolytische Spaltung eine massgebliche Rolle im Aktivierungsprozess spielt. Die präsentierten Ergebnisse erlauben ein tieferes Verständniss des derzeitigen Aktivierungsmechanismusses der Caspase-8 und möglicherweise anderer Caspasen.

Acknowledgements

First of all my gratitude goes to Prof. Dr. Markus G. Grütter, who gave me the possibility to join his group and offered me this interesting project, which I enjoyed working on very much. Special thanks also goes to Prof. Dr. Oliver Zerbe, who supervised me through the NMR experiments which formed the main part of my thesis. He guided me through this for me new field but also engaged in fruitful discussions about my work and writing. In addition, I want to thank my committee members Prof. Dr. Michael Hengartner and Dr. Elena Conti. Although they were not directly involved in my project they always took an interest in my work and provided me with valuable input.

Certainly I want to thank all my previous and current colleagues from the Grütter lab (Guido Capitani, Nicole Bischoff, Beat Blattmann, Florence Bourquin, Christophe Briand, Brian Brissoni, Bice Bruppacher, Magda Bukowska, Oliv Eidam, Sibylle Engeler, Dani Frey, Heinz Gut, Peter Gutte, Annette Haisch, Georg Hausammann, Thomas Heitkamp, Michael Hohl, Evi Jenny, Andi Kohl, Michaela Kramer, Mareike Kurz, Jana Lamp, Esti Lehnherr, Tobias Merz, Anshu Mittal, Damien Morger, Markus Müller, Dominik Possner, Heidi Roschitzki-Voser, Diego Sanchez, Thilo Schröder, Andreas Schweizer, Markus Seeger, Gabi Sennhauser, Christian Stirnimann, Celine Stutz-Ducommun, Rahel Urich, Christopher Weinert and Sara Züger) and the Zerbe group (Christina Ewald, Sowmini Kumaran, Jiri Mares, Alexey Neumoin, Reto Walser, Svava Wetzel and Chao Zou). Unfortunately, I cannot mention all the contributions of these people here. I just want to give a special thank to Alexey Neumoin and Jiri Mares as well as Christophe Briand for their introduction into the NMR and X-ray software, respectively. They

were very patient to answer all my silly questions. Further more I want to thank Beat Blattmann. When he did not go running with me through the woods, he was always open for questions and special plate request and was a good company for lunch breaks. In the initial phase of my thesis he provided me with beautiful salt crystals which finally lead me to do a successful NMR project. Very much I enjoyed supervising Sibylle Engeler during her Master's thesis. By doing an excellent job in her project she substantially contributed to the FADD project. Especially I enjoyed our fruitful discussions about the project. Another valuable contribution to this thesis came from Mark Monroe, Mareike Kurz and Nicole Bischoff, who were proofreading it. So if you like reading this thesis thank them, if you do not like it, blame it on me. Besides all the "lab rats" I also want to thank the Grütter secretaries Vreni Diezi, Ursi Iten and Salome Rittmeyer. They did a great job in managing the administrative site of the Grütter group as well as kept the boss in a good mood. I also do not want to forget to thank all the service people who ensured that life at the institute was running smoothly. The workshop guys Jean-Claude Tomassina, Adi Schmid and Sascha Weidner always made sure that the scientific instruments were up and running. The same holds true for the intranet and the computer support which was maintained by the IT service. In particular Steve Rast helped me with computer related problems. Ausserdem möchte ich mich bei meinen Eltern bedanken. Ohne ihre Unterstützung hätte ich es niemals so weit gebracht. Sie haben immer an mich geglaubt und mich jederzeit unterstützt. And finally I want to thank all the people I could not mention here, my friends in Zurich, people from other research groups who helped me out with discussions, reagents and introductions into certain equipment and the ASVZ with its great sport activities, which provided an important balance to my work in the lab.

Contents

List of Figures

List of Tables

List of Abbreviations

Proteins, Complexes and Diseases

Abbreviation	Full Meaning
ALPS	Autoimmune lymphoproliferative syndrome
Apaf1	Apoptosis protease-activating factor 1
ASC	Apoptosis associated speck-like protein containing a CARD
Bak	Bcl-2 antagonist/killer
Bax	Bcl-2 associated protein X
Bcl-2	B cell leukemia 2
Bcl-xl	B cell leukemia XL
BH3	Bcl-2-homology domain 3
CARD	Caspase-associated recruitment domain
CED	*C.elegans* cell death
DD	Death domain
DDAA	Double mutation of caspase-8: D374A, D384A
DED	Death effector domain
DISC	Death inducing signaling complex
ER	Endoplasmatic reticulum
FADD	Fas-associated death domain
FLIP	Flice (= synonym for caspase-8) like inhibitory protein
IAP	Inhibitor of apoptosis
ICE	Interleukin-1β-converting enzyme
LRR	Leucine-rich repeats
NLR	NOD-like receptor
PIDD	p53-induced protein with a DD
PC8	Procaspase-8
RAIDD	RIP-associated ICH-1/CED-3-homologous protein with DD
RIP	Receptor-interacting protein
TLR	Toll-like receptor

Reagents and Materials

Abbreviation	Full Meaning
AMC	7-amino-4-methylcoumarin
ATP	Adenosintriphosphat
cmk	chloro-methylketone
DDT	Dithioerithiol
EDTA	Ethylenediaminetetraacetic acid
GdHCl	Guanidine hydrochloride
LDAO	Lauryldimethylamine-oxide
MES	2-(N-morpholino)ethanesulfonic acid
PBS	Phosphate-buffered saline
TCEP	Tris(2-carboxyethyl)phosphine
TBS	Tris-buffered saline
TBST	TBS with 0.2% Tween-20

Methods and programs

Abbreviation	Full Meaning
BMRB	Biological Magnetic Resonance Bank
DAPI	4,6-Diamidino-2-phenylindole
HSQC	Heteronuclear single quantum coherence
hNOE	Heteronuclear Overhauser effect
NOESY	Nuclear Overhauser enhancement spectroscopy
PDB	Protein Data Bank
TOCSY	Total correlated spectroscopy
TROSY	Transverse relaxation optimized spectroscopy

Chapter 1

Introduction

1.1 Apoptosis - A programmed cell death

1.1.1 The history of a apoptosis

Apoptosis is a cell death program that is present in all mammalian and some plant cells. Several bacteria and yeast also have such a process genetically encoded [1]. The term was defined in 1972 by Kerr at al. [2]. However, it was used in the literature almost 2000 years ago by Hippocrates of Cos to describe a physiological form of tissue death observed at fractures that were covered by bandages [3]. The word 'apoptosis' is derived from the Greek roots 'apo' and 'ptosis', which together mean 'falling apart'.
Although the term apoptosis cannot be found in the literature again until 1972, fundamental research in the area was being performed in the mid 19th century (Figure 1.1, reviewed in [4]). In 1842, Karl Vogt first described cell death in the normal development of metamorphic toads [5]. Two decades later, in 1860, Rudolph Virchow distinguished between two forms of cell death - necrosis and necrobiosis - with the later describing morphological changes later defined to be characteristic for apoptosis [6]. A few years later, Walther Flemming, for the first time suggested that intracellular chemical changes rather than external mechanical forces were the cause of this type of cell death [7]. He was also the first one to describe chromatin disintegration, a hallmark of the apoptotic cellular death process. When in 1951 Glucksmann prepared a list of all types of cell death known to date, many

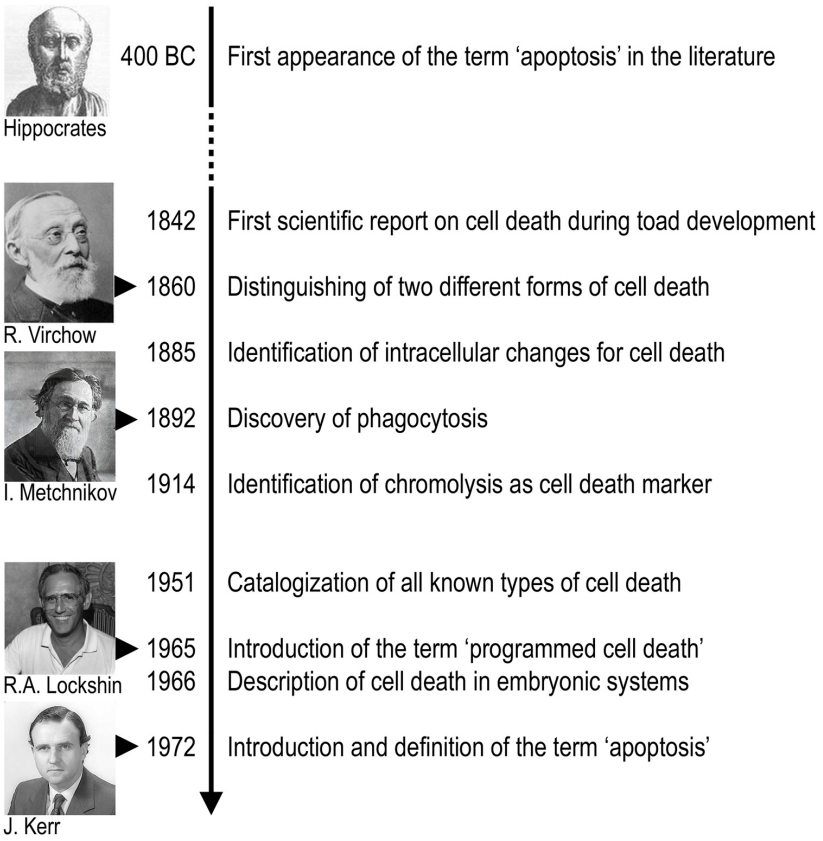

Figure 1.1: Historical review of apoptosis.
A more detailed description of the historical events in the discovery and definition of apoptosis is summarized in a review by Diamentis, et.al [4].

morphological changes such as chromatin condensation and nuclei fragmentation were included on that list [8].

Finally, in 1972 Kerr et al. defined the term apoptosis as a mechanism for the disposal of unwanted cells during embryonic development as well as normal tissue homeostasis throughout life [2]. In his fundamental publication he describes most of the morphological changes nowadays widely accepted to be linked to apoptotic cell death (Figure 1.2, [10]): In the early stage dying cells detach themselves from surrounding cells and round up, which can be easily observed under a normal light microscope. Next, small protrusions from the plasma membrane appear. This phenomenon is called membrane blebbing. Finally the whole cell condenses into 'apoptotic bodies', which will be engulfed and digested by macrophages. On the intracellular level most

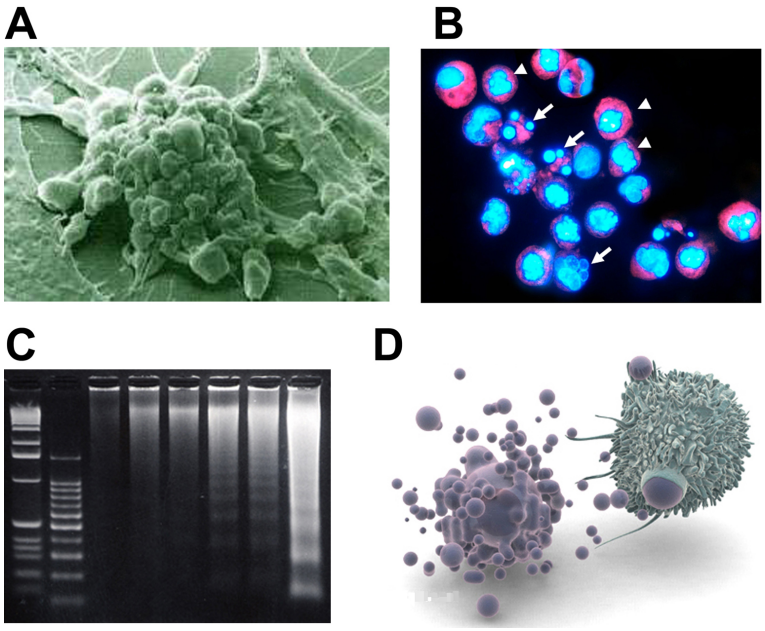

Figure 1.2: Morphological changes characteristic for apoptosis
A) Electron microscopy image of an apoptotic cell detached from surrounding cells. Extensive membrane blebbing is evident.
B) Chromatin condensation (arrow heads) and fragmentation (arrows) visualized by DAPI staining (adapted from Zoli et al. [9]).
C) DNA laddering on an agarose gel (adapted from: www.research.kobe-u.ac.jp/brce-mikitani/english.html). Following two marker lanes chromosomal DNA at increasing levels of fragmentation is visible.
C) Schematic drawing of the engulfment of an apoptotic cell (left) by a macrophage (right) (adapted from the U.S. National Library of Medicine).

changes are restricted to the nucleus. Chromosomal DNA condensates and is digested into smaller fragments. The condensed nucleus finally disintegrates into smaller particles. In contrast to the nucleus, which is effected early during apoptosis most other organelles seem to remain intact for at least some time. In some cases swelling or condensation of mitochondria and membrane permeabilization was described [10]. During the whole process of apoptosis the cytosolic contents of the cell is surrounded by the cellular membrane. This prevents release of the intracellular components and keeps an immune response from occurring. [11].

The introduction of modern DNA techniques and genetic model organisms such as *Caenorhabditis elegans* and *Drosophila melanogaster* in the early

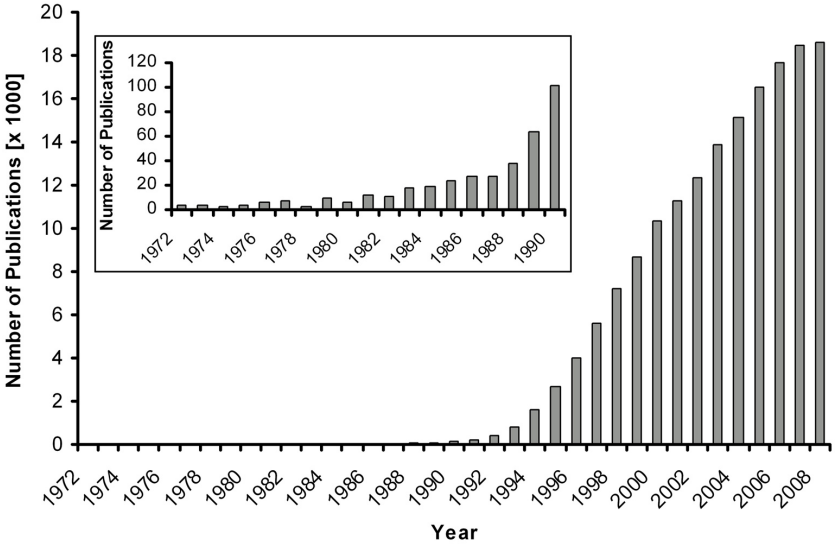

Figure 1.3: Publications on topics concerning apoptosis
Listed are all PubMed publications with the term 'apoptosis' appearing in either the title or abstract. The inset zooms in on the publications of the early years with a larger scale on the publications per year axis.

1970^{th} greatly advanced our understanding of apoptosis. In 1977, Sulston and Horvitz made the exciting discovery that during normal development in the nematode *C.elegans*, exactly 131 out of 1090 somatic cells undergo programmed cell death [12]. Further research on the worm lead to the discovery of the first apoptotic gene, *ced-3* in 1982 [13]. Many more pro- and antiapoptotic genes followed. Researchers all over the world started to investigate various aspects of apoptosis as evident by a rapidly increasing rate of publications on this topic (Figure 1.3).

1.1.2 Apoptotic pathways - the road to death

To date, two different apoptotic pathways have been distinguished - extrinsic and intrinsic - depending on the origin of the apoptotic stimulus. The extrinsic pathway is initiated by binding of an extracellular ligand or antagonist to an extracellular part of a transmembrane death receptor. A well studied example is the Fas mediated pathway. Upon an apoptotic stimulus the Fas ligand binds to the Fas receptor. This leads to the oligomerization of the receptor. Signal transduction from the Fas receptor to downstream proteins

is mediated by the adapter protein FADD. This FADD is responsible for the recruitment of the caspases-8 and -10 to a macromolecular complex which is termed the death inducing signaling complex (DISC). After activation at the complex, the caspases are released and process downstream targets, such as caspase-3 and -7, which in turn cleave further proteins, finally leading to self destruction of the cell. A more detailed description of the molecular interactions at the DISC and the activation of the caspases are given in chapter 1.2.1.

Apoptotic cell death can also be induced by internal stimuli such as cytotoxic stress or DNA damage [14]. As a response diverse proteins belonging to the BH3-only proteins are activated. If this activation overcomes a certain threshold it can compensate the inhibitory effects executed by antiapoptotic proteins of the Bcl-2 family. This results in the formation of Bax/Bak oligomers within the outer membrane of mitochondria and subsequent release of cytochrome *c* from the mitochondria [15]. Together with Apaf1 and caspase-9 and the cofactor ATP, cytochrome *c* forms the apoptosome which activates caspase-9 [16,17]. After activation, caspase-9 further cleaves downstream caspases -3 and -7, which subsequently lead to the execution of the cell [18].

Apoptosis can also be initiated by a combination of the two pathways described above. Whereas so called type I cells display the extrinsic pathway, some crosstalk between the extrinsic and the intrinsic pathway exists in type II cells. There, the formation of the DISC is reduced as compared with type I cells, which results in lower levels of active caspase-8. In order to achieve sufficient apoptosis an amplification of the signal is needed. This is achieved by cleavage of the Bcl-2 family protein Bid by caspase-8 to generate tBid [19]. tBid locates to the mitochondria and induces release of cytochrome *c*, which leads to activation of the intrinsic cell death pathway [20,21].

Induction of the intrinsic pathway can also be induced by the initiator caspase-2, which was shown to be able to promote cytochrome *c* release from mitochondria [22,23]. However, how this happens is not yet understood. In general, programmed cell death via caspase mediated cascades is a highly complex mechanism. We most likely only know about a small fraction of what is really going on in dying cells. However, a complete or at

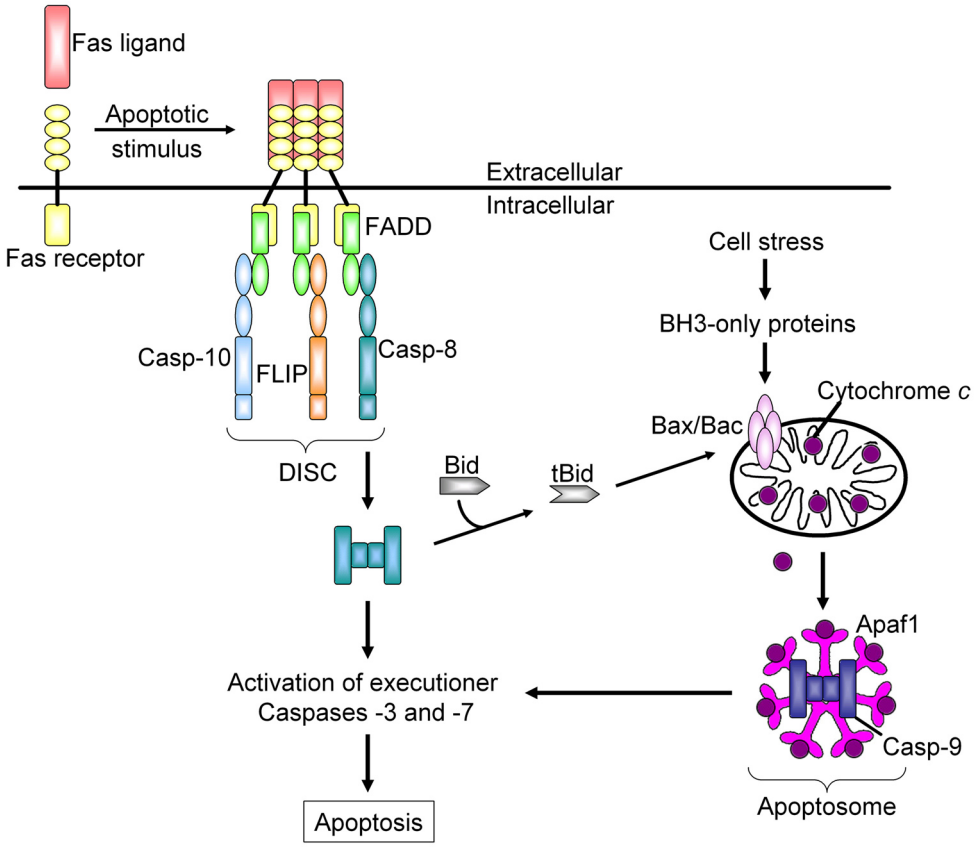

Figure 1.4: Apoptotic pathways.
The extrinsic Fas mediated pathway is displayed on the left side, the intrinsic pathway is shown on the right. Both pathways lead to activation of caspase-3 and -7.

least better understanding of the involved pathways is essential to fight many wide spread diseases. Already in 1973 Danielevicius suggested a direct link between improper apoptosis and the development of cancer [24]. Nowadays, it is a well known fact, that inappropriate cell accumulation is involved in many different types of cancer as well as autoimmune diseases [25–29]. In contrast, excessive cell death has been linked to stroke, Alzheimer's and Parkinson's disease [30]. Furthermore, many viruses directly influence the apoptotic pathways of their host, which leads to infectious diseases such as AIDS [1,31].

Group (Subfamily)	Cellular function	Group members	Substrate specificity
Group I (ICE)	Inflammatory mediators	Caspase-1	WEHD
		Caspase-4	(W/L)EHD
		Caspase-5	WEHD
		Caspsae-11	
		Caspase-12	WEHD
		Caspase-13	
		Caspase-14	WEHD
Group II (CED3)	Apoptotic initiators	Caspase-2	DEHD
		Caspase-8	IETD
		Caspase-9	(L/V)EXD
		Caspase-10	(L/V)EXD
Group III	Apoptotic executioner	Caspase-3	DEHD
		Caspase-6	VEHD
		Caspase-7	DEVD

Table 1.1: Overview of mammalian caspases and their substrate specificity

1.2 Caspases - the players of the death game

Caspases function in key positions along the apoptotic pathway. These enzymes form a class of endoproteases with a cysteine in the active site and have a specificity for aspartate in their substrates. The first caspase identified was ICE/caspase-1, which is involved in the proteolytic maturation of pro-interleukin-1β [32,33]. Fourteen different mammalian caspases are known to date. Caspases cleave a great variety of substrates, among them transcriptional and translational regulators, structure proteins and many kinases. The online database CASBAH (www.casbah.ie) lists all natural known caspase substrates [34].

Caspases can be grouped by how they function. They take part in inflammatory or apoptotic processes (Table 1.1). However, some take part in both processes, and therefore are not easily categorized. Apoptotic caspases can be further divided into apical initiator caspases and downstream executioners. In addition to their different positions within the apoptotic cascade initiators and executioners also differ in their domain architecture (Figure 1.5). They all contain a catalytic domain with a large ($\sim$20 kDa) and a small ($\sim$10 kDa) subunit, termed p20 or α and p10 or β. These units are

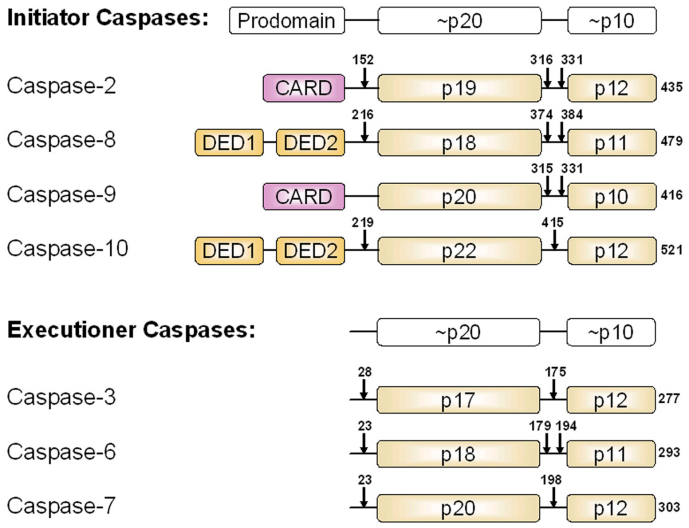

Figure 1.5: Domain organization of mammalian caspases. The position of the P1 aspartates are indicated by arrows and residue numbers. Proteolytic cleavage occurs after the assigned residues.

connected by a linker. The initiator caspases contain additional hexa-helical domains at their N-termini. These so called prodomains contain either one CARD or tandem DED domains and are linked to the catalytic domain by a flexible linker region. The executioner caspases contain only short, if any, prodomains.

Structural information on the catalytic domains of caspases is available (Figure 1.6). Executioner caspases and active initiator caspases are present in the cell as dimers, whereas initiator zymogens appear to be monomeric. Most of the structures solved today show dimeric active caspases with a variety of different small molecule inhibitors bound. All of these structures share the same overall fold: Each catalytic unit contains a six-stranded β-sheet with five parallel and one antiparallel strand. Within the dimer the six-stranded β-sheet is expanded to a twelve-stranded sheet with the antiparallel strands positioned at the dimerization interface. The individual protomers are thereby arranged in a head-to-tail fashion. The central β-sheet of each protomer is surrounded by five α helices, three and two flanking opposite sites of the β-sheet.

Protruding from this core are flexible loops: L1-L4 (Figure 1.6 E). They are

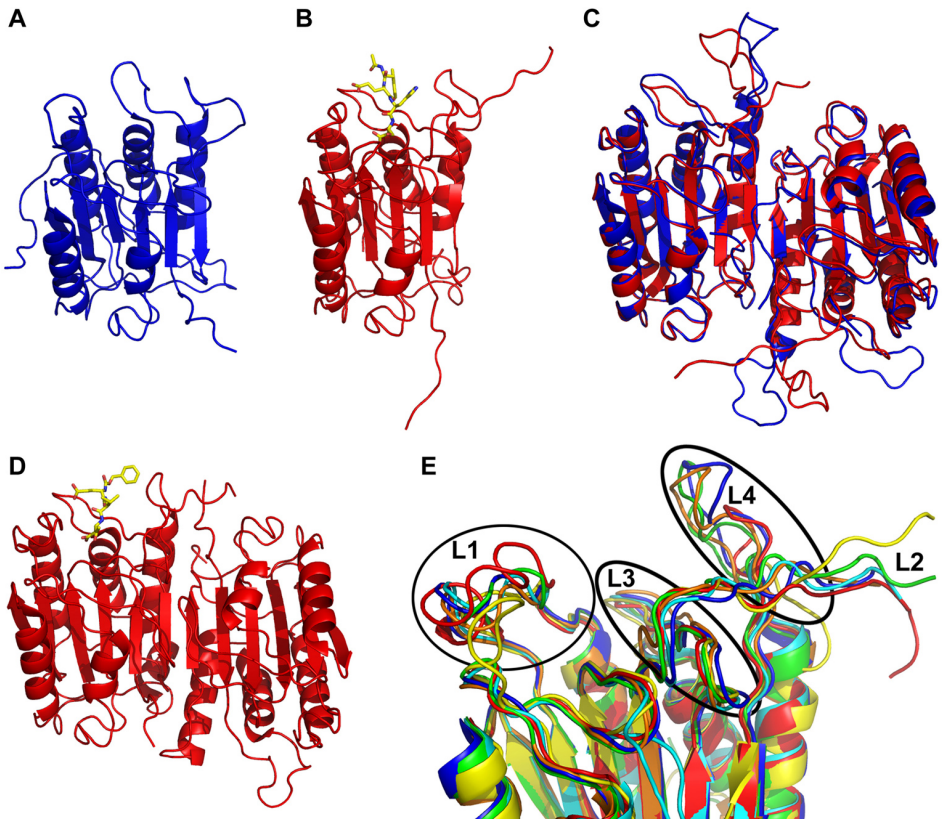

Figure 1.6: Structures of caspase zymogens (blue) and active caspases (red). Inhibitors are indicated as yellow sticks.
A) X-ray structure of the *Drosophila melanogaster* initiator procaspase Dronc (PDB code 2FP3).
B) First X-ray structure of a caspase - caspase-1 (PDB code 1IBC). Although the PDB file contains only a monomer of caspase-1 it is known to be a dimer.
C) X-ray structures of dimeric inactive procaspase-7 (blue, PDB code 1K88) and active caspase-7 (red, PDB code 1K86).
D) Structure of caspase-9 (PDB code 1JXQ). The inhibitor (yellow) is bound to only one monomer. In the second protomer is in a conformation not suitable for substrate binding.
E) Superposition of the active site conformation of different caspases. The individual enzymes are colored as followed: Caspase-1 = yellow, caspase-2 = green, caspase-3 = blau, caspase-7 = orange, caspase-8 = red, caspase-9 = cyan. The positions of the catalytic loops (L1-L4) are indicated.

all located on one side of the β-sheet and are involved in forming the substrate binding pocket. L2 contains the active site cysteine (C285 in caspase-1 numbering), which is part of a highly conserved amino acid sequence: QACxG. L1 and L3 display a similar length and position in all caspase structures solved to date. L2 and L4 are less conserved. Together the loops form the substrate binding pocket, which can accommodate the typical caspase recognition sequence: $\mathrm{X}^{P4}\mathrm{E}^{P3}\mathrm{X}^{P2}\mathrm{D}^{P1}$. P1, which represents the aspartate directly adjacent to the catalytic cleavage site and P3 are very invariant in substrates of all caspases. This is reflected in a high conservation of the corresponding S1 and S3 substrate binding pockets of the active enzyme, which are almost identical in shape in all caspase structures. The S1 pocket is lined by two conserved arginines positioned on L1 and L3 as well as a glutamine at L2 resulting in a highly basic pocket where aspartate can bind [35]. The S2 and especially S4 binding regions are less conserved and are responsible for substrate specificity. Depending on this substrate specificity, caspases can be divided into three different groups: Caspases-1, -4, and -5 possess a relatively wide S4 subsite and therefore share a preference for bulky hydrophobic residues at the P4 position. They belong to group I. Group II comprises caspases-8, -9, and -10. They prefer branched aliphatic side chains at P4 position. Caspases belonging to group III encompass caspases-3 and -7. This group has a requirement for aspartic acid in P4 due to a very narrow and positively charged S4 binding pocket.

1.2.1 Caspase activation

In order to bind and process their substrates, caspases need to be activated first. Thereby, executioner and initiator caspases apply different mechanism. Dimeric executioner caspases are activated by proteolytic processing at their intersubunit linker, resulting in the formation of L2 and L2' fragments, which are linked to the p20 and p10 subunits, respectively. Furthermore, this results in the rearrangement of the catalytic loops. Especially L2 and L2' undergo major structural changes. After cleavage L2 translocates towards the other protomer where it interacts with the corresponding L2'. These re-

arrangements are only possible after catalytic processing of the linker region. In contrast, it was shown that catalytic processing of initiator caspases is not sufficient for their activation [36]. Rather dimerization seems to be the stimulus for apical caspase activity. This was described first by the 'close proximity model' in 1998 and later on refined to the 'proximity-induced dimerization model' [37,38]. These models state that initiator caspases are activated when brought in close proximity to each other and subsequent homodimerization is enforced. This is achieved by recruitment of the enzymes to macromolecular activation platforms. Several of these complexes have been described over the years: The death inducing signaling complex - DISC, the apoptosome, the inflammasome and the PIDDosome (reviewed in [39–43]). They activate apoptotic as well as inflammatory caspases.

Death domains

An important feature for the activation of caspases on the activation complexes are homotypic interactions between domains belonging to the class of death domains (Figure 1.7, reviewed in [44,45]). Members of this class comprise the death domain (DD), the death effector domain (DED), the caspase recruitment domain (CARD) and the pyrin domain (PYD). They all share a common fold of a six α helices arranged in a Greek key topology. An exception is the pyrin PYD domain of NALP1 where the third α helix is disordered [46]. Interactions between the individual death domains of different proteins have so far only been observed between members of the same subfamily of death domains, i.e. CARD with CARD, DED with DED, etc (Figure 1.7 C, E). These interactions form the basis of the assembly of various complexes important for caspase as well as kinase activation [44,45]. Thus, death domains are important for proximity induced dimerization, proteolytic processing or phosphorylation of their adjacent domains.

The death inducing signaling complex - DISC

The extrinsic apoptotic pathway is initiated by binding of an extracellular Fas ligand to a transmembrane Fas receptor, followed by oligomerization of

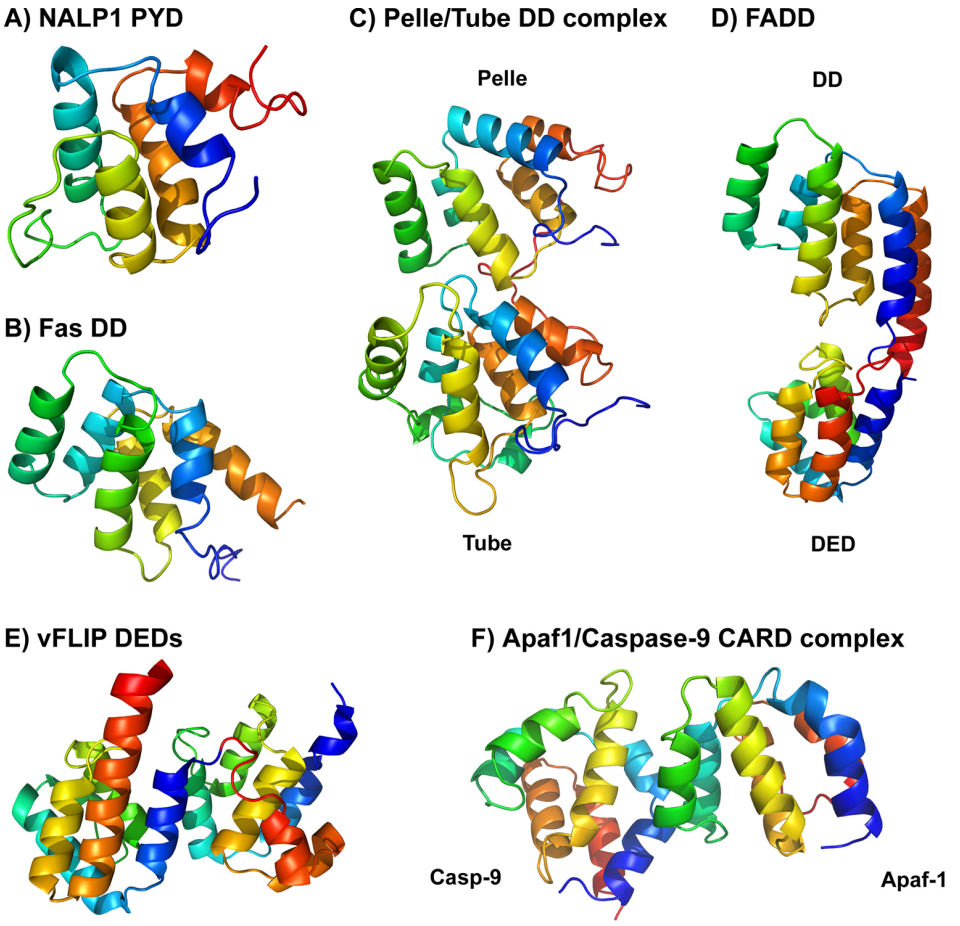

Figure 1.7: Structures of death domain family domains. Solution and X-ray structures of A) NALP1 PYD (1PN5), B) Fas DD (1DDF), C) Complex of the Pelle/Tube DD from *Drosophila melanogaster* (1D2Z), D) FADD with DED and DD (2GF5), E) tandem DD viral FLIP MC159(2BBR) and F) Apaf-1/caspase-2 CARD complex (3YGS). The Figure was prepared using PyMol (DeLano, Scientific). The helices of each death domain are colored in rainbow from blue at the N-terminus to red at the C-terminus. NALP1 PYD and the DDs of Fas, Tube and FADD are displayed in the same approximate orientation. FADD DED was superimposed with the first DED of vFLIP.

the receptor (Figure 1.8 A). Signal transduction from the Fas receptor to the downstream proteins is mediated by the adapter molecule FADD [45]. FADD is a two domain protein with an N-terminal DED and a C-terminal DD. The DD binds homotypically to the intracellular DD of Fas via electrostatic interactions. The structures of the individual DDs of both proteins as well

as the complex between them were solved (Figures 1.7B, 1.8A, [47–49]). Upon complex formation the FADD DD undergoes only minor structural changes whereas major rearrangements in the DD of Fas occur [49]. The sixth helix of the Fas DD shifts for about 40 Å which results in the formation of an extended helix comprising helices five and six. This opening exposes a hydrophobic patch where FADD binds. Furthermore, the authors stated that this elongated helix also undergoes oligomerization with proximal Fas/FADD complexes, resulting in further oligomerization of the DISC [49].
Via its N-terminal DED FADD is able to recruit procaspase-8 or -10 to the DISC. Both proteases contain tandem DEDs at their N-terminal prodomain, which are involved in the interaction with the FADD DED. As a result the caspases autoprocess themselves at their intersubunit linker followed by another cleavage event between the prodomain and the catalytic domain. The active dimeric caspase is released in the cytosol where it initiates the apoptotic catalytic cascade.
The individual domains of the different DISC proteins have already been characterized. However, their stoichiometry remains enigmatic. Efforts to isolate the DISC from cells or reconstitute it *in vitro* have been unsuccessful so far. This is most likely due to self aggregation of the proteins. This aggregation phenomenon might play a role in *in vivo* DISC formation, but that still remains to be investigated. At the moment it is unknown if the DISC exists in a single conformation. Different oligomerization states might exist.

Apoptosome

Structurally better defined than the DISC, is the composition of the apoptosome (Figure 1.8 B, [16,50]). The apoptosome is required for caspase-9 activation and is composed of cytochrome *c*, the cofactor ATP, the adapter protein Apaf-1 and caspase-9 [51]. Apaf-1 is a multidomain protein containing an N-terminal CARD, a central nucleotide binding and oligomerization domain and a C-terminal WD40 domain with 13 WD40 repeats. Without an apoptotic stimulus it exists in an inactive conformation with the individual domains accommodating a compact structure [52]. Upon the binding of

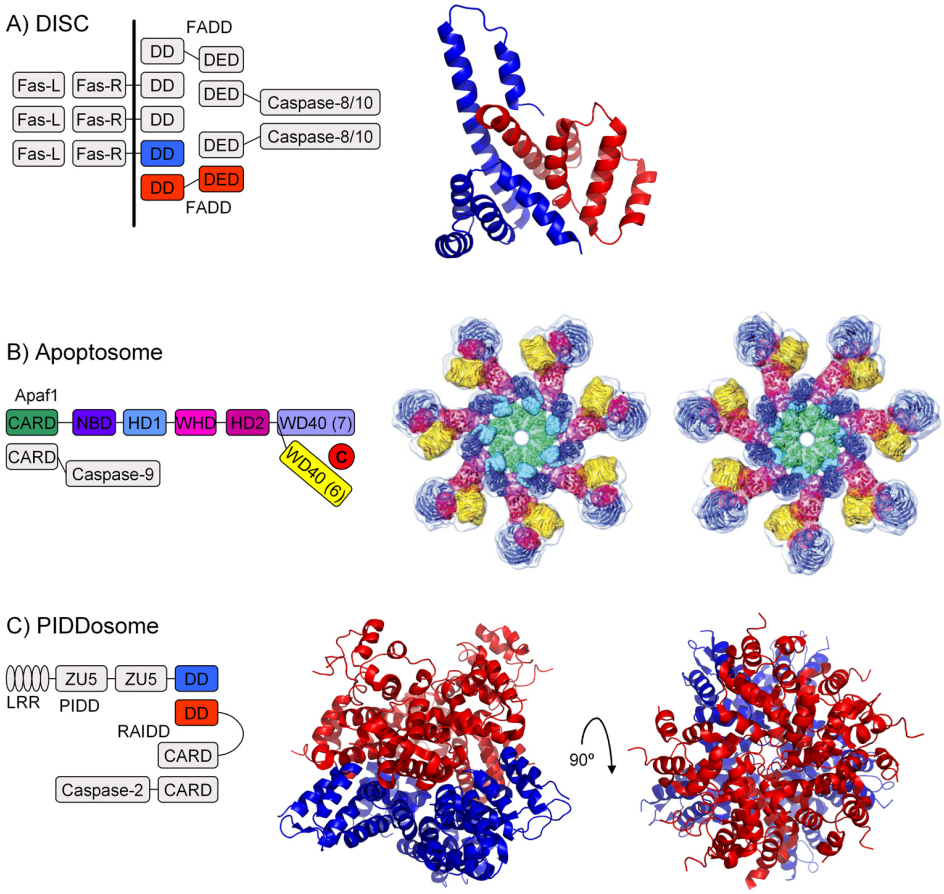

Figure 1.8: Activation platforms for apoptotic caspases
On the left hand side schematic drawings of the activation complexes are shown. Available structures of the whole complex or parts of it are shown on the right side. The applied color coding on the scheme and the structures indicate identical elements. The molecule structures in A) and C) were prepared using PyMol (DeLano, Scientific).
A) Death inducing signaling complex - DISC - with the corresponding X-ray structure of the Fas-DD/FADD-DED complex (PDB code 3EZQ)
B) Apoptosome. The right panel shows an EM structure at 12.8Å resolution at two different views rotated by 180°. The structural figures were adapted from Yu et al. [50].
C) PIDDosome. On the right hand side two different orientations of the PIDD-DD/RAIDD-DD complex are displayed (PDB code 2OF5). The second structure is rotated by 90° towards the viewer. The complex contains seven RAIDD-DDs and five PIDD-DDs.

ATP and cytochrome *c* Apaf-1 extends to an elongated structure, exposing the previously buried caspase-9 binding interface on its CARD. In this open conformation Apaf-1 assembles to a seven-wheeled macromolecular complex with a 1:1 stoichiometry of all involved proteins (Figure 1.8 B, [16,50]). The seven CARDs of Apaf-1 form a central ring with the caspase-9 binding site exposed. The other domains of Apaf-1 protrude from this ring. Cytochrome *c* was found to be bound between two β-propellers formed by seven and six WD40 repeats of the WD40 domain, respectively.
Caspase-9 is recruited to this complex by CARD/CARD interactions between its own prodomain and the N-terminal domain of Apaf-1 [53]. Binding of caspase-9 to the apoptosome results in dimerization. Autoprocessing is not required for the activation of caspase-9 [54,55]. Dimerization without cleavage is sufficient for full caspase-9 activation. In its dimeric form caspase-9 remains attached to the complex, while processing its targets. This observation supports the induced proximity model [37,38].

PIDDosome

Another activation platform is the PIDDosome, which is responsible for caspase-2 activation (Figure 1.8 C, [56]). This complex contains PIDD, the adapter protein RAIDD and caspase-2. Formation of it seems to be induced by an intracellular increase of PIDD [57], a protein not only involved in initiation of apoptosis but also in activation of NF-κB [58]. PIDD contains an N-terminal LRR domain, two ZU-5 domains and a C-terminal DD. It is often autoprocessed between the two ZU-5 domains and between the second ZU-5 and the DD and the site of processing decides between PIDDs pro- and anti-apoptotic functions [59]. Processing after the second ZU-5 results in separation of the DD from the rest of the protein. This single DD can then bind to the C-terminal DD of the adapter protein RAIDD. The resulting complex reveals an unusual stoichiometry of seven RAIDDs and five PIDD molecules (Figure 1.8 C).
Besides the DD RAIDD also contains an N-terminal CARD which recruits caspase-2 to the complex via homotypic CARD/CARD interactions. Bound to this complex caspase-2 is activated and can induce the intracellular apop-

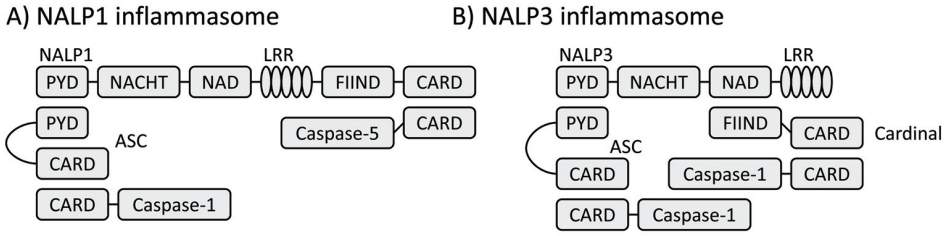

Figure 1.9: NALP inflammasomes for caspase activation.
Shown are two examples of inflammasomes containing NALP proteins. Other inflammasomes containing different NOD-like receptors are known.

totic pathway in response to intracellular stress. Therefore, it acts upstream of the mitochondria by inducing Bid cleavage, Bax translocation to the mitochondria and subsequent cytochrome *c* release [22,23].

The NALP inflammasomes

Upon tissue injury or infection, cellular pathways are activated which lead to inflammation. These pathways can be induced by the inflammatory caspases -1, -4 and -5. As their apoptotic counterparts, the initiator caspases -1 and -5 have been found to be recruited to macromolecular activation complexes, termed inflammasomes (Figure 1.9, reviewed in [41,42]). Different types of inflammasomes have been identified so far. They all contain proteins belonging to the family of NOD-like receptors (NLRs), such as the NALPs, IPAF and NAIPs [60]. NALP1, 2 and 3 have been shown to be involved in caspase-1 activation. Via their N-terminal PYD they bind the adapter protein ASC through homotypic domain interactions. In addition to PYD ASC also harbors a CARD domain which is involved in caspase-1 recruitment (Figure 1.9). The NALP3 inflammasome can bind an additional caspase-1 molecule via the CARD of the adapter protein cardinal (Figure 1.9 B). Furthermore, caspase-1 can be activated by binding to IPAF forming the IPAF inflammasome [61].
Despite the discovery of multiple pathways for caspase-1 activation no activation platform for caspase-4 is known. Caspase-5 can be activated by the NALP1 inflammasome by a mechanism different from caspase-1. It binds directly via its CARD to the C-terminal CARD of NALP1 (Figure 1.9 A, [62]).

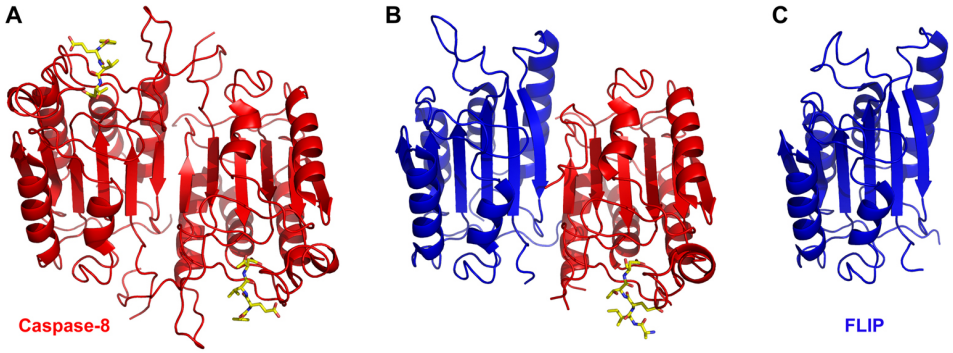

Figure 1.10: Caspase-8 structure and its interaction with FLIP
A) Structure of dimeric active caspase-8 (red, PDB code 1QDU) with a DEVD tetrapeptide (yellow) bound in the active site.
B) Heterodimer of the catalytic domains of procaspase-8 (red) and FLIP (blue, PDB code 3H11)
C) Structure of FLIP (blue, PDB code 3H13)

1.3 Caspase-8

Caspase-8 is the most apical caspase of the extrinsic apoptotic pathway and therefore belongs to the initiator caspases. It contains a prodomain of 180 amino acids, comprising two death effector domains (DED) followed by a 40 amino acid linker connecting the prodomain with the catalytic domain. The latter contains ~260 amino acids and can be divided into a large (p18 or α) and a small (p11 or β) subunit. These two subunit are linked by a 40 amino acid linker, which contains the two caspase-8 cleavage recognition motifs, VETD and LEMD. Processing at both sites results in separation of the two subunits and removal of a ten amino acid fragment during caspase-8 activation at the DISC and can occur intramolecularly as well as intermolecularly [63]. Following the subunit separation is a second cleavage step which releases the dimeric active caspase from the DISC-bound prodomain [64].
The structure of active caspase-8 with a bound inhibitor was first described in 1999 by two different groups (Figure 1.10 [65,66]). Both structures show dimeric caspase-8. However, in solution active caspase-8 exists in a monomer/dimer equilibrium with a dissociation constant of 50 μM [67]. This value is decreased by 10-fold upon inhibitor binding, indicating that addition of the inhibitor shifts the monomer/dimer equilibrium towards the dimer species.

The interface of this dimer is formed by hydrophilic and hydrophobic interactions and multiple hydrogen bonds [65,66]. In addition, the dimer seems to be stabilized by translocation of the cleaved linker fragments, which are termed L2 and L2' for fragments belonging to the α and β subunit, respectively. Thereby, L2 forms contacts with L2' of the other protomer and this interaction is thought to enhance dimerization stability [66].

Overall, caspase-8 represents the typical caspase fold described in Chapter 1.2 (Figure 1.10 A). The secondary structure elements of caspase-8 align well (rmsd $\sim$1Å) with the secondary structure elements of other caspase structures. Differences to other caspase structures are restricted to the loops which form the active site pocket and define the substrate specificity of caspase-8 (Figure 1.6 E). Loop1 is longer than in other observed caspases. It contains a short α helix, which seems to be unique to caspase-8. In caspase-8, loop1 is involved in substrate binding by forming direct contacts to the P1 aspartate and the P3 glutamic acid of a bound substrate [65]. Loop3 forms one side of the S4 pocket and therefore defines the substrate specificity at P4. Together the loops form a cleft on the surface, where natural and synthetic substrates or inhibitors can bind.

Caspase-8 was crystallized with different inhibitors, covalently bound to the active site cysteine [65,66,68–71]. All these structures reveal a positively charged S1 binding pocket, which is lined by several conserved residues: Arg413, Arg260 and Gln358 [66]. These residues form salt bridges with the P1 aspartate. Furthermore, the P1 α-carbonyl forms a hydrogen bond to the catalytically important His317. Besides the absolute requirement for aspartic acid in the P1 position, the P3 position in caspase-8 is also well defined. All of the solved structures accommodate a glutamic acid in the P3 position of the inhibitors. This residue forms hydrogen bonds to the conserved Arg413 and to Arg258 in loop1. The S4 pocket is formed by the bulky aromatic residues Trp420 and Tyr412, which explains the preference for small hydrophobic residues in the P4 position of the caspase-8 substrates [66]. Trp420 is the only tryptophan present in caspase-8. Besides forming the S4 pocket it also lines the S2 pocket [68]. Although it is located at the substrate binding site Trp420 is not buried by the inhibitor. The solvent accessible surface of it with and without inhibitor was calculated to be identical [67]. Thus, Trp420

has been used previously by several research groups to monitor structural changes in the active sites of caspase-8 during different states of activation using fluorescence changes [36,67].
It is currently unknown exactly how caspase-8 binds to the DISC since structural information on the prodomain of caspase-8 is still missing. However, the structure of the viral caspase-8 homologue FLIP MC159 has been solved and gives us some clues about the binding (Figure 1.7 C, [72]. As caspase-8 MC159 contains two DEDs responsible for protein-protein interactions with FADD. High sequence similarity between the caspase-8 prodomain and MC159 suggest a similar structure for caspase-8. MC159 contains two DEDs tightly packed to each other rather than separate domains connected by a flexible linker. Each of the two DEDs contains a hydrophobic patch at helices 2 and 5. This patch of DED1 is buried by helices 1 and 4 of DED2. In contrast, the hydrophobic region on helices 2 and 5 of DED2 is surface exposed. Recent mutagenesis studies imply an involvement of this region in binding to FADD [72]. In addition residues within helices 1 and 4 of FADD have been suggested to be involved in caspase-8 binding. Together, these observations imply an analogous binding of FADD to the DED2 of caspase-8 as is observed between DED1 and 2 of MC159 [73]. However, the accurate assembly of the two proteins into a complex has to be verified structurally.

1.3.1 Regulation of caspase-8

Caspase-8 regulation by FLIP

Caspase-8 represents the most apical caspase of the extrinsic apoptotic pathways. Since it is positioned at the beginning of a signaling cascade it is important that its activation and function is well regulated. In addition to Fas, FADD, caspase-8 and -10, and a caspase-8 homologue, called FLIP is also found in the DISC (Figure 1.8 A, [74,75]). This protein seems to be involved in direct caspase-8 regulation. Cellular FLIP is expressed in three different forms: a long splice variant c-FLIP$_L$ and shorter versions c-FLIP$_S$ and c-FLIP$_R$ [76,77]. The short splice variants are similar to the DED containing prodomain of caspase-8, whereas the long version contains an additional domain homologous to caspase-8 but inactive. Besides the cellular FLIPs, a

viral FLIP v-FLIP exists, which resembles the short cellular FLIPs in length. All splice variants compete with caspase-8 and -10 for binding to the DISC. The short splice variants were found to be inhibitors of caspase-8 by competing for the binding sites on FADD, whereas c-FLIP$_L$ can function either pro- or anti-apoptotic depending on its concentration in the cell [75,78].
The catalytic domain of caspase-8 and the corresponding sequence of c-FLIP$_L$ share 28% sequence identity and 44% sequence similarity. The structure of the domains are highly similar (Figure 1.10, [79]. The secondary structure elements of the two proteins superimpose well with an rmsd of 1.8 Å. Structural differences are located in the loops which form the active site in caspase-8 but do not so in c-FLIP$_L$. Apparently, c-FLIP$_L$ regulates caspase-8 activity by formation of a heterodimer with caspase-8 [79]. Interestingly, c-FLIP$_L$ also dimerizes with inactive procaspase-8, which is not able to homodimerize with itself. This indicates a higher affinity of procaspase-8 for c-FLIP$_L$ than for itself. In the hetrodimeric complex, procaspase-8 is found to be in the active conformation. At this stage it is able to process different substrates such as other procaspase-8 molecules and its dimerization partner c-FLIP$_L$. Catalytic processing of c-FLIP$_L$ in this heterodimer results in increased catalytic activity of the complexed caspase-8, independent of its own processing state [79]. Thus c-FLIP$_L$ is a potent enhancer of apoptotic activity when bound to the DISC. However, it is currently unclear whether the heterodimer is released from the DISC into the cytosol. c-FLIP$_L$-dependent activation of caspase-8 might be locally restricted to the DISC environment.

Phosphorylation of caspase-8

Phosphorylation and dephosphorylation has been shown to be a powerful tool to regulate protein expression, binding or function. An effect on apoptosis has been previously shown on caspase-9, whose activity was inhibited by phosphorylation [80–82]. Caspase-8 also undergoes phosphorylation in the presence of active Src kinase [83]. This kinase was found to be up-regulated in different colon cancers, together with an increase of phosphorylated caspase-8 in infected cells [83,84]. The phosphorylation site on caspase-8 was mapped to Tyr380, which is located in the linker region between the two subunits

and is conserved in other mammalian organisms [83]. *In vivo* studies by Cursi et al. revealed that phosphorylation at Tyr380 results in impaired receptor mediated apoptosis. Since, during catalytic processing a ten amino acid fragment containing Tyr380 is cleaved off, regulation of apoptosis by caspase-8 phosphorylation is most likely linked to some inhibitory effects on caspase-8 activation. In fact, it was suggested that modification of Tyr380 interferes with processing and thus activation of monomeric procaspase-8 to dimeric caspase-8 [83].

1.3.2 Caspase-8 for survival

Besides its role in cell execution caspase-8 is also involved in several pathways important for cell survival, such as embryonic development, monocyte differentiation, and T cell activation as well as innate immunity (summarized in [85]). Most of these pro-survival functions of caspase-8 are tightly linked to the NF-κB pathway. By cleaving RIP1, an antagonist of NF-κB, caspase-8 plays an important role in macrophage differentiation [86,87]. No macrophage differentiation was observed in caspase-8 deficient bone marrow precursor cells or upon addition of caspase inhibitor to normal cells [86,88]. Furthermore, specific caspase-8 inhibitors have also been found to decrease T cell activation and proliferation [26], suggesting a crucial role of caspase-8 in this process. Defects in T cell regulation are directly linked with diseases such as the autoimmune lymphoproliferative syndrome (ALPS)and a homozygous mutation (R248W) in caspase-8 has been identified in patients with this disease [25].

Caspase-8 dependent activation of NF-κB is not only important for T cell proliferation but also plays an important role in innate immunity. This defense mechanism against microbial infections is mediated by Toll-like receptors (TLR). For example, TLR4 activation results in apoptosis of dendritic cells and macrophages upon bacterial infections [89,90]. Recent studies have revealed the presence of small quantities of functional but uncleaved caspase-8 during NF-κB activation [91,92]. A possible explanation for this interesting finding might be that caspase-8 is regulated by c-FLIP$_L$ as described in 1.3.1. This hypothesis is strengthened by different studies which suggest an

involvement of c-FLIP$_L$ in NF-κB activation (summarized in [93]).
An interesting observation during the study of caspase-8 dependent NF-κB activation was the recruitment of the DISC into lipid rafts within the cell [94]. Therefore, the delicate balance between cell death and cell survival seems to be regulated by the specific location of active caspase-8 within the cell. In contrast to its cytosolic location during apoptosis, caspase-8 is bound to a different environment in the lipid rafts during its anti-apoptotic activities, exposing the protease to a different set of substrates.
To date it is not known whether the multiple involvement of caspase-8 in survival pathways is dependent on its enzymatic activity or if it serves merely as a scaffold. Although the presence of active caspase-8 contributes to some extend to the activation of NF-κB, it has been difficult to identify putative caspase-8 substrates. The dual killing and survival functions of caspase-8 will have to be investigated in more detail. Its apical position in the extrinsic pathway makes it a highly sought after target for drug development. However, currently it is not possible to influence the cell death mechanisms of caspase-8 without disturbing its survival functions and *vice versa*.

Chapter 2

Binding of Procaspase-8 to FADD

2.1 Introduction

Protein domains belonging to the superfamily of death domains are involved in a variety of different pathways. They play an important role in caspase activation during apoptosis and inflammation but also mediate protein/protein interactions in other situations (reviewed in [44,45]). Four different subfamilies of death domains have been distinguished so far: death domains (DD), death effector domains (DED), caspase recruitment domains (CARD) and pyrin domains (PYD). DDs and DEDs ar mainly involved in apoptotic signaling whereas PYDs play important roles in inflammation. CARDs have been found to be involved in both processes. The death domain superfamily proteins share a common hexa-helical fold in Greek topology arrangement. Structural and mutational studies revealed different regions on the surfaces of death domains to be responsible for protein/protein interactions [43,45,49,53,72,73,95–97]. However, death domain interactions are so far only known to occur between members of the same family, i.e. DD with DD, DED with DED, CARD with CARD and PYD with PYD.
The extrinsic pathway of apoptosis is initiated by formation of the death inducing signaling complex (DISC), which serves as a platform for caspase-8 activation (Figure 1.4; [98]). This complex is formed by homotypic DD/DD

and DED/DED interactions between the involved proteins. Upon an apoptotic stimulus an extracellular Fas ligand binds to the transmembrane Fas receptor, which contains a DD at its C-terminal cytoplasmic part. This DD directly interacts with the C-terminal DD of the adapter protein FADD. Via its N-terminal DED, FADD then recruits procaspase-8 and -10 as well as the caspase-8 homologue FLIP into the complex, the latter all containing tandem DEDs at their N-terminal prodomain. Binding of the procaspases leads to dimerization and thus activation of the enzymes.

Although the individual DISC components have been extensively characterized the structure and stoichiometry of the complex are unknown. Structural information is available for individual domains. The DDs of Fas and FADD and full-length FADD have been structurally investigated by solution NMR (Figures 1.7B, D and 1.8A on pages 12 and 14, respectively; [47,48,73]). In addition, information on the DD/DD interaction between Fas and FADD is known by a crystal structure of this complex [49]. Whereas the individual domains share the common hexa-helical fold of the death domain family, the structure of the complex reveals a different conformation in the sixth and last helix of the Fas DD upon binding of FADD. This helix shifts by approximately 40Å and forms an extension of helix 5. This conformational change exposes a hydrophobic surface on Fas, the binding site for FADD. Additional oligomerization mediated by the extended helix 5 and 6 was observed in the crystal structure, where each assymetric unit contains four Fas and four FADD molecules [49]. In general, the death domains involved in DISC formation are highly aggregation prone. However, whether this aggregation also occurs *in vivo*, enhancing oligomerization of the DISC and thus caspase activation, is still unknown.

So far, no structural information is available regarding the binding between FADD and the prodomain of caspase-8. The structure of full-length FADD was solved by NMR (Figure 1.7 D) but the prodomain of caspase-8 is structurally unknown. However, it can be assumed that it adopts a similar conformation as was seen for the caspase-8 homologue MC159, a viral FLIP (Figure 2.6 B on page 33, [72]). In this structure the tandem DEDs adopt a dumbbell-shaped conformation with the two DEDs representing the weights at each site (Figure 1.7 E). The first DED in the structure is different from

the typical death domain fold by a missing α helix 3 but two additional helices at the N- and C-terminal, respectively. Interactions between the two DEDs are of hydrophobic nature, with a hydrophobic surface of the first DED1 being in contact with a region in the second DED, which is located on the opposite site as the patch in the first DED. It is still unknown whether this interaction is representative for DED interactions. However, it is different from the interactions observed in homotypic complexes of other death domain superfamily members i.e. the DDs of Pelle and Tube or the CARDs of caspase-9 and Apaf-1 (Figure 1.7 C, F; [53,95].

The structure of MC159 and mutational studies on FADD suggest interaction between the two proteins [72,73,96,97]. The exact nature of the binding is still unknown but would provide important information to understand DISC formation and thus apoptosis regulation. This work was set out to biochemically and structurally characterize the interaction between FADD and the prodomain of caspase-8. For that pull-down studies were performed to determine, which parts of the prodomain are involved in FADD binding. Furthermore, pull-down experiments were used to analyze the importance of disulfide bridge formation in FADD binding as well as intermolecular prodomain oligomerization. Initial experiments were performed towards the determination of the three-dimensional structure of the FADD/caspase-8 prodomain complex.

A

	DED1	DED2	DED1 DED2	DED12	DED12 C163S	DED2 C163S
FADD	-	-	-	+	+	
FADD/DED12	-	+				-

C. Ghisleni, unpublished data

B

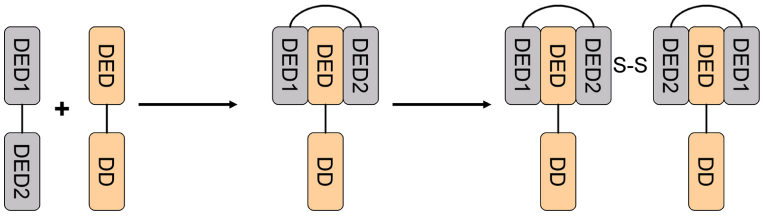

Figure 2.1: Summary of pull-down results from C. Ghisleni
A) Overview of the different protein combinations used in the pull-downs. FADD, either alone or in complex with bound DED12 was used as a bait to pull-down the proteins indicated on the top of the table. "+" and "-" indicate binding and no binding between the proteins, respectively. Combinations with no signs have not been investigated.
B) Schematic drawing of interpretation of pull-down results.

2.2 Results

2.2.1 Summary of previous results by Ghisleni, et al.

The following work is based on a diploma thesis by Claudia Ghisleni [99]. She designed and cloned single DED and double DED constructs of caspase-8 prodomain to perform pull-down experiments using GST-FADD bound to glutathione sepharose beads as a bait. In these experiments it was possible to pull-down the full-length caspase-8 prodomain DED12 but not the individual domains DED1 and DED2, suggesting that both domains are involved in binding FADD. Interestingly, simultaneous addition of separate DED1 and DED2 did not result in binding of either one of them. This indicates that both domains function as a single unit in FADD binding (Results summarized in Figure 2.1 A).

After protein purification mass spectrometry was performed to verify the correct protein masses. The obtained masses indicated the formation of a disulfide bridge between β-mercaptoethanol molecules from the buffer and

prodomain constructs containing DED2 either as a single unit or in combination with DED1. In addition, dimerization of these constructs was observed on SDS PAGE. The sequence of DED2 contains two cysteines in DED2 at position 130 and 163. Mass spectrometry in combination with proteolytic digest of the full-length prodomain indicates that Cys130 is surface exposed and involved in disulfide bridge formation whereas Cys163 is buried.
To investigate the role of Cys130 and Cys163 further, pull-down studies using the FADD/DED12 complex and single DED2 were performed (Figure 2.1 A). Interestingly, DED2 can be pulled down by the FADD/DED12 complex and this interaction was found to be inhibited at high concentrations of reducing agents or mutation of Cys163 to serine in DED2. Therefore, Ghisleni et al. suggested an additional oligomerization of the caspase-8 prodomain via disulfide bridge formation between DED2s of proximal procaspase-8 molecules (Figure 2.1 B). However, the biological relevance of this finding still is still unknown.

2.2.2 Pull-down experiments

The main goal of this work is the structural determination of a complex between FADD and the caspase-8 prodomain DED12. To get a better understanding of this system, first experiments were performed to confirm and expand the pull-down results described above [99]. A previously designed but unused DED12 C130S construct was included in the analysis and an additional DED2 C130S construct was designed. Furthermore, TEV protease cleavage sites were introduced right before the coding sequence for FADD and the full-length prodomain to allow removal of these tags prior to crystallization. An overview of the final constructs is shown in Figure 2.2.
Expression and purification of FADD and procaspase-8 was performed as described previously with minor differences. In contrast to the previous diploma work expression of all constructs was performed in BL21(DE3) cells. Different strains did not enhance expression or solubility levels. Very important was the use of unbaffled flask for expression of the prodomain constructs. Using baffled expression flasks resulted in complete insolubility of the proteins.

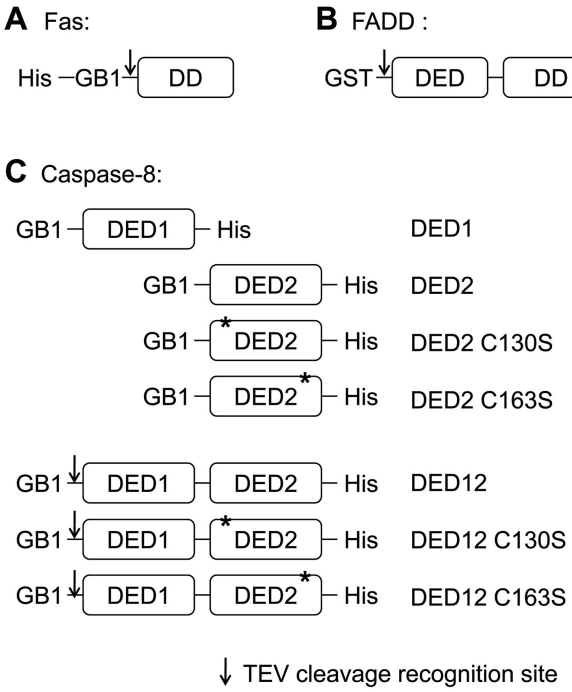

Figure 2.2: Overview of constructs used in pull-down experiments
Schematic drawing of the constructs for A) Fas, B) the bait protein FADD and C) the prodomain single (DED1 and DED2) and double constructs (DED12). The individual fusion tags are displayed. C130S and C163S mutations in DED2 are indicated by "*". The TEV cleavage sites are presented by arrows.

The expression level of GST-tagged FADD was very high. Purification of one liter of culture yielded more than 100 mg of soluble fusion protein with high purity (Figure 2.3 A). Expression of the prodomain constructs proved to be less effective. Especially, the full-length prodomain had a much lower expression level. Furthermore, purification of single and double DED constructs did not yield sufficiently pure material for structural work (Figure 2.3 B,C). However, for pull-down experiments the purity of the proteins was adequate. Western blot analysis of all proteins included in the pull-down experiments showed single bands for proteins carrying a C-terminal His-tag as displayed in Figure 2.3 D. Fas, FADD and GST-SGT1 do not contain a C-terminal His-tag and therefore were not detected.
The individual DEDs and full-length prodomain were analyzed for their abil-

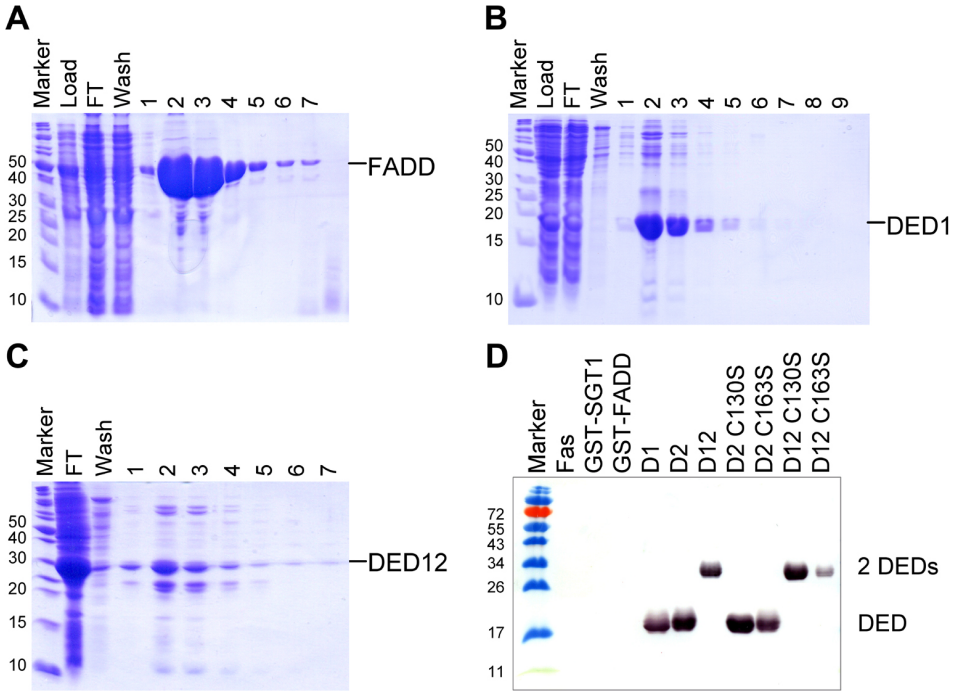

Figure 2.3: Purification of proteins for pull-down experiments
SDS PAGE of individual purification steps for A) GST-FADD, B) the single GB1-DED construct DED1 and C) the double GB1-DED construct DED12. The first lanes following the marker show the whole cell lysate, which was loaded on the column (Load), the unbound flow-through (FT) and the flow-through from washing the column (Wash). The numbers indicate the eluted fractions.
D) Western blot on purified proteins used in pull-down experiments. The individual proteins are indicated above the lanes. Detected was the C-terminal His-tag on the prodomain constructs. GST-FADD, GST-SGT1 and Fas do not have a C-terminal His-tag.

ity to bind FADD. A schematic drawing is displayed in Figure 2.4 A. GST-SGT1 was included in the pull-down as a negative control to exclude that the prodomain binds to the GST fusion tag. No binding was observed for the negative controls. As expected from former results [99], the individual DEDs did not bind to full-length FADD even when co-incubated. In contrast, full-length prodomain bound to FADD and this binding was not inhibited by mutation of either one of the cysteines or high concentration of DTT. Thus binding of procaspase-8 to FADD does not depend on disulfide bridge formation.

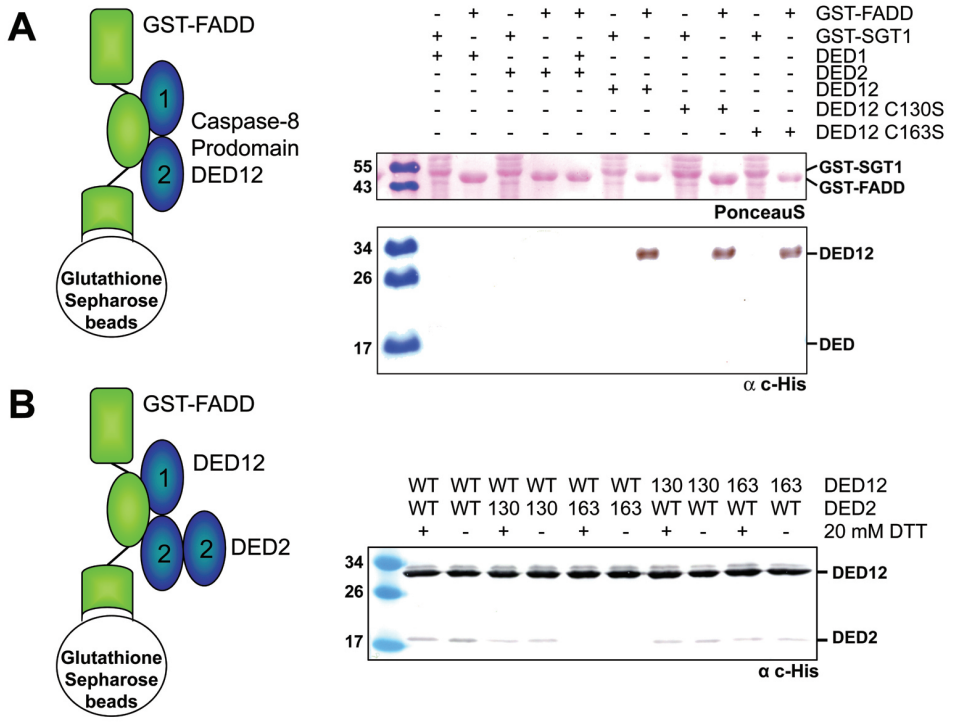

Figure 2.4: GST pull-down experiments to determine FADD/prodomain interactions
A) Pull-down of single or double DED constructs with GST-FADD as a bait. The proteins included into the pull-down are indicated above each lane
B) Binding of DED2 to the FADD/DED12 complex. Single and double domains were used as wild-type protein (WT) or with the C130S (130) or C163S (163) mutation as indicated above the blot.

Previous experiments by Ghisleni et al. suggested the formation of a disulfide bridge between cysteines in DED2. To verify this hypothesis wild-type DED2 or either one of the DED2 mutants were incubated with the FADD/DED12 complex (Figure 2.4 B). Indeed, it is possible to pull-down DED2 and DED2 C130S with the FADD/DED12 complex as observed by the appearance of an additional band for the single DED2 constructs. In contrast, no binding of DED2 C163S to DED12 was detected, which confirms the results by Ghisleni, et al. [99]. However, the reverse setup using wild-type DED2 and DED12 C163S leads to formation of a FADD/DED12/DED2 C163S complex as evident by bands for both prodomain proteins. In addition DED12 C130S

was also able to bind DED2 as effectively as wild-type DED12. Thus, mutation of either one of the two cysteines in DED12 does not prevent binding of DED2. Furthermore, addition of high concentrations of DTT did not abolish this interaction indicating that the interaction between DED12 and DED2 is not dependent on disulfide bridge formation.

2.2.3 Analysis of the biological relevance of disulfide bridge formation *in vivo*

To complement the results from mass spectrometry and the pull-down experiments we characterized the influence of the cysteine mutations *in vivo*. Preliminary experiments were performed by transfecting Cos cells with full-length wild-type caspase-8 or either one of the cysteine mutants C130S and C163S (Figure 2.5). Expression of all constructs was confirmed by detection of caspase-8 in Western blots. Activity of caspase-8 was analyzed by co-expression of caspase-8 with its substrate caspase-3. Processing of caspase-3 into the small and large subunit indicates that all caspase-8 constructs are active (Figure 2.5 A).

An interesting observation from the initial expression tests was that the C130S mutant shows higher signals in the Western blots as compared to wild-type caspase-8 and C163S, although the same amount of DNA was used for transfection (Figure 2.5). This effect could either be attributed to a higher expression level, an increased stability or to a decrease in proteolytic processing of this mutant. A reduced self processing rate would result in lower levels of active caspase-8 in the cells and therefore less caspase-3 processing. However, levels of cleaved caspase-3 are slightly elevated using C130S and this increase correlates well with the increased expression level. Thus the C130S mutant is as active as wild-type and C163S but is expressed at higher levels or has an increased stability.

Higher expression levels for C130S as compared to wild-type and C163 were also observed using the corresponding catalytic mutants of caspase-8 (C285A) for transfection. These C285A mutants are incapable of self-processing and therefore stay in their full-length form. All of these mutants

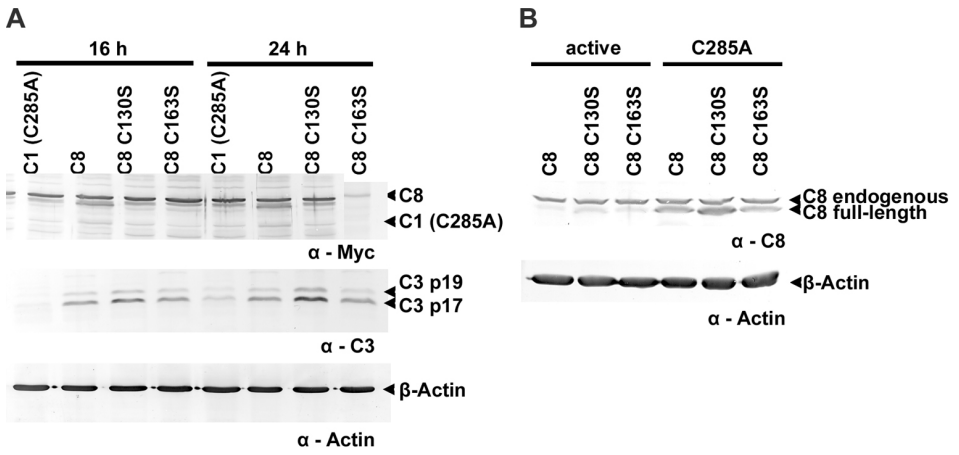

Figure 2.5: Overexpression of wild-type caspase-8 and cysteine mutants in Cos cells.
A) Expression analysis of inactive caspase-1 (control) and active caspase-8 constructs at 16 and 24 hrs after transfection by detection of a C-terminal Myc-tag. Caspase-8 activity was analyzed by processing of caspase-3 into the individual subunits. The large subunit (p17/p19) was detected using a specific caspase-3 antibody. Equal expression levels of β-actin allow comparison of the samples.
B) Expression analysis of active vs. inactive caspase-8 constructs analagous to A). Detected was the p18 subunit of overexpressed and endogenous caspase-8.

show a more intense signal for full-length caspase-8 on western blots as compared to their active counterparts. The lower levels of the full-length active caspase-8 mutants are most likely due to partial processing and thus formation of active caspase-8.

2.2.4 Comparison of the caspase-8 prodomain with viral FLIP MC159

In addition to the pull-down experiments and the *in vivo* studies described above we compared the caspase-8 prodomain with its homologue FLIP of which a crystal structure is available (Figure 2.6 A; [72]). In that structure the two DEDs are arranged side by side with α helices 2 and 5 of DED1 forming hydrophobic contacts with α helices 1 and 4 of DED2 which are located on the opposite side of DED2 than helices 2 and 5. Sequence com-

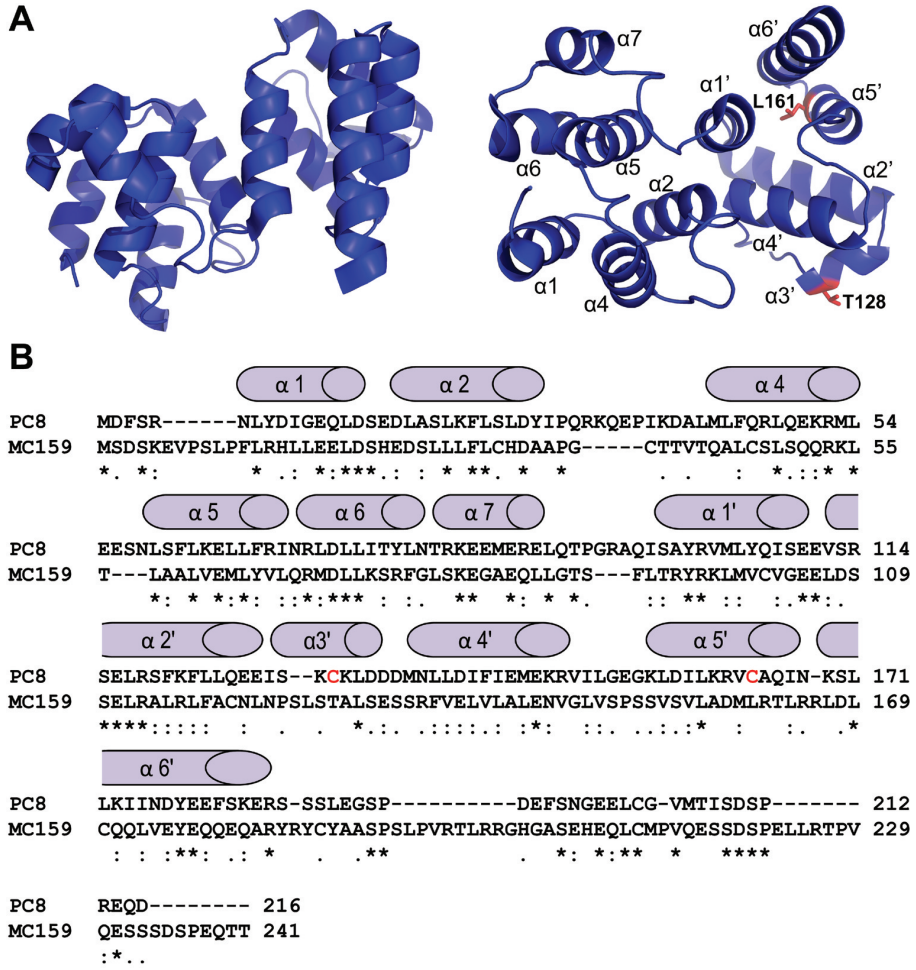

Figure 2.6: Comparison of the procaspase-8 prodomain with viral FLIP MC159
A) Crystal structure of MC159 (PDB code 2BBR). The second view is rotated by 90° around a horizontal axis. The helices are numbered according to generell DED numbering. Helix 3 of DED1 is missing. The MC159 residues aligning with the cysteines in the caspase-8 prodomain that were mutated in this study are indicated as red sticks.
B) Sequence alignment of procaspase-8 (PC8) and MC159. The positions of the α helices in MC159 are displayed above the sequence. The labeling of the helices corresponds to A). The mutated cysteines of caspase-8 are indicated with red letters. "*" defines sequence identity. ":" and "." stand for high and less sequence similarity, respectively.

parison of the prodomain caspase-8 with FLIP revealed about 25% sequence identity and 37% similarity indicating that both proteins are also likely to be structurally similar. This allows allocation of the approximate positions of Cys130 and Cys163 in the corresponding region of the FLIP structure. According to this analysis, Cys163 is buried between helices 1, 5 and 6 of DED2. Therefore, a biological relevant role of Cys163 in caspase-8 oligomerization is unlikely. In contrast, Cys130, which is located in helix 3 is probably surface exposed and therefore available for intermolecular contacts.

2.2.5 Complex formation between full-length FADD and the prodomain of caspase-8

According to the pull-down experiments described in this work, complex formation between FADD and caspase-8 prodomain is feasible. The main goal of this work is to characterize this complex structurally. Therefore, sufficient amounts of pure material are needed. Different strategies were applied to obtain the complex: i) Expression and purification of individual proteins and subsequent complex formation, ii) separate expression of proteins and co-purification of the combined proteins and iii) co-expression and purification of the complex. In the following paragraph initial experiments for all three strategies will be described.

For expression and purification of individual FADD and DED12 the constructs from the pull-down studies were used. While separate expression and purification of FADD was possible, it proved to be difficult for the caspase-8 prodomain, which precipitated during the purification procedure. It was even impossible to obtain sufficient concentrations of DED12 to screen for more optimal buffer conditions. A different strategy to stabilize DED12 during the purification process was the addition of purified GST-FADD during cell lysis. However, subsequent affinity purification did not yield detectable amounts of complex.

Besides the instability of DED12 another particular problem during the purification of DED12 was that the protein did not bind efficiently to the Ni-NTA column as observed by significant amounts of it in the flow-through (Figure 2.3 C). This suggests that accessibility of the C-terminal His-tag

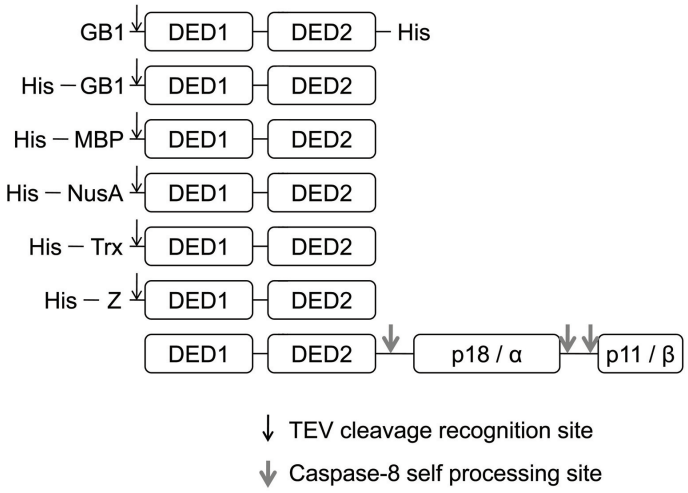

Figure 2.7: Overview of available caspase-8 prodomain constructs
Schematic drawing of different prodomain fusion constructs and full-length caspase-8. The individual fusion tags are displayed. The TEV cleavage sites are presented by small, caspase-8 self-processing sites by thick arrows. All constructs were also designed carrying either a C130S or C163S mutation.

might be restricted. To possibly enhance binding to the column as well as protein stability new DED12 constructs were designed in which the His-tag was N-terminal to the GB1 solubility tag (Figure 2.7, second construct). However, the new protein proved to be as unstable as the previous construct. The use of other solubility enhancing tags such as MBP, NusA etc. (Figure 2.7) did not improve purification or protein stability of individual DED12, either.

Fortunately, the new fusion constructs with the N-terminal His-tag harbor a different antibiotic resistance (kanamycin) than the FADD construct (ampicillin). This allows co-expression of FADD and DED12. Previously, GST-FADD and His-GB1-DED12 were individually expressed in the same cells using the same expression conditions. Therefore, the same strategy was applied for co-expression. Surprisingly, the expression level for FADD, which was very high when expressed individually, dropped dramatically when co-expressed with DED12. Although both proteins are in the soluble protein fraction after cell lysis binding to the GST affinity column seems to be inhibited (Figure 2.8 A). A significant fraction of protein was found in the

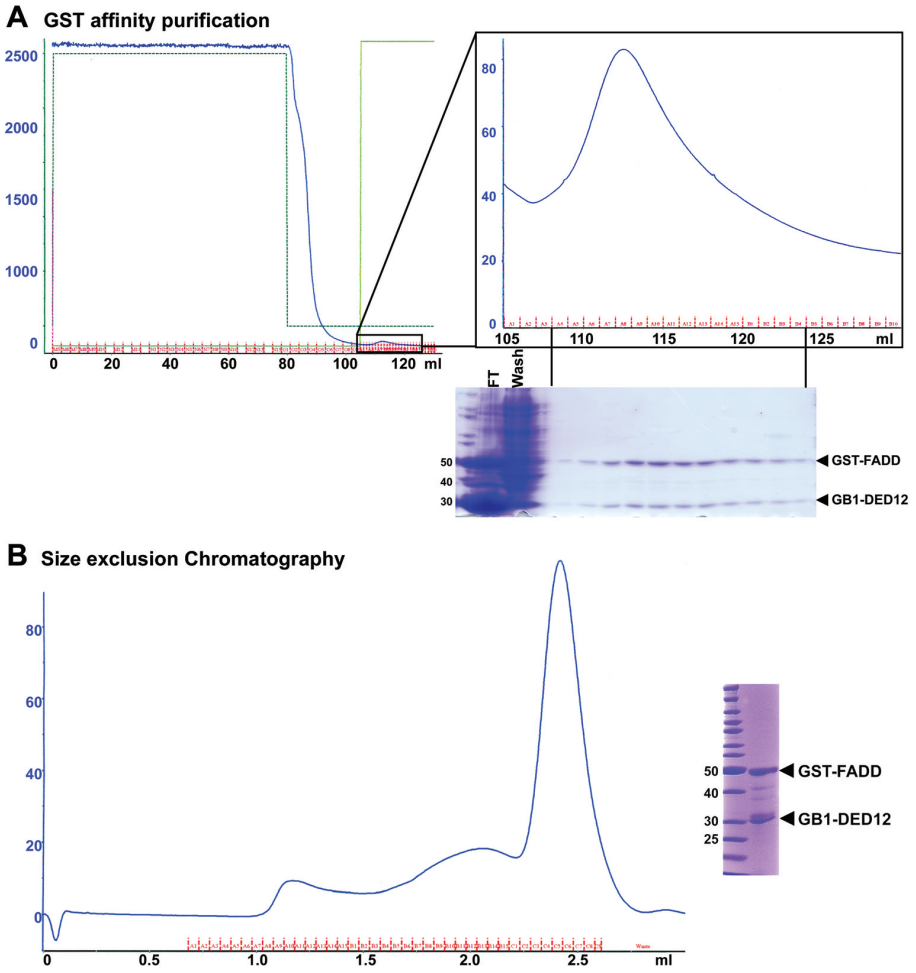

Figure 2.8: Purification of coexpressed FADD and DED12
A) Complex purification using GST Trap column. The area where the protein elutes (small box) is displayed at a larger scale on the right side. The SDS gel with the corresponding fractions (TCA precipitation) is indicated below the diagram.
B) Analytical size exclusion chromatography using an S200 superdex column. The peak fractions were submitted to TCA precipitiation and analyzed by SDS PAGE (right)

flow-through and only small amounts of protein eluted from the column. Nevertheless, the eluted peak contains FADD and DED12 in approximately 1:1 stoichiometry as judged by the intensity of the bands on an SDS gel. This material also eluted as a single peak from an analytical size exclusion column (Figure 2.8 B).

2.3 Discussion and Future Directions

Caspase-8 and -10 are activated through binding to the death inducing signaling complex DISC. This complex is formed by trimerization of Fas and subsequent FADD and caspase-8 and -10 binding. According to the available crystal structure Fas and FADD bind to each other in a 1:1 ratio [49]. Our preliminary co-expression experiments indicated also equal ratios of FADD and caspase-8. Additionally, studies by Ghisleni et al. suggested a further dimerization of caspase-8 prodomains via disulfide bridge formation resulting in additional DISC oligomerization. So far there is no information about the overall stoichiometry of the individual components in the DISC. However, it seems that this caspase activation platform is a higher oligomeric complex [49].

This work was set out to characterize a complex between FADD and its binding partner caspase-8 but also to evaluate the importance of two cysteines, Cys130 and Cys163, in the second DED of the caspase-8 prodomain. Therefore, we used an expanded set of prodomain mutants in biochemical experiments as well as *in vivo* studies. Previous experiments suggested that Cys130 is located on the protein surface whereas Cys163 is buried inside the protein [99]. This finding is supported by comparison of the procaspase-8 with the structurally characterized viral FLIP MC159. The more surprising was the finding that mutation of the buried Cys163 in single DED2 interfered with binding to full-length caspase-8 prodomain. A possible explanation is that mutation of this internal residue effects folding of the domain and thus interrupts oligomerization. In contrast, mutating Cys163 in full-length prodomain seems to be ineffective on protein folding, since this domain is able to bind FADD as effectively as wild-type prodomain. Furthermore, mutation of Cys163 in full-length caspase-8 did not effect its expression *in vivo* and this protein is able to processes caspase-3 as effectively as wild-type caspase-8. Thus this cysteine is not important for FADD interaction or intermolecular self aggregation as proposed by Ghisleni et al. who suggested a biological relevance of this cystein [99].

In contrast, Cys130 shows a different behavior than wild-type in prokaryotic as well as eukaryotic expression. In both systems the C130S mutants are

better expressed and more stable than the corresponding wild-type protein. Because Cys130 is located on the surface of the protein it might theoretically be involved in oligomerization of the prodomains. Inhibition of this oligomerization has a positive effect on caspase-8 stability and caspase-3 processing, which is contrary to the hypothesis of Ghisleni et al. [99]. Therefore, this study reveals that there is no biological relevance of the two cysteines in DISC formation and thus caspase-8 activation. Wild-type caspase-8 prodomain as well as both cysteine mutants are able to bind FADD equally well in pull-down experiments and the corresponding full-length constructs are able to process caspase-3 *in vivo*.

Preliminary studies on expression and purification of the FADD/prodomain complex indicate that it is possible to obtain this complex but so far, it was impossible to purify sufficient amounts of it for crystallization. A useful information from the eukaryotic expression studies is the slightly increased stability of the C130S mutant as compared to wild-type DED12. Since, the C130S mutation does not interfere with binding of FADD future experiments will be performed using this mutation for the DED12 constructs.

The high aggregation tendency of DED12 necessitates the use of solubility tags for expression and purification. Although proteins can in principle be crystallized in the presence of fusion tags these tags could also induce crystallization artifacts. Therefore, it is advised to remove these tags prior to crystallization. However, this most likely results in instability of the individual prodomain but might be possible after formation of the FADD/DED12 complex, assuming that FADD stabilizes DED12. Optimal conditions for these fusion proteins alone and in complex with FADD have to be determined by buffer screening (see Chapter 2.4.2).

Alternatively, a previous work by Roy et al. reported refolding of functional full-length caspase-8 from inclusion bodies [39]. Preliminary experiments using either catalytically active or inactive (C285A) full-length caspase-8 showed that it is possible to refold functional protein with this procedure (S. Engeler, unpublished results). Both variants were able to bind FADD in pull-down experiments, indicating that the prodomain was properly folded. Furthermore, the catalytically active construct was able to cleave the tetrapeptidic Ac-DEVD-AMC substrate, verifying successful refolding of the catalytic

domain. This full-length caspase-8 will provide a different strategy to obtain the FADD/DED12 complex. Full-length caspase-8 can be incubated with FADD. Afterwards, processing of the natural cleavage site between the prodomain and the catalytic domain of caspase-8 will give rise to the desired complex. An N-terminal His-tag of the prodomain can then be used for further purification of this complex.

One possibility for the poor recovery of the complex from affinity columns might be that as a complex binding of the affinity tags to the column resin is compromised. For example, individual GST-FADD binds well to the GST Trap column (Figure 2.3 A) whereas the complex is found mostly in the flow-through (Figure 2.8 A). This problem could be circumvented by cloning a longer linker between GST and FADD or removal of the GST-tag prior to complex formation. The latter strategy requires the optimization of buffer conditions for untagged FADD. A TEV based buffer screen (see Chapter 2.4.2) using high concentrations of GST-FADD might provide first ideas about more optimal buffer conditions for stable untagged FADD.

A different strategy would involve the use of only the FADD DED instead of full-length FADD for complex formation. A previous study describing the structure of a complex between the DDs of Fas and FADD states an increased stability of this complex when using only the DD of FADD instead of the full-length protein [49]. Analogous, the use of the single DED could stabilize the FADD/DED12 complex.

This section describes different strategies to obtain a a stable complex between FADD and the prodomain of caspase-8. Although the main goal is to crystallize this complex additional biochemical and biophysical experiments have to be performed to gain a better understanding of the stability and solubility properties of it. In addition, analytical ultracentrifugation or light scattering have to be used to elucidate the exact stoichiometry of the complex, and to answer questions, such as whether this complex is of higher molecular order electron micrsocopy could provide further insight. In addition, the binding affinity between FADD and the prodomain will be analyzed by Biacore experiments. A particular interesting question to answer is whether there is a difference in binding affinity of full-length caspase-8 versus only the prodomain to FADD.

2.4 Experimental procedures

2.4.1 Protein design, expression and purification

DNA sequences coding for human caspase-8 residues 1-84, 93-180 and 1-180 were cloned into the pET-20b(+) vector (Invitrogen) to yield the constructs DED1, DED2 and the full-length prodomain DED12, respectively. The vector was modified to contain an N-terminal GB1 solubility tag. Additional Cys to Ser mutations were introduced by Quikchange mutagenesis (Stratagene). Full-length prodomain constructs were further modified to contain a TEV cleavage site, which was introduced by ligation of annealed oligos containing the TEV coding sequence into a *BamH*I site directly N-terminal to the DED12 sequence. All constructs contain a C-terminal hexa-His-tag. Full-length FADD was cloned C-terminally to the GST-tag into the pGEX-6 vector (Qiagen). An additional TEV site was introduced prior to the FADD coding sequence as described above.

FADD an the prodomain constructs were either separately expressed or co-expressed in BL21(DE3) cells in LB media. Protein expression was induced with 1 mM IPTG at OD_{600} = 0.5. Caspase-8 constructs were expressed in unbaffled flasks for four hours at 37°C. FADD was produced at 18°C over night. Cells were harvested, resuspended in PBS or 20 mM Tris 8.0, 100 mM NH_4Cl, 0.5 mM TCEP for FADD and caspase-8 prodomain constructs, respectively. Cells were lyzed by French press (2 passes at 10,000 - 12,000 PSI), the soluble protein fractions clarified by centrifugation at 24,000 x g for 30 min and applied to the corresponding affinity columns, equilibrated with the corresponding lysis buffer. The caspase-8 prodomain constructs were purified by Ni-NTA. Elution was achieved by addition of 200 mM imidazole to the described lysis buffer. FADD was loaded onto a GST trap and eluted with lysis buffer containing 10 mM reduced glutathione.

2.4.2 Protein stability tests

The individual proteins and complexes were tested for their optimal buffer conditions using an incomplete factorial screen [100]. Screening was per-

formed against buffers with pH values between 4.5 and 9.0 and different salts at various concentrations. Plates were set up using a Phoenix liquid handler (Art Robbins Instruments). To screen for optimal protein stability drops were mixed containing 100 nl protein and 100 nl mother liquor. Protein stability after TEV cleavage was assayed by mixing drops of 800 nl protein and 800 nl mother liquor and addition of 100 nl TEV protease (stock concentration 2 mg/ml) to the mix. All plates were incubated at 20°C and monitored for several days. Buffer conditions were precipitation was observed were considered as not optimal.

2.4.3 Pull-down experiments and Western Blot

All pull-down experiments were performed in 100 mM sodium phosphate buffer pH 7.0, 100 mM NaCl, 1 mM PMSF, 0.5% NP40, and either 1 or 20 mM DTT. 50 μl glutathione sepharose beads (Amersham) were equilibrated with the pull-down buffer and incubated with GST-FADD for two hours at 4°C. Unbound FADD was removed by washing the beads four times with the pull-down buffer. The required FADD binding proteins were added in five-fold excess, incubated and left over protein washed out as described before. If indicated, a third component was added following the same procedure. The washed beads were resuspended in 80 μl SDS loading buffer, proteins were separated by SDS PAGE and blotted onto a PVDF membrane. The membrane was blocked with 5% milk in high-TBST (50 mM Tris pH 7.0, 500 mM NaCl, 0.2% Tween-20) for one hour at room temperature. Alkaline phosphatase conjugated $\propto$-His scFv-PhoA antibody (Qiagen) was dissolve 1:1000 in high-TBST containing 0.5% milk and incubated for one hour. Afterwards, the membrane was washed twice each with high-TBST, high-TBS (50 mM Tris pH 7.0, 500 mM NaCl) and H_20. Alkaline phosphatase activity was detected by addition of 100 μl NBT-BCIP (Fluka) in 5.7 ml 100 mM Tris pH 8.8, 10 mM NaCl, 5 mM $MgCl_2$.

2.5 Acknowledgments

The fundamental work was done by Claudia Ghisleni under supervision of Christophe Briand. The GST-SGT1 protein used in pull-down experiments was a kind gift of Michala Kramer. Eukaryotic expression and analysis of full-length caspase-8 and the corresponding cysteine mutants was performed by Gabriel Sollberger at the group of Sabine Werner at the ETH Zurich.

Chapter 3

Structural and biochemical studies on procaspase-8: New insights on initiator caspase activation

Nadine Keller[1], Jiří Mareš[2], Oliver Zerbe[2], Markus G. Grütter[1*]

[1]Institute of Biochemistry, University of Zurich, CH-8057 Zurich, Switzerland
[2]Institute of Organic Chemistry, University of Zurich, CH-8057 Zurich, Switzerland

*corresponding author

Structure (2009), Vol **17**, No. 3, pp. 438-448.

Author Contributions: Nadine Keller was involved in the design of the project and in the writing of the manuscript. She carried out all biochemical experiments, analyzed the NMR spectra and performed the structure determination and evaluation.

3.1 Abstract

Caspases are proteases with an active-site cysteine and aspartate specificity in their substrates. They are involved in apoptotic cell death and inflammation, and dysfunction of these enzymes is directly linked to a variety of diseases. Caspase-8 initiates an apoptotic pathway triggered by external stimuli. It was previously characterized in its active inhibitor bound state by crystallography. Here we present the solution structure of the monomeric unprocessed catalytic domain of the caspase-8 zymogen, procaspase-8, showing for the first time the position of the linker and flexibility of the active site forming loops. Biophysical studies of carefully designed mutants allowed disentangling dimerization and processing, and we could demonstrate lack of activity of monomeric uncleaved procaspase-8 and of a processed but dimerization-incompetent mutant. The data provide experimental support in so-far unprecedented detail, and reveal why caspase-8 (and most likely other initiator caspases) needs the dimerization platform during activation.

3.2 Introduction

Apoptosis is a highly regulated process in multicellular organisms where unwanted or diseased cells self-destruct. It plays a crucial role in all higher organisms. During embryonic development it is important in shaping the nervous system, organs and extremities [101]. Later on, various intra- or extracellular signals, such as genome damage, cytotoxic stress or environmental insults, can trigger apoptotic cell death [102,103]. Moreover, it functions in the regulation of immune response, for example, in elimination of virus-infected cells or selection of educated immune T cells [29,104]. Defects in the apoptotic machinery are closely linked to a variety of developmental and neurodegenerative diseases as well as cancer [28,30]. Because of its central role in maintaining homeostasis of cells in multicellular organisms including mammals and humans, apoptosis has been extensively studied to provide a better basis to fight diseases in which it is deregulated [105]. However, despite extensive research apoptotic signaling is not fully understood, and major questions remain unanswered, in particular concerning the nature of and the interaction between the different proteins involved in this process.
A crucial role during apoptosis is played by caspases, a class of cysteine proteases with specificity for aspartic acid in the P1 position of their substrates. A subgroup of them, called executioner caspases, is responsible for the cleavage of a variety of substrates, which ultimately result in morphological changes associated with apoptosis [106]. They are produced in the cell as inactive dimeric zymogens, and become activated by proteolytic processing of a linker, an event that is orchestrated by upstream so-called initiator or apical caspases. Processing separates each catalytic unit of the dimer into a large ($\sim$p20 or α) and a small ($\sim$p10 or β) subunit, and is subsequently followed by a rearrangement of the linker and loops in order to form the active site of the executioner caspases [107].
Although the activation mechanism of executioner caspases is well understood, the exact mechanism of activation of initiator caspases still needs to be established. In contrast to the dimeric executioners of apoptosis, the initiators are expressed as inactive monomeric zymogens. These apical caspases are activated upon binding via their N-terminal prodomains to macromolec-

ular complexes, such as the death inducing signaling complex (DISC), the apoptosome or PIDDosome [40,57,96]. By that means they are brought into close proximity and dimerize. Subsequent autoproteolytic cleavage of the zymogens results in separation of the catalytic unit in two subunits. An additional cleavage event between the prodomain and the catalytic domain allows release of the active enzyme from the activation complex. It was long debated, whether dimerization or cleavage is responsible for initiator caspase activity. Muzio et al. introduced the induced proximity model, which postulates dimerization as the sole requirement for initiator caspase activation [37]. Experiments on caspase-8, using inducible dimerization systems, revealed that caspase-8 can be activated by dimerization, independent of cleavage of the linker. This finding was later confirmed by other groups using different experimental approaches, some of which were also applied to other caspases [36,64,67,108].

Caspase-8 is involved in the extrinsic pathway of apoptosis; extrinsic, because of the origin of the apoptotic stimulus. This pathway starts with binding of an extracellular Fas ligand to the transmembrane Fas receptor. Ligand binding induces oligomerization of the receptor, which probably triggers intracellular conformational changes. This results in binding of the adaptor molecule FADD to the Fas receptor via homophilic death domain interactions. FADD further recruits procaspase-8, which binds via its N-terminal prodomain comprising two death-effector domains. This prodomain is joined via a 50-residue linker to a $\sim$270 amino acid catalytic domain, which contains two caspase-8 cleavage sites for autoproteolytic processing. Two additional cleavage sites exist within the catalytic domain, allowing it to be processed into two different subunits, termed α or p18 and β or p11.

Several structures of active cleaved caspase-8 with different inhibitors bound have been determined over the last years, and substantially improved our understanding of substrate binding and specificity [65,66,68]. In contrast, to date knowledge on the structure of the zymogen and on conformational differences between the zymogen and the active enzyme is still missing. Here we present the structure of the catalytic domain of caspase-8 in its zymogen state that, together with biochemical studies using mutants with different properties for processing and dimerization, allows a description of the activa-

tion and dimerization mechanism of caspase-8. We experimentally identified two different factors important for dimerization and showed the importance of cleavage on the stabilization of active caspase-8.

3.3 Results

3.3.1 Procaspase-8 structure determination

To investigate the activation mechanism of caspase-8, we determined the solution structure of a single-chain mutant of caspase-8 by using nuclear magnetic resonance (NMR) techniques. Therein, Cys285 within the catalytic domain was replaced by Ala in order to prevent intersubunit cleavage (the numbering follows the caspase-1 nomenclature; Cys360 in full-length caspase-8). Moreover, to facilitate the recombinant production, the prodomain was excluded in the construct that will be designated in this work as procaspase-8.

This mutant was expressed as a single-chain construct in E. coli, purified to homogeneity and characterized by biochemical methods. Analytical ultracentrifugation measurements displayed a single peak at ∼30 kDa, characterizing it as purely monomeric (Table 3.1). This view was additionally confirmed by the line widths in the [^{15}N, ^{1}H] heteronuclear single quantum coherence (HSQC) NMR spectra (Figure 3.1 A) even at concentrations as high as 1mM, and this observation is in clear contrast to the behavior of active caspase-8, which exists in a monomer-dimer equilibrium.

Backbone and side-chain assignments were completed to 80% and 82%, respectively. Triple-resonance experiments on deuterated samples were used for backbone assignments, while HCCH total correlated spectroscopy (TOCSY)-type experiments were used for assigning the side-chain resonances. A detailed description of the assignment process is provided in the Supplementary Material. Assignments in the proton-nitrogen correlation maps could not be made for the first ten N-terminal amino acids and for residues from loops 4 and 5. This is particularly surprising because no peaks without assignments remained in the [^{15}N, ^{1}H]-HSQC spectrum. From inspection of the corresponding strips in the 3D triple-resonance and ^{15}N-resolved nuclear Overhauser enhancement spectroscopy (NOESY) spectra accidental overlap of these peaks with other amide resonances can be excluded. Moreover, spectra recorded at both 500 and 900 MHz did not yield additional signals. We suspect that those signals are broadened beyond detection due to conformational exchange processes. Excluding these regions the completeness

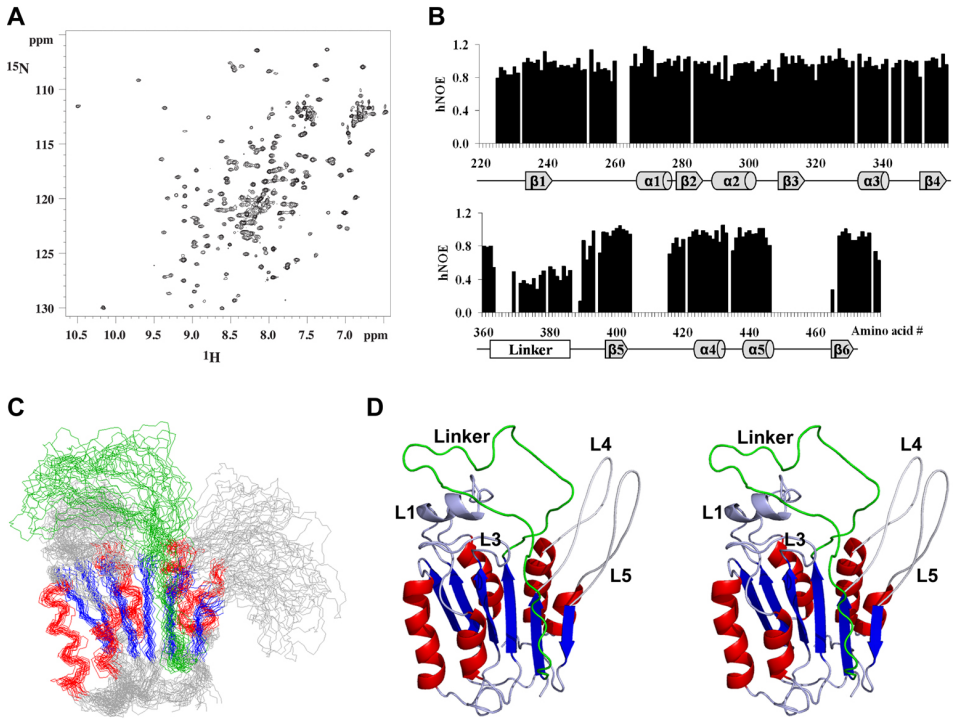

Figure 3.1: Dynamic analysis and solution structure of procaspase-8.
A) 700 MHz [^{15}N, ^{1}H]-HSQC spectrum of procaspase-8 recorded at 305K.
B) ^{15}N $\{^{1}$H$\}$-NOE of the backbone amide moieties of procaspase-8. Values between 0.7 and 1 indicate rigidity of the protein, whereas values below 0.5 imply increasing flexibility. Values below 0 indicate complete loss of structure. Blank regions are due to amides that have not been assigned.
C) Superposition of the backbone atoms of secondary structural elements of the 20 lowest-energy structures of procaspase-8 as determined by NMR. The central β sheet is colored blue; the surrounding α helices are shown in red. The linker is depicted in green. The graphic was produced using MolMol [109].
D) Stereo model of best energy structure of the 20-structure bundle. The color coding is the same as described in C. The nomenclature of the different loops as used in this publication is annotated on the structure. Loops 4 and 5 are not defined in the NMR structure and are modeled as smooth loops in the presented stereo view. The actual position of these loops is unknown. For functional stereo view use Figure of publication [110]. This graphic was prepared using PyMOL (DeLano Scientific LLC, http://www.pymol.org).

of the remaining parts of the structure was 93% and 95% for backbone and side-chain assignment, respectively.

Once the backbone assignment was completed $^{15}N\{^{1}H\}$-NOE measurements were exploited to analyze the backbone dynamics of procaspase-8 (Figure 3.1 B). Heteronuclear NOE values larger than 0.7 indicate that the backbone of procaspase-8 is stably folded. In contrast, values in the linker region decreased to between 0.4 and 0.5, characterizing this long loop as being more dynamic or flexible but still partly structured, a result that was later confirmed in the final structure.

The final structure calculation was based on 2229 NOE-derived upper distance limits, and 236 torsion angle restraints, obtained from the analysis of ^{13}C α/β chemical shifts using the program TALOS (Supplemental Data). The 20 structures with the lowest energies were selected from a total of 200 computed structures and further refined using the AMBER force field. The rmsd of the resulting ensemble of conformers is 1.6 Å, determined by fitting over the secondary structure elements (see Supplementary Table S1 for refinement statistics). The conformer with the best energy statistics will be used below to represent the NMR ensemble and to discuss the structural features of procaspase-8 in solution.

3.3.2 The structure of procaspase-8

The structure of procaspase-8 displays the characteristic caspase fold (Figure 3.1 D). Therein, a six-stranded β sheet is formed by five parallel and one anti-parallel β strand. This core unit is surrounded by five α helices, two and three of which flank the two sides of the β sheet. Protruding from these elements are four loops and the linker region. All loops extend from the same side of the protein. Loop 1 contains a short α helix, encompassing Ala245 to Lys250, which was also observed in active caspase-8. Loop 2 constitutes the 40-residue long linker that connects the two subunits of the catalytic domain and traverses across the central β sheet along one side of the protein. The loops and the linker region of procaspase-8 display increased flexibility when compared with elements of secondary structure. The less rigid character of these regions is reflected in increased values of the rmsd (4.24 Å for backbone

atoms) compared with those of regions of regular secondary structure (e.g., 1.27 Å for backbone atoms of the β sheet).
The β strands and α helices of procaspase-8 superimpose well with the corresponding regions from active caspase-8 (rmsd of 2.4 Å on average, Figure 3.2 A). Significant differences between the two structures are contained in the loops and in the linker region, which in the active enzyme form the binding pocket with the active-site Cys. In procaspase-8 loop 1 is rotated along a perpendicular axis by ∼90° compared with caspase-8 (Figure 3.2 B). In the zymogen this loop is partially located where the active site will be formed in caspase-8. In procaspase-8 the position of this loop is defined by eleven NOEs between loop 1 and 3, as well as by several contacts to the linker, that partially cover loop 1 (Figure 3.2 B, 3.3). Loop 3 is shifted slightly toward the putative binding pocket (Figure 3.2 C). Although the difference is small, the corresponding signals are significantly shifted in the active caspase-8 spectrum (see Supplemental Data for spectra). Even though the backbone cannot be traced through loops 4 and 5 in the presented structure, we conclude that the substrate-binding pocket is not present in procaspase-8. Furthermore, the linker that is cleaved during activation covers most of the putative active site region (Figure 3.2 E). Modeling of the DEVD tetrapeptide as observed in the caspase-8 X-ray structure into the corresponding region of procaspase-8 clearly indicates that binding is impossible in the zymogen conformation.

3.3.3 Location, orientation and processing of the linker

To our knowledge, the structure presented here is the first example of a procaspase in which the position of the linker is structurally defined. Although the backbone dynamics reflected in the $^{15}N\{^1H\}$-NOE reveal the linker region to be more flexible (Figure 3.1 B), its approximate conformation is determined by various NOE restrains that anchor the loop at various positions (Figure 3.3). For example, the position of the linker in the vicinity of the active site is defined by contacts formed between four linker residues (Thr373, Gln376, Tyr380, Leu381) and two residues from loop 1 (Arg248, Gln249). In addition, NOEs are observed between linker residue Y392 and three residues located in loop 3 (K320), in the third α helix (I333) and in the

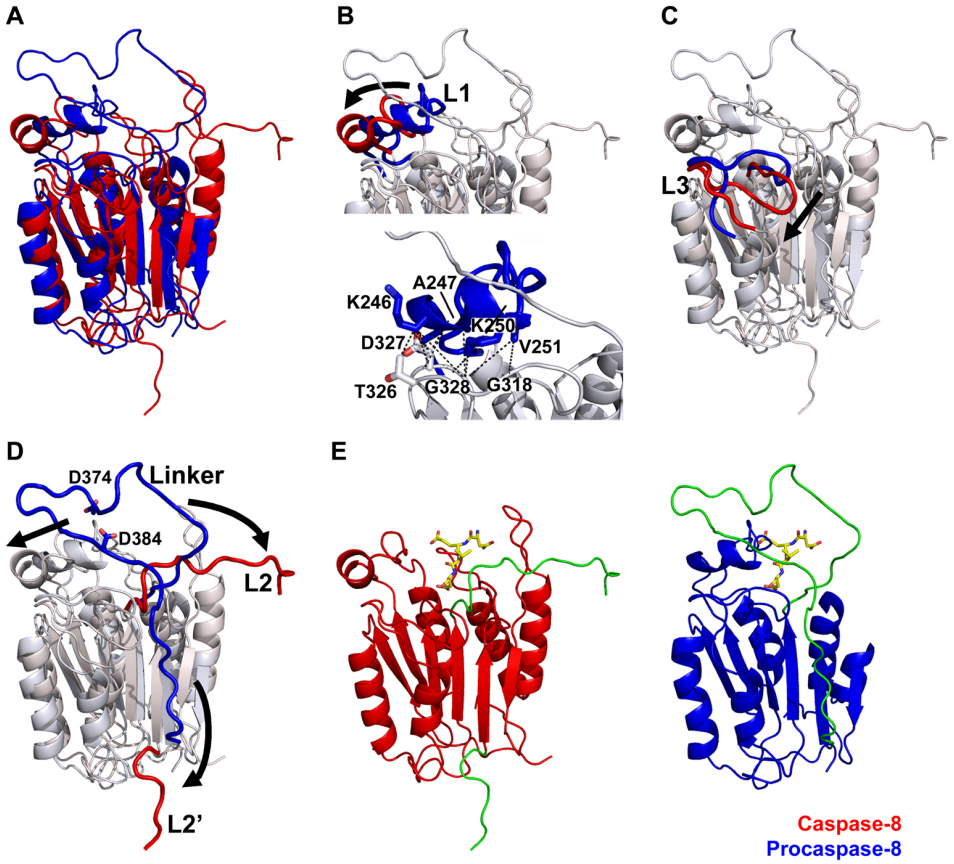

Figure 3.2: Comparison of procaspase-8 (blue) with active caspase-8 (red), respective linker rearrangements and substrate binding.
A) Superposition of the solution procaspase-8 structure with one caspase-8 monomer (1QTN). The missing loops 4 and 5 are omitted in the procaspase-8 structure.
B-D) Differences in the positions of the loops and the linker. The molecules are depicted in light colors with the regions of interest shown in bright colors. Arrows indicate the rearrangements of the loops and the linker fragments during caspase-8 activation.
B) The top panel shows the rearrangement of loop 1 from procaspase-8 to caspase-8. The lower panel shows the NOE restrains defining the position of the procaspase-8 loop 1 respective to loop 3. For simplicity protons are omitted and restrains applied to the corresponding carbons. The involved residues are presented as labeled sticks.
C) Rearrangement of loop 3 during caspase-8 activation.
D) Relocation of the linker after processing. The P1 Asp of the two cleavage sites are shown as labeled sticks. The arrows define the movement of the C-terminal part of the α subunit (L2 loop) and the N-terminal part of the β subunit (L2' loop). The central ten amino acids of the linker are removed during processing.
E) Binding of a DEVD tetrapeptide (yellow sticks) to the active site pocket of caspase-8 and modeling of the inhibitor into the corresponding region of procaspase-8. The linker is shown in green.

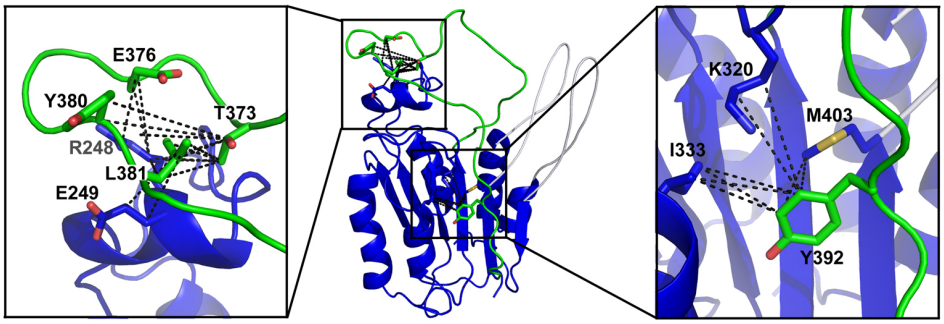

Figure 3.3: Definition of the position of the linker by NOE-derived restrains. Observed NOEs between linker residues (green) and the rest of the protein (blue) are indicted by dashed lines. For clarity the hydrogen positions are omitted and the constraints applied to the corresponding carbons.

fifth β strand (M403), thereby establishing the position of the linker relative to the core of the protein. Whereas the linker in procaspase-8 forms multiple intramolecular contacts, the cleaved fragments in the active caspase-8 dimer are dramatically shifted in position (Figure 3.2 D). The C-terminal end, which is denoted as the L2' loop, detaches from the protein core. The N-terminal fragment, termed L2 loop, extends along the top of the molecule towards the second protomer, where it is trapped into a pocket formed by the core and the L2' loop of the second monomer (Figure 3.5 B). The active-site cysteine is located at the N-terminal end of the linker close to the end of the last (3rd) β strand of the α subunit. In the published X-ray structures of caspase-8, this cysteine is easily accessible to the substrates. In the procaspase-8 NMR structure, Ala285, which replaces the active site cysteine, is buried by the linker. Movement of the linker shifts the active site cysteine by about 6 Å into a substrate-accessible position in active caspase-8.
The procaspase-8 linker contains two potential cleavage sites, VETD and LEMD. The present literature and our own data indicate that both cleavage sites can be processed intermolecularly by a proximal protease, which could either be another caspase-8 dimer or a different protease such as granzyme B [36,37,64]. Interestingly, cleavage sites might also be susceptible for intramolecular self-processing by the active site cysteine. Analysis of the ensemble of conformers derived from NMR shows a high flexibility in the linker region with some conformers adopting an arrangement of the linker with the

cleavage recognition motifs close to the region, where the active site is formed in caspase-8. Dimerization might be the trigger responsible for forming the binding pocket and shifting the linker into it. Thus, we postulate that the two cleavage sites can be processed in different fashions, intermolecular as well as intramolecular.

3.3.4 Both cleavage sites have to be processed for full activity of caspase-8

Different processing experiments have shown that both cleavage sites can be processed intermolecularly but the question remains whether cleavage at one particular site is required to allow access to the second site. Accordingly we designed single-chain active caspase-8 mutants with Ala in the P1 position of either one of the two cleavage recognition motifs (Figure 3.4). At high concentrations both mutants, D374A and D384A are processed into the individual subunits by cleavage at their intact cleavage site.

Because both sites can be processed individually, we have addressed how single processing of the linker at these unique sites influences dimerization and activity. In this study the double mutant DDAA (D374A, D384A) and wild-type caspase-8 define the initial and final states during activation from the zymogen to the active protein. Table 3.1 summarizes the data on oligomerization as derived from analytical ultracentrifugation.

Both single-point mutants are less prone to forming dimers, but the affinity for homodimerization is much more reduced in the case of D384A. At a concentration of 100 μM this mutant exists exclusively as a monomer, whereas low populations of dimers are encountered at higher concentrations. Thus, processing at both cleavage sites is necessary for forming dimers at levels comparable to those of the wild-type protein.

Structural changes in the active site of these mutants were monitored by shifts of the fluorescence maxima of a single tryptophan, Trp420, which is located in the β subunit near the S2 and S4 subsites of the active-site pocket and is able to form a hydrogen bond to the P1 Asp of the substrate [68]. Thus, structural changes close to the active site can be monitored conveniently by fluorescence spectroscopy (Table 3.1). Absorption maxima at

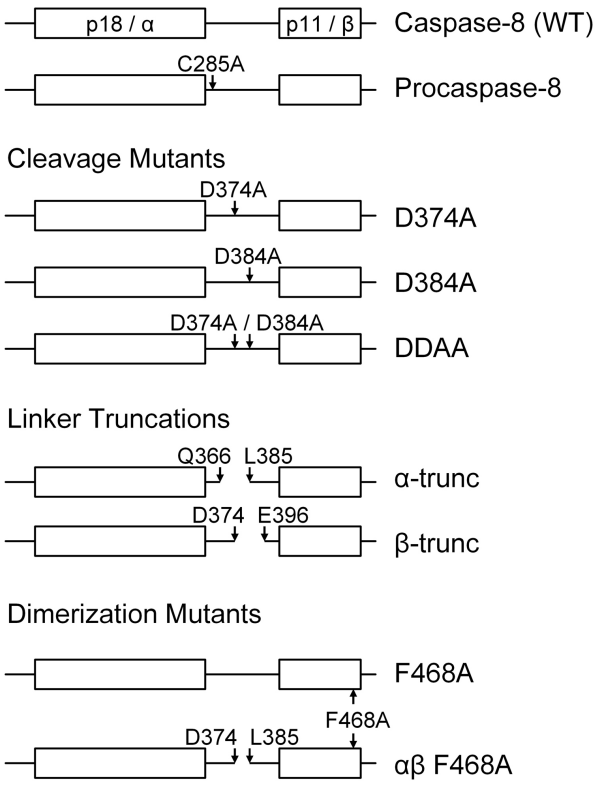

Figure 3.4: Overview of caspase-8 constructs. Shown is the catalytic domain of caspase-8. The two subunits are defined as squares. The positions of the single amino acid substitutions and truncations are indicated (full-length caspase-8 numbering; C285A in accordance with caspase-1 numbering).

350.57 nm and 353.47 nm occur for wild-type caspase-8 and the DDAA mutant, respectively, indicating a more exposed Trp environment in DDAA than in caspase-8. The absorption maxima in the single-point mutants are 351.3 nm in case of D374A, which is closer to the value of caspase-8, and at 352.3 nm for D384A, which resembles more the one of procaspase-8. These data point to a clear difference in the structural organization of the active site in procaspase-8, caspase-8 and the partially processed enzymes.

In order to characterize the relationship between dimerization, structural active-site rearrangements and activity we measured the enzymatic activity of all mutants using the artificial Ac-DEVD 7-amino-4-methylcoumarin (AMC) substrate (Table 3.1). As expected from previous studies, the double mutant DDAA is strongly impaired in activity. D374A shows only a mild

Mutant	Fluorescence λ_{max} [nm]	Activity [rfu/s] (% wild type)	Concentration [μM]	Sedimentation coefficient S_{exp}	Monomer/Dimer [%]
Procaspase-8	353.38	—	1200	2.4 ± 0.033 / —	100 / —
Caspase-8 (=WT)	350.57	11.37 ± 0.71 (100%)	100	2.7 ± 0.020 / 4.0 ± 0.030	33 / 67
			250	2.4 ± 0.022 / 3.9 ± 0.035	29 / 71
			500	2.2 ± 0.021 / 3.4 ± 0.033	21 / 79
D374A	351.38	8.80 ± 0.82 (77%)	100	2.4 ± 0.013 / 3.7 ± 0.020	48 / 52
			250	2.3 ± 0.014 / 3.8 ± 0.023	40 / 60
			500	2.4 ± 0.020 / 3.9 ± 0.032	39 / 61
D384A	351.94	7.37 ± 0.76 (65%)	100	2.8 ± 0.017 / —	100 / —
			250	2.6 ± 0.020 / 3.7 ± 0.028	58 / 42
DDAA	353.47	0.11 ± 0.01 (1%)	100	2.4 ± 0.016 / —	100 / —
			250	2.4 ± 0.019 / —	100 / —
			500	2.5 ± 0.022 / —	100 / —
			1000	2.4 ± 0.021 / —	100 / —
α-trunc	351.53	0.33 ± 0.03 (3%)	100	2.3 ± 0.035 / 3.8 ± 0.057	70 / 30
			250	2.5 ± 0.022 / 3.8 ± 0.034	48 / 51
β-trunc	349.52	12.42 ± 1.01 (109%)	100	3.0 ± 0.020 / 4.1 ± 0.029	31 / 69
			250	2.4 ± 0.020 / 3.8 ± 0.031	22 / 78
			500	2.2 ± 0.029 / 3.5 ± 0.047	18 / 82
F468A	353.38	0 (0%)	100	2.4 ± 0.022 / —	100 / —
			250	2.5 ± 0.021 / —	100 / —
			500	2.2 ± 0.029 / —	100 / —
$\alpha\beta$F468A	353.38	0 (0%)	100	2.4 ± 0.019 / —	100 / —
			250	2.5 ± 0.024 / —	100 / —
			500	2.2 ± 0.019 / —	100 / —

Table 3.1: Biochemical analyses of caspase-8 mutants

decrease in activity when compared with wild-type caspase-8, likely due to reduced dimerization propensity. Considering the highly reduced tendency for dimerization, it was surprising that D384A displays a substantial amount of activity.

3.3.5 Dimerization is important for caspase-8 activity

Activation of initiator caspases has often been explained using the induced proximity model, which proposes a direct relationship between dimerization propensity and activity [37]. Previously, it has been shown that the dimerization mutant T390D (Thr467 in our structure) is unable to induce apoptosis in HEK293 cells [108]. This mutant introduced a negative charge into the dimerization interface of caspase-8, which most likely results in repulsion between the monomers. Because the previous results allow no statements regarding the processing capability of that mutant we further elucidate the role of dimerization and processing for caspase-8 activity by characterization of a F468A mutant (Figure 3.4). Phe468 is located next to the previously mutated Thr in the terminal β strand of caspase-8. It is important to note that mutation of the Phe to Ala does not introduce repulsive effects similar

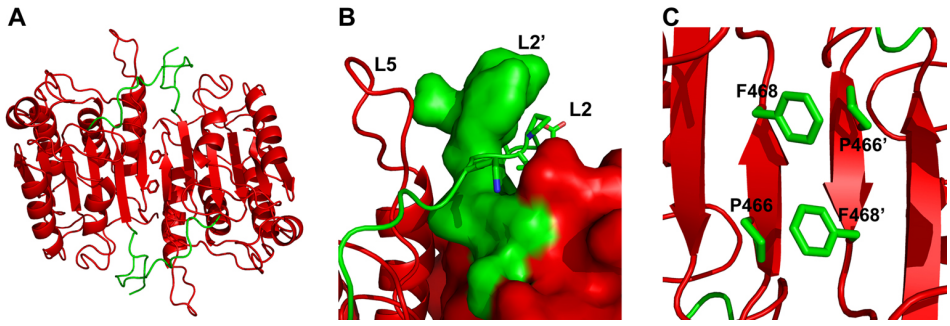

Figure 3.5: Structural features important for dimerization of caspase-8
A) Backbone trace of caspase-8. The caspase-8 dimer is shown in red and the linker in green.
B) Close-up highlighting L2 loop interactions. Caspase-8 has the same orientation as in A, with one caspase-8 protomer being shown as a cartoon and the other as a surface presentation. The L2 loop of one protomer occupies a pocket formed by the L2' loop and the core of the other protomer. L2 loop residues which are deleted in the α-trunc mutant are shown as sticks.
C) Interaction of Pro and Phe residues at the dimerization interface. The molecule is rotated by 180°compared with A, now viewing from the back side of the dimer. Side chains of Pro466 and Phe468 are shown as green sticks.

to those observed for T390D. Instead, Phe468 forms intermolecular contacts with Pro466 of the other protomer (Figure 3.5 C). Interactions of Pro and aromatic residues are known to play a pivotal role in the formation of tertiary and quaternary structures [111–113].

As anticipated, the F468A mutant of caspase-8 cannot process itself, although the active site cysteine is present. No cleavage was observed, even at a concentration of 1 mM at 305 K for several days (data not shown). This mutant exclusively exists as a monomer according to analytical ultracentrifugation. Moreover, the [^{15}N, ^{1}H]-HSQC spectrum is highly similar to the one of procaspase-8, both with respect to line widths and position of the vast majority of peaks (see Supplemental Data for more details) Furthermore, no binding of the artificial Ac-DEVD-AMC substrate was observed (Table 3.1), clearly indicating that dimerization is a precondition for caspase-8 activity and self-processing.

Although mutants at the dimerization interface were previously designed as single-chain constructs, we also introduced a F468A mutation into an individual β subunit (Figure 3.4). Upon mixing with an unmodified α subunit,

the processed enzyme was reconstituted. This $\alpha\beta$-F468A mutant can not dimerize and as the corresponding single-chain mutant it possesses no activity, indicating that cleavage alone is not sufficient for activity (Table 3.1). Surprisingly, both the single- and the two-chain F468A mutants display the same fluorescence maximum, indicating very similar active-site arrangements in both proteins (Table 3.1). Furthermore, [^{15}N, ^{1}H]-HSQC spectra of F468A and $\alpha\beta$-F468A are mostly identical (Supplemental Data). Peaks corresponding to the linker residues from the L2 and L2' loop in $\alpha\beta$-F468A have not changed their positions, whereas signals from the ten amino acids removed upon cleavage and their directly adjacent residues disappeared. Previous studies from the Salvesen group indicate that cleavage alone is not sufficient for activity [36,108]. The above results allow us to conclude that cleavage does not immediately result in the rearrangements of the L2 and L2' loops, which are necessary to form the active site. After cleavage both linker fragments remain in the zymogen conformation. In contrast to the $\alpha\beta$-F468A mutant, signals in the [^{15}N, ^{1}H]-HSQC spectra belonging to residues in the L2 and L2' loops of dimeric wild-type caspase-8 are largely shifted, indicating different positions of these loops in the dimeric cleaved protein (Supplemental Data). Thus we conclude that dimerization is necessary to induce loop rearrangements not only in uncleaved caspase-8 but also in the cleaved enzyme.

3.3.6 Caspase-8 processing is important in stabilizing the active dimer

The observation that monomeric procaspase-8 possessing an intact linker is transformed into cleaved dimeric active caspase-8 suggests that the linker might regulate dimerization in two different ways: the unprocessed linker could sterically interfere with dimerization, or the cleaved linker could stabilize the formed dimer. The linker does not directly influence dimerization because it is not positioned in the dimerization region. That result is consistent with prior research on dimeric procaspase-7 that defines that linker in a place similar to the linker in procaspase-8 [114] (Figure 3.6).
Several groups have stated that the L2 loop contributes important interac-

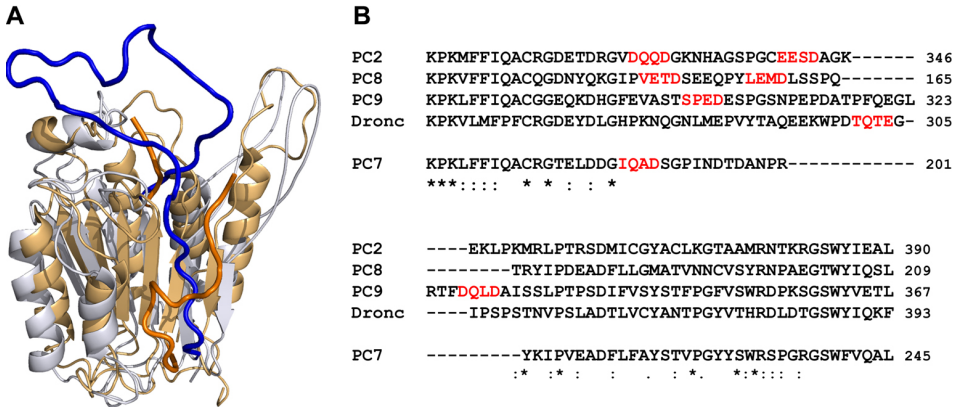

Figure 3.6: Structure and sequence comparison of procaspase-8 with other caspases
A) Superposition of procaspase-8 (blue) and procaspase-7 (brown, Protein Data Bank code: 1K88). The proteins are depicted in light colors with the linker residues indicated in bright blue and brown, respectively. The X-ray structure for procaspase-7 reveals only the termini of the linker.
B) Sequence alignment of the linker segment of different initiator procaspases and the executioner procaspase-7. The caspase cleavage recognition motifs are highlighted.

tions for stabilizing the caspase-8 dimer [108,115]. However, to our knowledge no experimental evidence for this hypothesis can be found in the literature. In order to experimentally test this hypothesis, a set of mutants was designed where the α and β subunits were truncated C and N terminally, respectively (Figure 3.4). In active dimeric caspase-8, the L2 loop is sandwiched between the L2' loop of the other protomer and its core (Figure 3.5 B). The truncations are made such that the interacting parts of the two subunits are removed. Dimerization states of these α-trunc and β-trunc mutants were analyzed by analytical ultracentrifugation. At a concentration of 100 μM the dimeric form in wild-type caspase-8 is populated to 67% whereas only 30% dimers can be detected for the C-terminally truncated a mutant (Table 3.1). This mutant is also almost completely devoid of activity. In contrast, the β-trunc mutant revealed a slight but reproducible increase in dimerization accompanied by a small increase in activity. This result was very surprising because it was believed that the L2' loop is needed to stabilize the dimer and the active site [108].

3.4 Discussion

Programmed cell death is a biological process of prime importance, and therefore has been in the focus of research for a long time [116]. It was almost a decade ago that Salvesen and coworkers introduced the induced-proximity model to explain activation of initiator caspases [37]. The concepts and mechanisms for triggering initial steps during apoptosis were clearly described in their seminal work [36,117,118], but some of the molecular and structural events underlying this mechanism await experimental verification. This work is set out to present structural and biochemical data that describe these events and allow refining of the mechanism.

Activation of procaspase-8 is achieved through dimerization with subsequent processing of the intersubunit linker [36,37,64,67]. To our knowledge, the structure of procaspase-8 described in this work for the first time reveals the position of the intersubunit linker in an initiator procaspase. The active-site mutant of procaspase-8 is monomeric and assumes the typical caspase fold. The long intersubunit linker is partially flexible but clearly located on one side of the central β sheet. High local concentrations of caspase-8 *in vivo* or *in vitro* trigger its cleavage, and the resulting species is predominantly dimeric [37,66]. Using a set of mutants, two factors particularly important for dimer stabilization are observed: i) formation of contacts involving the cleaved linker fragments, and ii) π-Pro interactions at the central dimerization interface. The combination of structural, biochemical, and biophysical data in this work support many aspects of the induced-proximity model in unprecedented experimental detail and additionally augment new aspects to refine the mechanism.

An interesting general observation is that the intersubunit linker in initiator caspases is longer compared with those found in executioner caspases (Figure 3.6 B). The presented structure of procaspase-8 reveals this linker to be highly flexible. The linker might thereby adopt different conformations, some of which are suitable for substrate binding, explaining basal activity of unprocessed initiator caspases. Dimerization most likely triggers conformational changes in the linker and the catalytic loops, allowing the active site pocket to form and become accessible for substrate binding, even without

proteolytic cleavage. This hypothesis is supported by the observation that caspase-9, which acts *in vivo* as an uncleaved dimer [55], possesses a much longer linker that upon dimerization might allow rearrangement of the unprocessed linker and result in formation of the active site. This implies that the longer linker of the initiator caspases might be important for their basal activity.

The induced proximity model proposes that dimerization is the trigger for initiator caspase activity but not cleavage (reviewed in [115,119,120]). This view is strongly supported by our data on the F468A mutants. Single-chain F468A is monomeric and structurally highly similar to procaspase-8 but cannot process itself. The cleaved form is again structurally similar to procaspase-8, and therefore it is evident that dimerization but not cleavage is the event responsible for the structural changes.

Proximity-induced dimerization of procaspase-8 at the activation platform DISC is necessary to induce cleavage of the linker, which subsequently results in increased affinity for dimerization even when caspase-8 is released from the DISC [108]. The L2 loop of the cleaved linker extends over the other protomer as shown in several X-ray structures [65,66,68]. This interaction stabilizes the dimer by formation of several hydrogen bonds to the other protomer, and the resulting structural changes additionally allow formation of the active site. Without this stabilizing effect caspase-8 activity is reduced to almost the zymogen level. Surprisingly, regardless of the multiple interactions between the L2' and the L2 loops, the L2' loop seems to not contribute significantly to dimer stability. Truncation of the L2' loop results in only a modest effect on dimerization propensity and activity. This observation suggests that interactions of the L2 loop with proximate residues of the β subunit of the second protomer are sufficient to keep L2 in place. In contrast, L2 to L2' interactions, even though they might be comparably strong, do not seem to critically contribute to dimer stability. Considering that L2' is not located in vicinity of the active site, alterations in its position or length are not expected to influence activity, compatible with the results of this study.

Interestingly, not only truncation of the L2 but also elongation of the L2 and L2' loops has an effect on dimerization. We could clearly demonstrate

that processing of both cleavage sites is important to achieve full caspase-8 activity. Elongation of either one of the linker fragments by an additional ten residues significantly affects dimerization and catalytic activity. An optimal length of the linker fragments after autoproteolytic processing seems to be crucial for optimal caspase activity. Analysis of different mammalian caspase sequences revealed that, in contrast to executioner caspases, they all contain two cleavage sites in their intersubunit linkers (Figure 3.6 B). Thus, one could speculate that nature developed a mechanism to process the longer linker of initiator caspases into fragments with an optimal length for dimer stabilization and active-site rearrangement.

The crystal structure of the caspase-8 dimer and our linker truncation experiments revealed stabilizing interactions of residues from the processed linker [65,66]. Although these interactions most likely make a significant contribution to dimer stability, they are obviously insufficient to induce dimerization at the low concentrations *in vivo*. The κ_D for homodimerization of the caspase-8 catalytic domains was proposed to be in the low micromolar range, well above its nanomolar *in vivo* concentration [67,108]. Instead, binding of their prodomains to the activation complex increases their apparent concentration and thereby enforces dimerization. Subsequently, depending on the specific type of caspase, the dimers are stabilized differently. Caspase-9, for example, remains attached to the apoptosome during its course of action [121]. In contrast, caspase-2 forms a stable disulfide bridge in the dimerization interface [122]. In the case of caspase-8 the dimer is stabilized twofold: by translocation of the cleaved linker followed by formation of stabilizing intersubunit contacts, and through interactions at the dimerization interface. The structure of the caspase-8 dimer reveals close proximity of Phe468 to Pro466 of the other protomer. Interactions between Pro residues and π-systems are strongly stabilizing in nature [111–113]. Replacement of Phe468 by Ala completely abolishes affinity for dimerization, and makes the mutant cleavage-incompetent. Because the overall fold is not affected by the Phe to Ala mutation, it indicates that an interaction directly required for dimerization has been removed.

Each of the analyzed mutants – the cleavage site mutants, the linker truncation mutant α-trunc, and the dimerization mutants F468A (Figure 3.4) –

reveal a significant impact on the affinity for dimerization accompanied by changes in catalytic activity. This strongly suggests that a combination of both, dimerization affinity and proper cleavage is necessary to achieve full caspase-8 activity. The two dimer-stabilizing effects analyzed in this article provide an explanation for the stability of caspase-8 dimers even after release from the DISC. Our structural and mutational studies prove that dimerization is indispensable for formation of the active site and thus for catalytic activity. This finding fully supports the proximity-induced dimerization model. In addition, our data demand a refinement of this model: it has to take into account that cleavage is necessary to retain dimerization after the enzyme is released from the activation complex, and is thus closely linked to the activation process of initiator caspases.

3.5 Experimental Procedures

3.5.1 Protein design, expression and purification

For single-chain constructs the DNA sequence coding for human caspase-8 amino acids 217-479 was cloned into pQE50 (Qiagen). The plasmid was transformed into M15 (pREP4) cells (Qiagen) and the protein expressed in LB medium at 37°C overnight. Two-chain constructs encompassed amino acids 217-374 for the α subunit and 385-479 for the β subunit. The fragments were cloned into pET-11d(+) (Invitrogen) and expressed in BL21(DE3) cells as described above. Amino acid substitutions were generated by Quikchange (Stratagene) mutagenesis. Linker truncations were prepared by insertion of a preliminary stop codon in the α subunit or deletion Quikchange mutagenesis on the β subunit.

Purification protocols were adapted from published procedures [66,123]. Cells were harvested, resuspended in phosphate-buffered saline (PBS) and lyzed by french press. The soluble protein fraction was removed by centrifugation, inclusion bodies washed in 20 mM Tris pH 8.0, 1 mM ethylenediaminetetraacetic acid (EDTA), 0.1% LDAO and solubilized in 6.5 mM GdHCl, 20 mM Tris pH 8.0, 2 mM EDTA, 100 mM dithiothreitol (DTT).

Refolding of two-chain constructs was achieved by dilution of equimolar amounts of the solubilized subunits into 100 mM HEPES pH 7.5, 10% sucrose, 0.1% CHAPS, 10 mM DTT. After incubation over night at RT the precipitate was removed by centrifugation. The soluble fraction was concentrated, dialyzed against 20 mM HEPES pH 7.5, 10% sucrose, 10 mM DTT and applied to a ResourceQ anion exchange column (Amersham). Elution was done with a NaCl gradient and protein fractions were applied to a Superdex 200 (Amersham) using 20 mM Tris, pH 8.0, 100 mM NaCl, 10 mM DTT.

The solubilized inclusion bodies of the single-chain constructs were added to an equal volume of acetic acid and the sample dialyzed against 50% acetic acid. Afterwards the solution was suspended rapidly in nine volumes H2O and immediately diluted in nine-fold excess of 1 M Tris pH 8.0, 5 mM DTT. Refolding was performed over night at RT and aggregates removed by centrifugation. During the subsequent concentration step autocatalytic pro-

cessing took place for those mutants that are able to form a proper active site. Final purification was achieved by size exclusion chromatography as described above.
Isotope labeling for NMR experiments was done by expression in M9 minimal media supplemented with $^{15}NHCl_4$ and ^{13}C-glucose as the sole nitrogen and carbon source. Deuteration was obtained by substitution of H2O with D2O. Purification was performed as described above and the final NMR sample rebuffered into 20 mM deuterated Tris pH 8.0, 100 mM KCl, 10 mM DTT. The $\alpha\beta$-F468A mutant was generated by addition of catalytic amounts of unlabeled active caspase-8 to labeled single-chain F468A and subsequent size exclusion chromatography.

3.5.2 Assignment and structure calculation

All NMR experiments were recorded at 305 K on a Bruker Avance 600 or 700 MHz spectrometer. For backbone assignment an approximately 79% deuterated, uniformly ^{13}C, ^{15}N-labelled sample was used. HNCACB / HN(CO)CACB spectra [124] and HN(COCACB)CG / HN(CACB)CG spectra [125] were used to link sequential amide moieties via matching pairs of Cα/Cβ and Cγ resonances. In addition, assignment was conducted via matching carbonyl frequencies derived from the HNCO / HN(CA)CO experiments [126]. Sequential amide protons were linked in the HN(CACO)NH experiment [127]. A proton-detected version of the steady-state $^{15}N\{^1H\}$ heteronuclear Overhauser effect sequence was used for measurement of the heteronuclear NOE [128].
Side chain assignments were performed using HCCH-type experiments, starting from assigned Cα, Cβ and Cγ pairs [129,130] whose carbon chemical shifts were corrected for the deuterium isotope shifts [131]. The aromatic spin system were linked to the aliphatic side chains using data from CB(CGCD)HD / CB(CGCDCE)HE spectra [132]. Proton frequencies within the aromatic spin systems were assigned using a ct-HMQC-TOCSY experiment [133].
Backbone and side chain assignment was accomplished in the software CARA [134]. Thereafter, ATNOS [135] was used to automatically pick and integrate

^{15}N- and ^{13}C-resolved NOESY spectra. In addition to NOE-derived upper-distance bounds, chemical shift information was used to derive torsion-angle restraints in the program TALOS [136]. After the first structure calculations, peak lists were further modified using the program XEASY [137] and assignment of NOESY crosspeaks was continued using the AUTOASSIGN module of CYANA [138,139]. To improve convergence during the early stages of the assignment/structure calculation process the preliminary structure after the first cycle was replaced by template coordinates derived from caspase-8 (excluding the loops and the linker). So far unassigned fragments were defined as proxy residues [140] and CYANA was used to define the proximate positions of these residues in the structure. The resulting coordinates for the procaspase-8 structure were energy-minimized in explicit water using the AMBER force-field [141,142].

3.5.3 Protein characterization

The final masses of all purified constructs and cleavage products were confirmed by ESI MS. Protein concentration was determined by UV and Bradford assay (Pierce).

Analytical ultracentrifugation was performed with an Optima XL-1 centrifuge (Beckman Coulter) and a TI50 rotor using epoxy centerpieces (12 mm) with sapphire windows. Samples were run at 20°C and 42000 rpm. Absorption was measured between 280 and 305 nm, depending on protein concentration. Results were analyzed using Sedfit [143].

Tryptophan fluorescence emissions spectra were recorded on a Fluorolog4 (Jobin Ivon) with a Peltier Temperature controller set to 20°C. 2 μM samples were excited at a wavelength of 290 nm. Five consecutively measured spectra were collected between 310 and 400 nm and averaged. The slit widths for excitation and emission were 10 nm and 5 nm, respectively.

Activity measurements were performed in black 96-well Nunclon microtiter plates on a GENios platereader (Tecan) using the Magellan6 software. The final sample volume of 100 μl contained 100 nM enzyme in assay buffer (20 mM PIPES pH 7.2, 1 mM EDTA, 100 mM NaCl, 0.1% CHAPS, 10% sucrose). The reaction was started with addition of Ac-DEVD-AMC substrate

at a final concentration of 100 μM and AMC release was monitored by fluorescence emission at 465 nm after excitation at 360 nm. Measurements were performed in triplicates and the standard deviation was calculated.

3.6 Accession numbers

Coordinates, chemical shifts and restraints have been deposited in the PDB and BMRB database under accession codes 2K7Z and 15932, respectively.

3.7 Acknowledgments

This work was supported financially by the Swiss National Science Foundation (grant 31-1022181 to M.G. Grütter) and a specific targeted research project funded by the European Commission (CAMP Project LSHG-2006-018830). We thank Alexey Neumoin for support with the NMR software. Nadine Keller is a member of the PhD program in Molecular Life Science, Zurich.

3.8 Supplementary material

3.8.1 Assignment and structure calculation

Backbone resonances of procaspase-8 were assigned using a triply labeled ^{2}H, ^{13}C, ^{15}N-labeled sample. Purification of the protein in aqueous solution and a refolding step in the procedure assured a quantitative back exchange of the backbone amide moieties. Backbone assignment was heavily based on sequential and intraresidual HN, Cα and Cβ correlations derived from constant-time HNCACB and HN(CO)CACB [124] experiments. As noticed by others the high-resolution from these experiments and the sign information of the peaks that additionally reports on the number of adjacent carbon atoms was crucial for identification of residue type and sequential assignment. Nevertheless, additional HNCG and HN(CO)CG [125] experiments to assign the gamma carbons were required to resolve ambiguities, and in addition proved to be very helpful for side chain assignment purposes. Furthermore HNCA(CO)NH [127] and HNCO as well as HNCACO [126] spectra were used to link sequential HN and Cα via carbonyl moieties, respectively. Only the combination of these experiments allowed unambiguous sequential assignment of the backbone, which was confirmed by connectivities from the 3D ^{15}N NOESY. A comparison of the proton-nitrogen correlation map with a ^{15}N-TROSY spectrum of deuterated active (wild-type) caspase-8 displayed much similarity, with many peaks located at identical chemical shifts (Fig. 3.7). Nevertheless, a number of peaks disappeared, and many new peaks appeared. Transfer of the assignments from procaspase-8 revealed that the peaks due to loop residues were mostly shifted and those from the linker region were either completely missing or strongly shifted in the caspase-8 spectra. In contrast, the position of many of the other peaks remained basically unchanged indicating that the two structures comprise the same overall fold, with major differences restricted to the loops, the linker region and dimerization interface. This finding was confirmed in the final procaspase-8 structure. Deuteration of the sample used for sequential assignment leads to a deviation of the carbon chemical shifts depending on the number of protons attached to them as well as the neighboring carbons. In order to proceed with side chain assignment using the Cα, Cβ and Cγ already obtained from

the experiments described above the carbon chemical shifts had to be corrected according to Venters, et.al. [131]. The corrected shifts were used in combination with constant-time-[^{13}C,^{1}H]-HSQC, HCcH-TOCSY and hCCH-TOCSY experiments to assign aliphatic side chains [129,130,144]. Edited constant-time-^{13}C-HSQC spectra were used to identify aromatic carbons and carbonyls. The adjacent protons were assigned by ^{13}C-NOESY experiments. Aromatic side chains were assigned by the combination of the HCCH-type, ct-HMQC-TOCSY [133] and ^{13}C-NOESY spectra and linked to the corresponding aliphatic side chains using CB(CGCD)HD and CB(CGCDCE)HE spectra [132]. After complete assignment the structure determination was continued as described in Materials and Methods. Since the proton nitrogen correlated experiments described above suggest a similar secondary structure fold for procaspase-8 as observed for caspase-8 we substituted the PDB file computed in the first cycle of the CYANA calculation with a template PDB from caspase-8 (one monomer of 1QTN). Since the loops and the linker were expected to be different, they were excluded in the template PDB. An additional structure calculation using the final set of upper-distance restraints confirmed that the template structure did not bias the final outcome of the calculation, and that the NMR conformer ensemble reflects the conformational space solely sampled by experimental restraints. During the side chain assignment process we obtained assignment for side chains and side chain fragments, which were not sequentially assigned so far, mainly due to missing signals in the proton nitrogen correlation experiments described above. Furthermore, several glutamine residues showed shift ambiguities, which did not allow a precise sequential assignment. To identify the sequential and structural position of these residues they were defined as Proxy residues [140]. The work of Ab, et al. presented a proxy library containing shifts of amino acid fragments as well as some complete amino acids. We expanded this library to include proxies for all 20 amino acids. The structure calculation by CYANA suggested the positions of the defined proxy residues based mainly on NOE restrains. The correct position was manually verified and gave rise to assignments of nine additional residues.

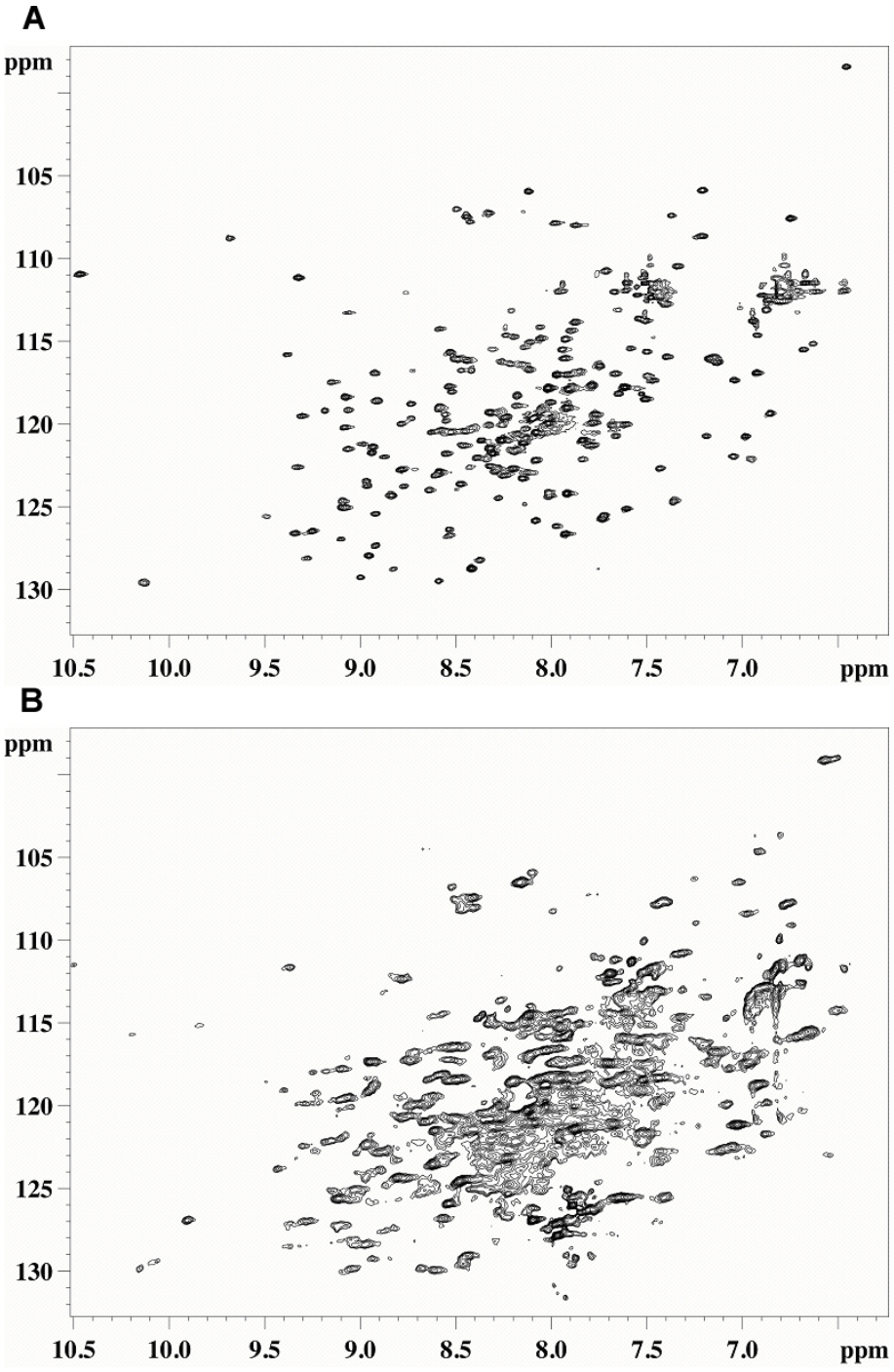

Figure 3.7: [^{15}N, ^{1}H]-HSQC spectra of
A) inactive monomeric procaspase-8 (of which the structure was determined in this paper)
B) active dimeric caspase-8 (TROSY spectrum at 700 MHz)

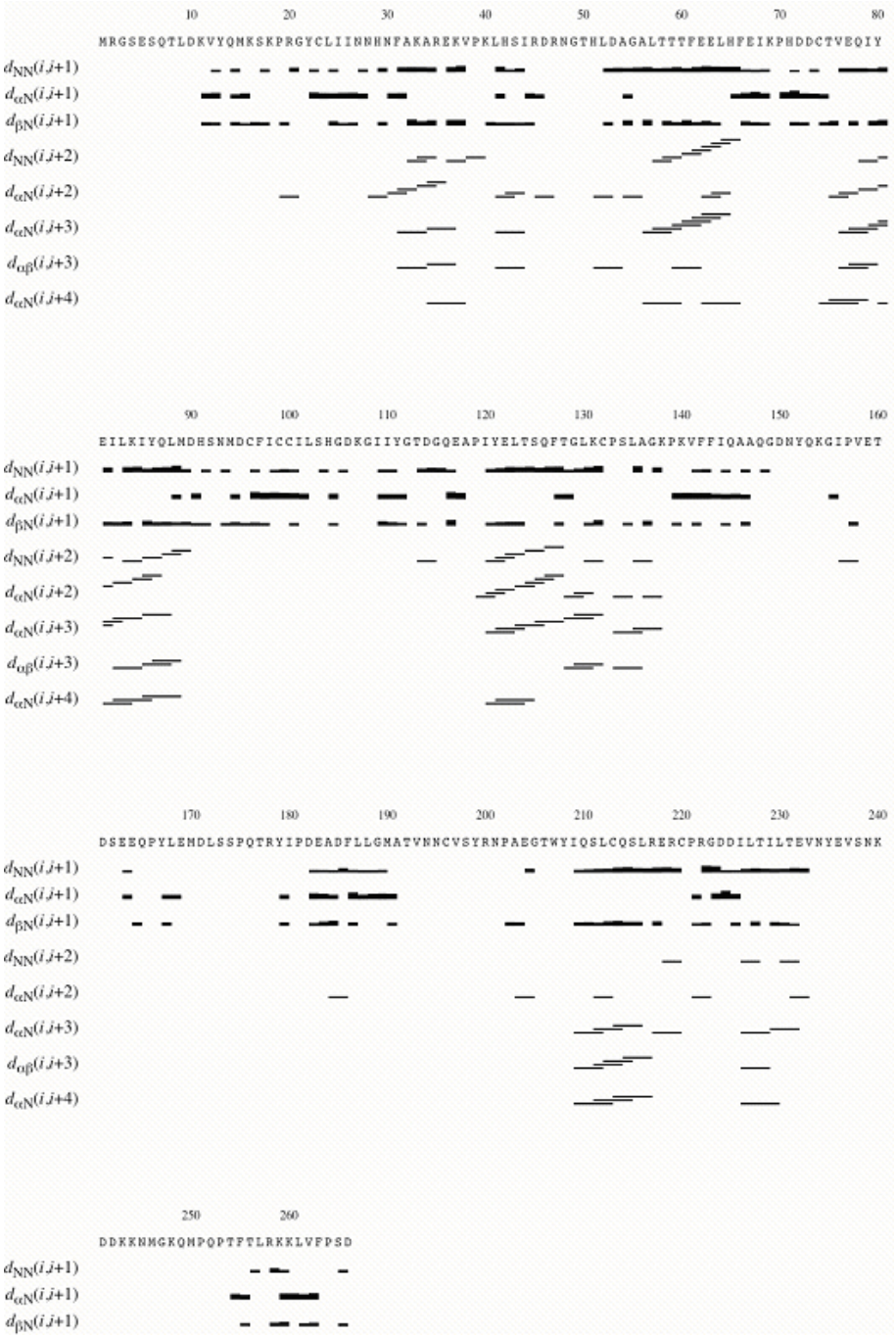

Figure 3.8: Restraints used in the Structure Calculation

NMR distance restraints:	
Total NOE	2229 (100.0 %)
Intraresidual, $\|i-j\|$=0	629 (28.2 %)
Sequential, $\|i-j\|$=1	710 (31.9 %)
Short-range, $\|i-j\|$=1	1339 (60.1 %)
Medium-range, 1<$\|i-j\|$<5	429 (19.2 %)
Long-range, $\|i-j\|$=5	461 (20.7 %)
Restrained α helical hydrogen bonds per monomer	none
Maximal distance restraint violation	0.23 Å
AMBER energies:	
Total (mean and s.d. of 20 conformers)	-4363 ± 185 Kcal/mol
van der Waals	-683 ± 40 Kcal/mol
RMS deviations from idealized geometry:	
Bond lengths	0.013 Å
Bond angles	1.7°
Ramachandran plot statistics:	
Residues in most favored regions	73.3 %
Residues in additionally allowed regions	25.4 %
Residues in generously allowed regions	0.9 %
Residues in disallowed regions	0.4 %
RMS deviations from the mean coordinates for bb (heavy) atoms	
N, C^{α}, C' of residues from β strands[a]	1.27 ± 0.23 (2.04 ± 0.25) Å
N, C^{α}, C' of residues from β strands and α helices[b]	1.64 ± 0.29 (2.34 ± 0.32) Å
N, C^{α}, C' of all residues exluding missing regions[c]	4.24 ± 0.85 (5.05 ± 0.81) Å

[a] backbone atoms of the β strands (residues 235-240, 311-314, 353-356, 399-401, 466-469, 280-285) were used for the superposition.
[b] backbone atoms of the β strands (residues 235-240, 311-314, 353-356, 399-401, 466-469, 280-285) and α helices (residues 267-276, 289-302, 333-337, 422-432, 439-446) were used for the superposition.
[c] Loop 4 (405-414) and loop 5 (447-463) are not defined and excluded from the analysis.

Table 3.2: Structural statistics

3.8.2 Comparison of single-chain and two-chain F468A

The [^{15}N, ^{1}H]-HSQC spectra of F468A is highly similar to unprocessed procaspase-8. The vast majority of peaks are identical. Differences between the F468A mutant and the procaspase-8 C285A mutant (C360A according to numbering used in this work) are encountered in the region around the active site residue 360 (compare Fig. 3.7A and 3.9A). Peak positions of procaspase-8 do not match for peaks corresponding to residues Ala359 to Gln362. The peak belonging to Gln358 is slightly shifted and decreased in intensity indicating that it is mildly affected by the C285A mutation. In ad-

dition to single-chain F468A we measured the spectrum of cleaved F468A. The protein was generated by processing of labeled single-chain F468A using catalytic amounts of unlabelled active caspase-8. During purification the protein was refolded into its zymogen conformation and afterwards processed, mimicking the natural activation process of caspase-8. The spectrum for two-chain F468A is again highly similar to the ones obtained for procaspase-8 and single-chain F468A. Figures 3.10A to C expand a region of the [^{15}N, ^{1}H]-HSQC spectra of procaspase-8 and single as well as two-chain F468A with the peaks for the linker residues annotated at positions observed in procaspase-8. Assignments belonging to non-linker residues are omitted for clarity. From these data we conclude that peaks belonging to the linker residues not excised during processing do not significantly change their positions, whereas peaks corresponding to the central ten amino acids disappear. This strongly suggests that in the absence of dimerization residues from the L2 and L2' loop do not change their conformation significantly upon cleavage.

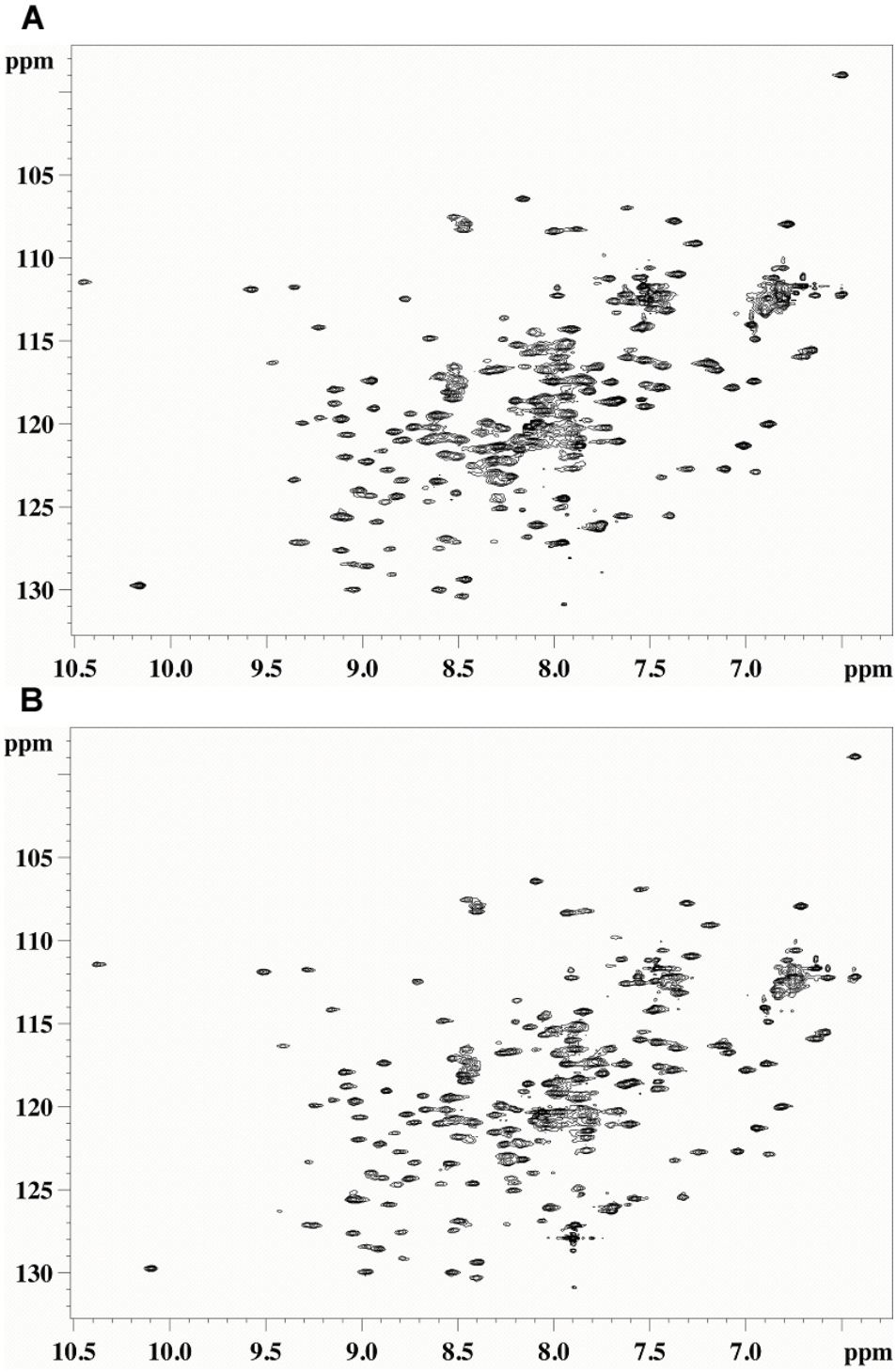

Figure 3.9: [^{15}N, ^{1}H]-HSQC spectra of
A) Unprocessed F468A
B) Proteolytically cleaved $\alpha\beta$-F468A

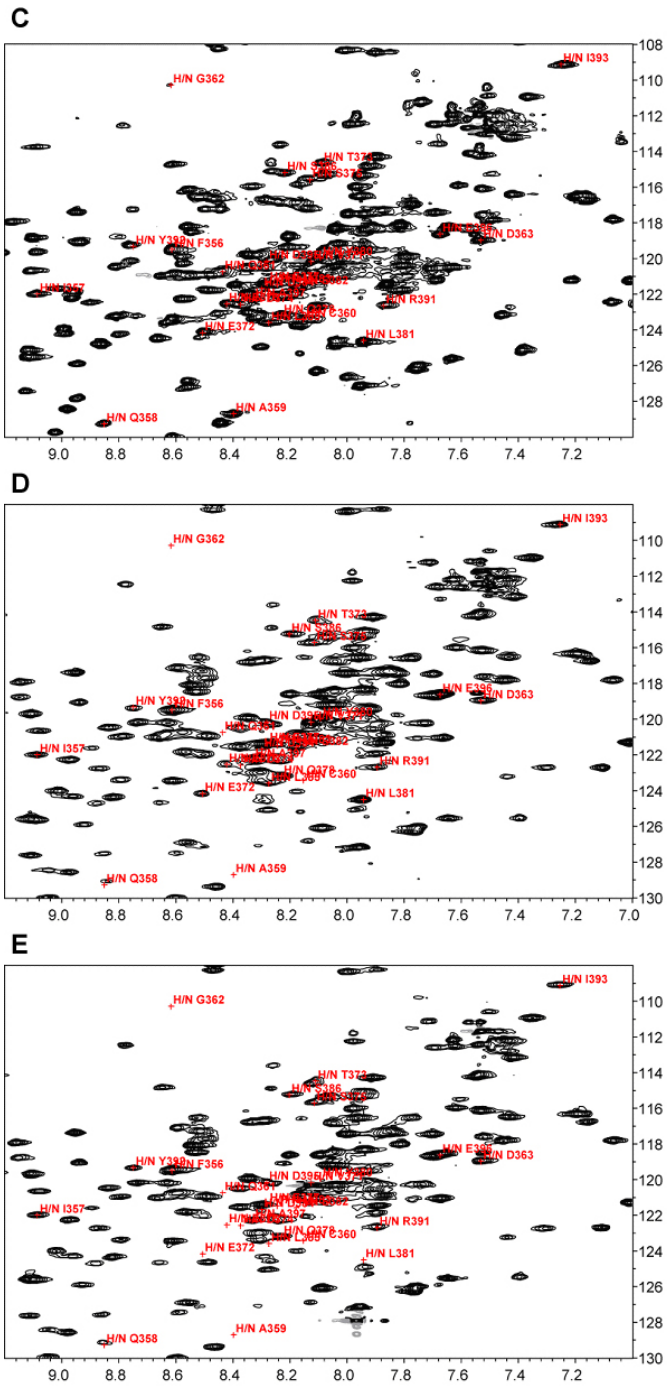

Figure 3.10: Expansion of the [^{15}N, ^{1}H]-HSQC spectrum of
A) PC8 from Figure S1A
B) F468A (spectrum 3.9A)
C) $\alpha\beta$-F468A (spectrum 3.9B)

Chapter 4

Studies of the Molecular Mechanism of Caspase-8 Activation by Solution NMR

Nadine Keller[1], Markus G. Grütter[1], Oliver Zerbe[2*]

[1]Institute of Biochemistry, University of Zurich, CH-8057 Zurich, Switzerland
[2]Institute of Organic Chemistry, University of Zurich, CH-8057 Zurich, Switzerland

*corresponding author

Submitted manuscript

Author Contributions: Nadine Keller was involved in the design of the project and in the writing of the manuscript. She carried out all biochemical experiments and analyzed the NMR spectra.

4.1 Abstract

Caspases are the key players of apoptosis and inflammation. They are present in the cells as latent precursors, procaspases, and are activated upon an apoptotic or inflammatory stimulus. The activation mechanism of caspases has been extensively studied by biochemical and biophysical methods. Additional structural information on active caspases with a variety of different inhibitors bound in the active site is available. In this study we investigated the cleavage mechanism of caspase-8 from its zymogen to active caspase-8 via solution NMR and by biochemical methods. The intermolecular cleavage reaction using the catalytically inactive C285A procaspase-8 mutant is triggered by adding caspase-8 and followed by ^{15}N, ^{1}H-NMR spectroscopy. The spectrum that initially resembles the one of procaspase-8 gradually over time changes to the one of caspase-8, and disappearing peaks display exponential decaying intensities. Removal of either one of the cleavage recognition motifs in the linker or phosphorylation at Tyr380 is shown to reduce the rate of the cleavage reaction. The data suggest that dimerization repositions the linker to become suitable for intermolecular processing by the associated protomer. Furthermore, analysis of inhibitor binding to the active caspase-8 reveals an induced fit mechanism for substrate binding.

4.2 Introduction

Caspases are cysteine-dependent enzymes with specificity for aspartic acid in the cleavage recognition motif of their substrates and are involved in apoptosis and inflammation [106,145–147]. In apoptosis, initiator caspases are the most apical enzymes, which receive the apoptotic signal and activate downstream executioner caspases. Initially, caspases are produced in the cells as inactive zymogens, the procaspases [105,106,145,146]. Inflammatory and apoptotic initiator procaspases are monomeric and contain an N-terminal prodomain that facilitates their recruitment to macromolecular activation platforms such as the death inducing signaling complex (DISC) [39,96], the apoptosome [40,50], the PIDDosome [43,57] or the inflammasome [41]. Through binding to these complexes their apparent concentration is increased and dimerization is induced. Dimerization then triggers activation of the initiator caspases as proposed by the induced proximity model [37,108]. While forced into mutual proximity at the activation complexes, autoproteolytic cleavage of the intersubunit linker occurs. A second cleavage event between the prodomain and the catalytic domain releases the active caspase from the activation complex [64]. For executioner caspases cleavage of the intersubunit linker constitutes the major event for activation while for initiator caspases it is dimerization [148].

Fundamental insight into the mechanism of caspase activation has been derived from crystal structures, with most of the structures of active caspases determined in the presence of inhibitors [149]. Additional crystal structures of inflammatory caspase-1 and executioner caspase-7 in the absence of inhibitors report on structural changes upon inhibitor binding, suggesting an induced fit mechanism of substrate binding [114,150]. Furthermore, a few zymogen structures are available, e.g. for *Drosophila melanogaster* Dronc [151], for executioner procaspase-7 [114], for inflammatory procaspase-1 [152], and for procaspase-8 [110]. The latter was solved by solution NMR and for the first time revealed the position of the intersubunit linker in a monomeric zymogen.

Caspase-8 is one of the best-studied initiator caspases. The recently determined solution structure of procaspase-8 and the available crystal structures

of caspase-8 in the presence of various inhibitors provide important information to decipher the activation mechanism of caspase-8. Additional mutational studies dissected the interplay between dimerization and proteolytic cleavage [36,37,63,64,67,108,110]. Although dimerization is required and by itself sufficient for caspase-8 activity, cleavage of the intersubunit linker at two different recognition motifs is important for dimer stabilization and thus is essential for caspase-8 activity [110]. While the importance of dimerization and cleavage is established experiments that describe the transition from the inactive zymogen to the activated and to the inhibitor-bound caspase-8, are not available presently. Attempts to describe the structure of caspase-8 in the absence of an inhibitor failed so far. In this work we interrogate the activation mechanism from monomeric, unprocessed zymogen to processed, dimeric caspase in the absence of inhibitors using solution NMR as the primary tool. We follow the cleavage reaction in the NMR tube by monitoring procaspase-8 processing using ^{15}N, ^{1}H correlation NMR spectroscopy. In addition, we determine to which extent the efficiency of caspase-8 processing is influenced by the dimerization propensity, by phosphorylation at Tyr380 and by limited proteolysis of the intersubunit linker. Finally, NMR data are used to evaluate how the structure of the free caspase-8 differs from the inhibitor-bound form.

4.3 Results

4.3.1 Processing of procaspase-8 into active caspase-8

To characterize the events leading to activation of caspase-8 on a molecular level we followed the cleavage process from procaspase-8 to active caspase-8 by NMR. ^{15}N-labelled procaspase was mixed with catalytic amounts (1:10000) of unlabelled caspase-8. Processing of procaspase-8 by caspase-8 was monitored by recording [^{15}N, ^{1}H]-TROSY spectra. Since only procaspase-8 is labeled, initially the spectrum resembled the one of procaspase-8, for which an assignment was obtained previously [110] and gradually over time changed into the spectrum corresponding to caspase-8. At the beginning of the experiment the narrower lines of procaspase-8 allowed recording spectra in 1 hour intervals. During biochemical processing a decrease of the signal intensity in the spectra occurred for most resonances reflecting the formation of dimeric caspase-8 accompanied by slight precipitation. Significant line-broadening is observed for the methyl resonances (Figure 4.1B) correlating well with increased processing as independently monitored by SDS PAGE (Figure 4.1A).

While most of the peaks remained unchanged a significant number of peaks decreased in intensity, and new peaks appeared (Figure 4.2). A few very strong peaks appeared in the random coil region. Since these signals were absent in spectra of the separately produced caspase-8, in which the intersubunit fragment was removed during purification, they most likely correspond to the fragment excised during cleavage.

Comparing peak integrals over time we observed an exponential decay of all peaks (Figure 4.1C). After approximately 30 hours the peaks in the [^{15}N, ^{1}H]-TROSY spectra contain about 30% of their original intensity. An example is depicted in Figure 4.1C, were signals from the C-terminus, which is identical in procaspase-8 and caspase-8, are presented. In contrast, signal intensity for all regions affected by processing is below 5% of their initial values. Unfortunately, the time resolution is insufficient to allow distinguishing whether events occur simultaneously or in sequential order.

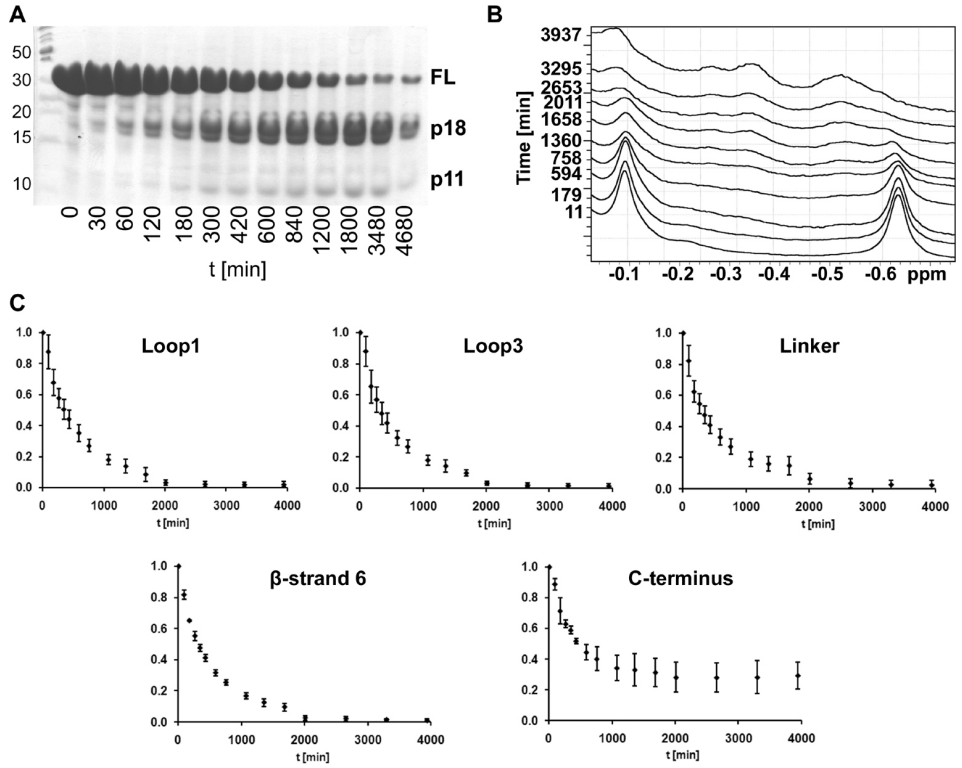

Figure 4.1: Processing of procaspase-8 into caspase-8. Labeled procaspase-8 was incubated in a 1:10.000 ratio with unlabelled caspase-8. Cleavage was monitored simultaneously by SDS PAGE and NMR.
A) SDS PAGE with procaspase-8 samples obtained at indicated time points during the cleavage process.
B) Regions of 1D proton spectra displaying the methyl region recorded at indicated time points.
C) Time course of signal decrease in [^{15}N, ^{1}H]-TROSY spectra. Peak intensities present averages for all residues from the segment indicated on the plots. Error bars reflect the standard deviation from the mean.

4.3.2 Caspase-8 undergoes structural changes during processing and during inhibitor binding

Processing of procaspase-8 into caspase-8 is accompanied by large spectral changes that are difficult to interpret. Furthermore, during the long measurement time protein precipitated resulting in a decrease in protein concentration leading to a reduction in signal intensity. Therefore, we decided to characterize the product of the cleavage reaction in its purified form. Ac-

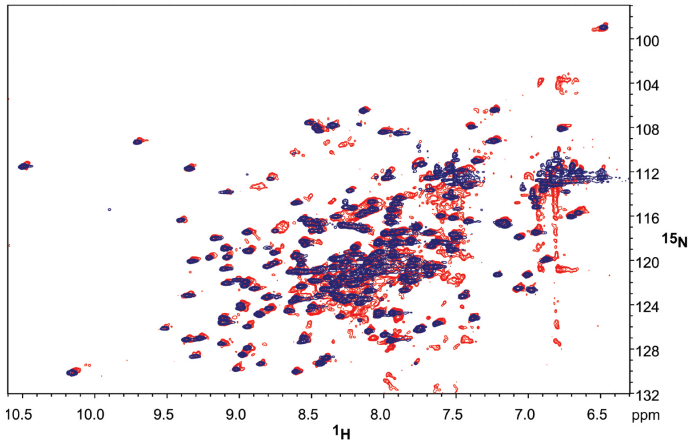

Figure 4.2: Comparison of [^{15}N, ^{1}H]-TROSY spectra of procaspase-8 (C285A) at the beginning and the end of cleavage reaction.

cordingly, caspase-8 was prepared from the active wild-type procaspase-8 in ^{15}N,^{2}H-labelled form. spectra recorded on the cleavage-incompetent C285A procaspase-8 mutant and caspase-8 indicates that both proteins are structurally highly similar (Figure 4.3A). Only signals corresponding to the loops and the linker as well as from residues of the β strand 5 and 6, which in procaspase-8 are in close proximity to the intact linker, were significantly shifted in position. In addition, β strand 6 forms the dimerization interface in active caspase-8, and therefore residues from these strands are expected to experience chemical shift changes.

During processing, the oligomerization state of the enzyme changes (Table 4.1) At the approximate concentration used in the NMR experiments procaspase-8 is purely monomeric whereas caspase-8, that is known to exist in a concentration-dependent monomer/dimer equilibrium [67,110], is present as a dimer at 81%. The increasing population of dimeric states during caspase-8 activation is also apparent from the line-widths of methyl signals in proton spectra (Figure 4.3B). In addition, the peaks are shifted in position indicating that they belong to residues undergoing structural changes or become involved in forming intermolecular contacts.

Structural information is available for procaspase-8 and inhibitor-bound caspase-8 but not for the inhibitor-free enzyme. The above-described data allows comparing caspase-8 in its zymogen and in the inhibitor-free state. In

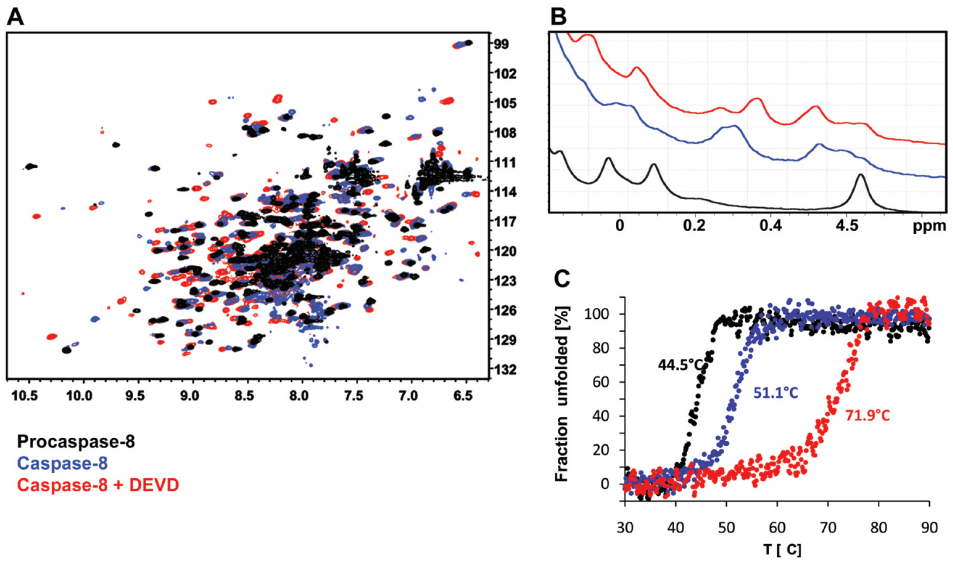

Figure 4.3: Comparison of procaspase-8 (black) with caspase-8 in the absence (blue) and presence (red) of the tetrapeptide DEVD inhibitor.
A) Overlay of a [^{15}N, ^{1}H]-HSQC spectrum with [^{15}N, ^{1}H]-TROSY spectra of caspase-8 in the absence or presence of the Ac-DEVD-cmk inhibitor. Differences in peak positions indicate changes in the environment of the corresponding amide moieties due to conformational changes or contacts to the inhibitor.
B) Section of the high-field region of a 1D proton spectrum displaying methyl signals. Line-widths are correlated with protein size such that increasing molecular weight during dimerization results in broader lines. Furthermore, differences in peak positions were observed as also seen in A).
C) Thermal denaturation of procaspase-8 and caspase-8 before and after inhibitor binding followed by CD spectroscopy. CD signals recorded at 222 nm were used to calculate the fraction of folded protein. The melting temperatures for the individual proteins are indicated in the plot.

order to assess how the free enzyme differs from the published inhibitor-bound crystal structure we added the irreversible Ac-DEVD-cmk inhibitor and monitored changes by chemical shift mapping. Interestingly, significant changes in peak positions occur. Analysis of the crystal structure of DEVD bound to caspase-8 reveals that about 21 amino acids are either directly involved in inhibitor binding or are in close vicinity. Surprisingly, comparison of the [^{15}N, ^{1}H]-TROSY spectra of caspase-8 in presence and absence of the inhibitor reveals that more than 70 peaks are shifted, suggesting further

Mutant	Sedimentation coefficient [S_{exp}]	Monomer/Dimer [%]
Constructs used in NMR experiments (800 μM)		
Procaspase-8	2.5 ± 0.031 / —	100 / —
Caspase-8	2.3 ± 0.022 / 3.9 ± 0.035	19 / 81
Caspase-8 + DEVD	2.2 ± 0.021 / 3.5 ± 0.034	11 / 89
Constructs used in cleavage experiments (250 μM)		
Procaspase-8	2.5 ± 0.019 / 3.7 ± 0.029	33 / 67 (29 / 71)*
D374A (C285A)	2.4 ± 0.019 / 3.9 ± 0.031	44 / 56
D384A (C285A)	2.7 ± 0.018 / 3.8 ± 0.025	67 / 33
F468A	2.5 ± 0.019 / —	100 / —

Table 4.1: Data derived from analytical ultracentrifugation of constructs used for the NMR and the cleavage experiments. Samples were measured at concentrations of 800 μM and 250 μM for NMR and cleavage experiments, respectively. Constructs used for the cleavage experiments harbor the active site mutation C285A and were processed by caspase-8 addition at a 1:1000 ratio. *The value in brackets was obtained previously at the same concentration for active caspase-8 which underwent autoproteolytic processing [110].

structural changes to take place upon inhibitor binding. Considering that the majority of the secondary structure elements are identical it is likely that these peaks belong to the active site forming loops or be located at the dimerization interface. However, the population of the dimer in presence vs. absence of inhibitor as determined by analytical ultracentrifugation is 81% and 89% (Table 4.1), respectively, and hence the difference is too small to explain the changes observed in the spectra. Moreover, a number of new peaks appear with rather strong intensity that must belong to residues in more flexible regions such as the active site forming loops.

To access the influence of activation and inhibitor binding on the overall protein stability the melting points of the proteins were determined by CD spectroscopy (Figure 4.3C). Dimerization and cleavage of the zymogen results in improved protein stability characterized by a 6.6 degree increase in the melting temperature for caspase-8 compared to procaspase-8. An even more pronounced stabilizing effect was observed upon inhibitor binding to caspase-8, which elevates the melting temperature by approximately 20 degrees.

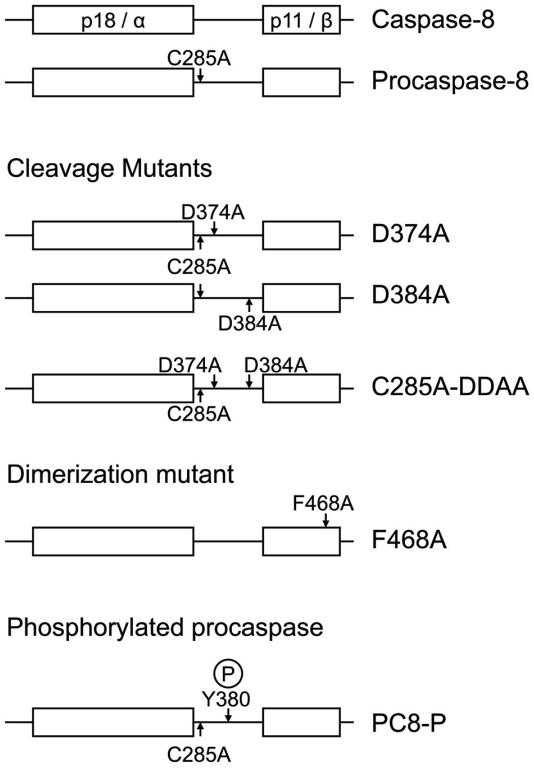

Figure 4.4: Overview of caspase-8 mutants used in this study indicating positions of individual mutation sites.

4.3.3 Determinants of the processing rate of procaspase-8

In the following we analyze to which extent the rate of processing of procaspase-8 by the addition of catalytic amounts of the active enzyme is influenced by the propensity for dimerization, by phosphorylation of procaspase-8 and by insufficient cleavage of the intersubunit linker. Therefore, we mutated either one of the Asp cleavage motifs in the linker, introduced a mutation at the dimerization interface or phosphorylated procaspase-8 *in vitro* (Figure 4.4). In order to prevent self-activation the constructs harbor an additional C285A mutation. To all mutants active caspase-8 was added in catalytic amounts (1:1000), the reaction was stopped at indicated time points, and the rate of processing was analyzed by SDS PAGE and densitometry.
Over time the intensity of the bands corresponding to full-length protein decreased and new bands for p18/p19 and p11/p12 subunits became visible. Integration of the bands corresponding to full-length protein revealed

a double-exponential decay (Figure 4.5 A). While the procaspase-8 mutants are rapidly processed in the beginning of the experiment cleavage rates are reduced later on. We believed this to be mainly due to a decrease in enzymatic activity of caspase-8 over time and therefore we determined the activity of caspase-8 using the fluorogenic Ac-DEVD-AMC substrate. After 3000 minutes caspase-8 retains 1% of its original activity (Figure 4.5B). The same experiment was performed by further addition of 1000 equivalents of the procaspase-8 mutant C285A-DDAA that cannot be cleaved due to the double mutation D374A D384A (DDAA) and also cannot process other substrates. This mutant does not compete with the Ac-DEVD-AMC substrate for the active site of caspase-8 in contrast to procaspase-8. Surprisingly, addition of C285A-DDAA resulted in increased caspase-8 activity (Figure 4.5C) and retarded caspase-8 deactivation (Figure 4.5B) indicating that it is able to interact with caspase-8, most likely via heterodimerization. Furthermore, analytical ultracentrifugation revealed that the affinity for dimer formation in cleaved procaspase-8 is only slightly lower than for caspase-8 (Table 4.1).

Despite the time dependent deactivation of caspase-8, a comparison of the cleavage efficiencies for the various substrates can still be made because all cleavage reactions have been performed under identical conditions and hence deactivation of caspase-8 and therefore remaining active caspase-8 is expected to be comparable at identical time points. Interestingly, all the analyzed mutants are less efficient in processing when compared to procaspase-8. While initial processing rates are similar within the range of the experimental error pronounced differences are observed after approx. 5-10 hours. In case of the Asp mutants the processing rate is more strongly affected for D384A. Analytical ultracentrifugation data of the cleavage products of both mutants reveals that the affinity for dimerzation is impaired compared to cleaved procaspase-8, and that this reduction is larger for D384A than for D374A. Moreover, F468A shows a significant decrease in the processing rate as compared to procaspase-8 underlining the important role of dimerization for activation.

Previous studies by Cursi et al. revealed a negative effect on Fas-induced apoptosis after phosphorylation of caspase-8 by Src kinase [83]. Src kinase

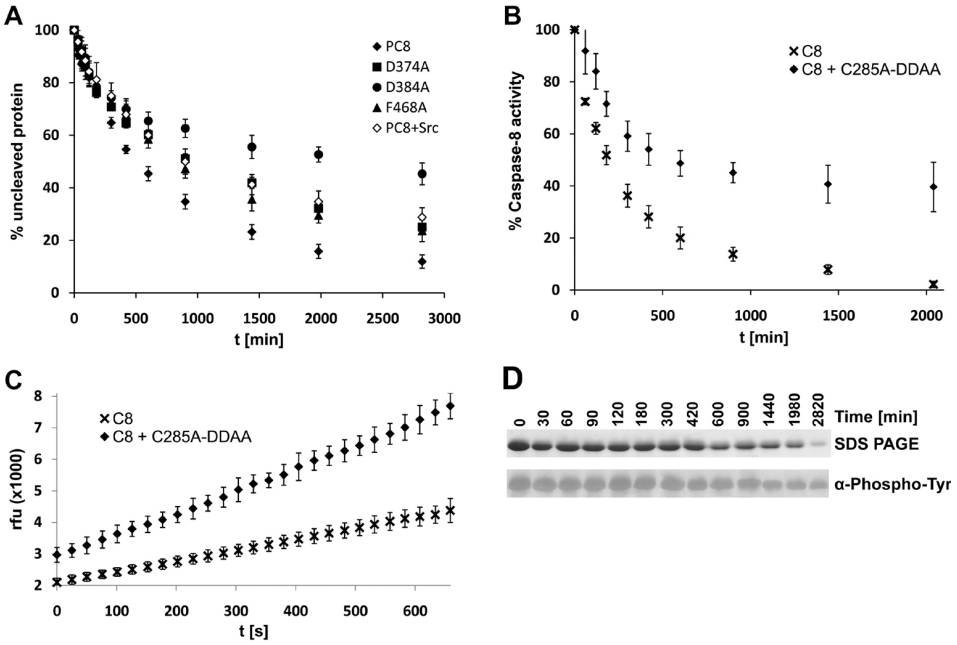

Figure 4.5: Processing of various procaspase-8 mutants by caspase-8
A) Time course of processing for various mutants (see panel) of procaspase-8 displaying the percentage of unprocessed protein at indicated time points. Processing was determined by SDS PAGE and densitometry on bands corresponding to uncleaved enzyme.
B) Time-dependent deactivation of caspase-8 in the absence and presence of the inactive uncleavable C285A-DDAA mutant monitored by conversion of the fluorogenic Ac-DEVD-AMC substrate.
C) Influence of inactive uncleavable procaspase-8 C285A-DDAA on caspase-8 activity.
D) SDS PAGE and corresponding Western blot of phosphorylated procaspase-8 following addition of caspase-8.

phosphorylates caspase-8 specifically at Tyr380, which is located between the two cleavage recognition motifs within the linker and is excised during processing. In this study, we phosphorylated caspase-8 *in vitro* with Src kinase. Phosphorylation of caspase-8 was detected by Western blot using a specific phospho-tyrosine antibody (Figure 4.5D). The rate of conversion for phosphorylated procaspase-8 is slower than for its unphosphorylated counterpart (Figure 4.5A). Interestingly, the band observed on SDS PAGE decreases faster in intensity than the band on the western blot, indicating that the un-

phosphorylated enzyme is preferably cleaved (Figure 4.5D). Phosphorylation at Tyr380 can reduce the rate of processing and thus caspase-8 activation and apoptosis by either sterically blocking access to the cleavage sites or by altering the conformation of the linker.

4.4 Discussion

Activation of inflammatory and apoptotic initiator procaspases proceeds through dimerization, which is stabilized by subsequent proteolytic processing. And although our understanding of the underlying molecular processes has greatly advanced with the development of important concepts like the induced-proximity model [37,108] the exact molecular details are still not fully understood. Only a few procaspase structures are available such as for *Drosophila melanogaster* Dronc [151], for executioner procaspase-7 [114], for inflammatory procaspase-1 [152] and for procaspase-8 [110]. Much more structural information is available on active caspases, but more than 90% of the pdb structures are of caspases in presence of bound inhibitors. Currently, no structural information is available for inhibitor-free apoptotic initiator caspases, which exist in an equilibrium of monomers and dimers that together with an increased flexibility of the active site forming loops and the linker most likely prevented crystallization and impedes NMR analysis. In contrast dimeric structures for caspase-1 and -7 have been published in both the inhibitor free and inhibitor-bound states [114,150].

In this work we have investigated cleavage of procaspase-8 and subsequent binding of substrates applying chemical shift mapping and biochemical methods. In the conducted experiments trace amounts of active caspase-8 triggered conversion of procaspase-8 mutants that are deficient of autoprocessing. Previous studies on procaspase-8 and caspase-8 stated that caspase-8 has no specificity for its own zymogen [64]. The experiments presented in this work, however, clearly demonstrate processing of the zymogen after addition of caspase-8 indicating that caspase-8 does have a specificity for procaspase-8.

Cleavage of procaspase-8 results in an apparent increase in molecular weight and large structural differences in the loops and at the dimerization interface. In principle, cleavage can be accomplished in three different ways: i) by an intramolecular process, ii) by an intermolecular process in which the participating Asp and Cys residues are part of different protomers within the same dimer (intradimeric) or iii) by an intermolecular process involving a proximal caspase dimer (interdimeric). All constructs that were tested for

cleavage contained the active site C285A mutation and are incapable of self-processing and therefore require intermolecular cleavage. The observation that an inactive, cleavage-incompetent C285A-DDAA mutant increases the activity of caspase-8 suggests that heterodimerization between procaspase-8 and caspase-8 occurs. Considering the vast excess of the procapase-8 mutants over active capase-8 (1000:1 in the biochemical and 10000:1 in the NMR experiments) caspase-8 is more likely to associate with procaspase-8 than with itself, which supports the intra-dimeric cleavage hypothesis. In addition, the concentration of caspase-8 was in the nanomolar range where caspase-8 homodimer formation (Kd of $\sim$50 μM, [67]) is unlikely, whereas our assay concentration of procaspase-8 (250 μM) was well above this threshold. While the affinity of caspase-8 for procaspase-8 may be lower than for caspase-8 formation of the heterodimer could result in immediate processing. Finally, intra-dimeric attack by Cys285 is expected to be favored kinetically. Our *in vitro* experiments support this view since they reveal a correlation between dimerization and cleavage of the substrate. Processing is slowed down in the dimerization-incompetent F468A mutant. Although F468A is incompetent for *homo*-dimerization because cross-strand intermolecular interactions of Phe468 with Pro466 have been removed, due to the pseudo-symmetry in the heterodimer one of the two Pro-Phe contacts remain. We expect the Kd for formation of the *hetero*dimer to be lower than the corresponding value for formation of the *homo*dimer in caspase-8, and this is reflected in the reduced processing rate. The connection between the rate of processing and the affinity for dimerization for the cleaved enzyme might also explain the reduced processing rates for the cleavage mutants D374A and D384A. Both mutants display a reduction in dimerization affinity, which is more pronounced in the slower processing D384A mutant.

If such intra-dimeric attack takes place the linker must undergo a dramatic conformational change in order to bring Asp374 and Asp384 into proximity of the catalytic Cys285 from the other protomer. One plausible scenario is that the relocation of the linker is triggered by dimerization that pushes loop 4 and possibly loop 5 towards that active site thereby displacing the linker segment from that region. We noticed that resonances from loops 4 and 5 were completely absent in the ^{15}N, ^{1}H-correlation spectra of procaspase-8,

indicating that these two loops interconvert between at least two different states, and hence intrinsically sample a larger conformational space [110].
The proposed conformational change is very large but precedence for such a linker topology is found in the crystal structure of procaspase-1. Although procaspase-1 is monomeric in solution it was crystallized as a dimer with the linker located in a cleft at the dimer interface and the cleavage motif for the first processing site positioned close to the active site of the second protomer (Figure 4.6 C, [152]). Furthermore, the linker in procaspase-1 is similarly positioned as the cleaved linker of active caspase-1 and -8 (Figure 4.6 A). Loops 3 and 4 (corresponding to loops 4 and 5 in procaspase-8) are slightly shifted towards the active site supporting their role in linker displacement. Thus the structure of the procaspase-1 displays all structural elements that are required for the proposed mode of cleavage for procapase-8 and we have taken this as a model of how the structure of procaspase-8 could change during dimerization.
Previous studies state that dimerization is the prime event in initiator caspase activation that triggers structural rearrangements of the active site forming loops leading to formation of the active site [36,67,108,110,117,118]. Our chemical shift mapping experiment using the DEVD inhibitor indicates that dimerization is not sufficient to form a proper active site, and that additional significant changes occur upon inhibitor binding. This statement is supported by similar conclusions drawn from the comparison of crystal structures of caspase-1 and caspase-7 in presence or absence of inhibitors and their corresponding zymogens [114,150]. In both enzymes structural differences are observed in the active site forming loops 3 and 4 and in the linker fragments with the inhibitor-free form being a structural intermediate between the zymogen and the inhibitor-bound species (Figure 4.6 B). Moreover, loops 3 and 4 are arranged in a way that the substrate-binding pocket is not properly formed in the absence of inhibitors. Furthermore, the cleaved linker fragments L2 and L2' of the associated protomers interact with each other in all inhibitor-bound crystal structures while they are separated in inhibitor-free caspase-7 [114]. Mutants of caspase-8 in which the L2 loop is truncated experience a significant shift towards the monomeric state for caspase-8 suggesting their importance for dimer stabilization [110]. Struc-

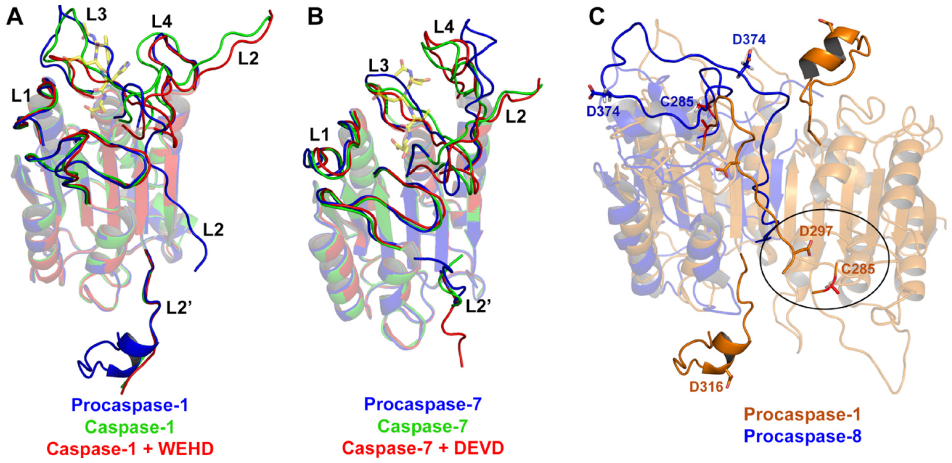

Figure 4.6: Comparison of different caspase activation states.
A) Superposition of procaspase-1 (blue, pdb code 3E4C) and caspase-1 in the absence (green, pdb code 1SC1) and presence (red, pdb code 1IBC) of a tetrapeptidic WEHD inhibitor (yellow). The active site forming loops are labeled and indicated in bright colors. The tetrapeptidic inhibitor is presented as sticks.
B) Superposition of procaspase-7 (pdb code 1K88) and caspase-7 in the absence (pdb code 1K86) and presence (pdb code 1F1J) of a tetrapeptidic DEVD inhibitor. The color coding and labeling is the same as described in A).
C) Comparison of the linker orientation in dimeric procaspase-1 (brown) and monomeric procaspase-8 (blue, pdb code 2K7Z). The active site cysteine and the Asp residues in the cleavage motifs are presented as sticks. All figures were prepared using PyMol (DeLano Scientific LLC, http://www.pymol.org).

tural differences of the L2 loop between inhibitor-free and inhibitor-bound caspase-8 could explain the higher dimer affinity upon inhibitor binding, a common phenomenon for initiator caspases [67].

Previous experiments on caspase-7 revealed an increased overall protein stability upon inhibitor binding by 17.9 degrees [153], which is in the same range as observed for caspase-8. Since caspase-7 is dimeric both in the absence and presence of inhibitor the enhanced stability must be largely independent from dimerization. Therefore, we speculate that the increased overall stability of caspase-8 upon addition of the inhibitor is rather due to rigidification of the loops around the active site and possibly may also involve loop4 and 5, which in procaspase-8 undergo conformational exchange [110].

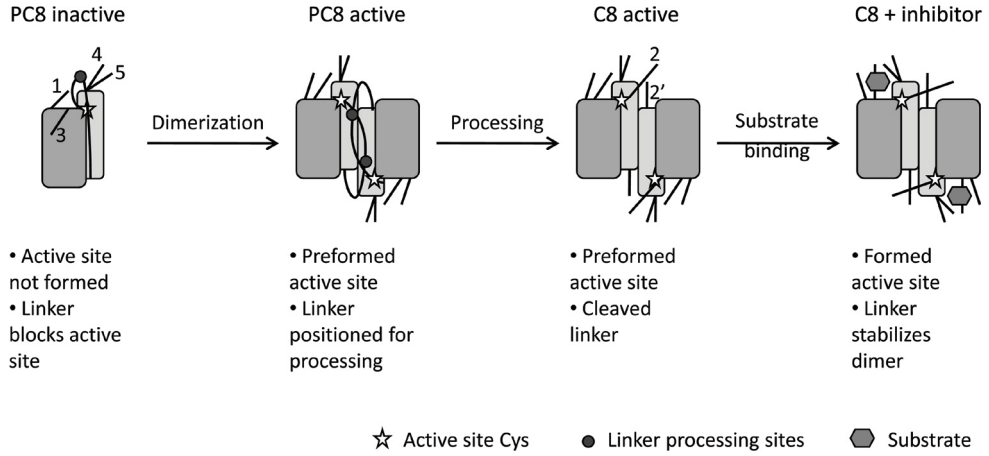

Figure 4.7: Schematic drawing of the caspase-8 activation mechanism. The large and small subunits are indicated by large and small boxes, respectively. The active site forming loops and the linker are depicted as lines and labeled according to the nomenclature used in Keller *et al.* 2009 [110].

Further support for the induced fit mechanism can be found in the structure of dimeric caspase-9, where only one active site is occupied by the inhibitor revealing a different conformation when compared to the empty site in the other protomer [118]. Although the authors suggested that the unoccupied site resembles the zymogen conformation, it might as well be a structural intermediate between the zymogen and the inhibitor-bound form. Furthermore, structural differences between inhibitor-free and inhibitor-bound form were also observed for caspase-3 [154]. In that case, however, conformational differences are restricted to side chains (especially 3 hydrophobic residues lining the S2 pocket). These observations together with our data suggest that substrate binding to the active site pocket during caspase activation probably generally occurs via an induced-fit mechanism. Whether the changes in caspase-8 involve larger conformational changes of the loops as observed for caspase-1 and -7 or minor side chain rearrangements as seen in caspase-3 cannot be distinguished based on our experiments. However, the data confirm that dimerization is the prime event during caspase-8 activation and allow expanding the current model of initiator caspase activation (Figure 4.7). We propose that dimerization helps relocating the cleavage motifs within the linker to become accessible for intermolecular cleavage and initiates pre-

building of the active site, which finally forms upon substrate binding.
Caspase-8 activation at the DISC is a very complex issue that is difficult to address *in vitro* and certainly requires additional biochemical experiments under conditions that better mimic the DISC environment. The model for caspase-8 activation proposed in this work provides a working hypothesis that may help guiding the design of such experiments.

4.5 Materials and Methods

4.5.1 Protein design, expression and purification

The DNA sequence coding for human caspase-8 amino acids 217-479 was cloned into a pQE50 vector (Qiagen). Amino acid substitutions were generated by Quikchange^{TM} mutagenesis (Stratagene) mutagenesis. The plasmids were transformed into M15 (pREP4) cells (Qiagen), and the protein was expressed at 37°C overnight either in LB (unlabeled protein) or in M9 (^{15}N-labeled protein) medium. M9 minimal media was supplemented with $^{15}NH_4Cl$ as the sole nitrogen source. Deuteration was achieved by growing cells in D2O.

The purification protocol was adapted from published procedures [66] and was described previously [110]. Cells were harvested, resuspended in PBS buffer and lyzed by french press. The soluble protein fraction was removed by centrifugation, inclusion bodies washed in 20 mM Tris pH 8.0, 1 mM EDTA, 0.1% LDAO and solubilized in 6.5 mM GdHCl, 20 mM Tris pH 8.0, 2 mM EDTA, 100 mM DTT. The solubilized inclusion bodies were added to an equal volume of acetic acid and the sample dialyzed against 50% acetic acid. Subsequently the solution was suspended rapidly in nine volumes H2O and immediately diluted in nine-fold excess of 1 M Tris pH 8.0, 5 mM DTT. Refolding was performed over night at room temperature and aggregates were removed by centrifugation. Final purification was achieved by size exclusion chromatography on a Superdex 200 column (Amersham) using 20 mM Tris, pH 8.0, 100 mM NaCl, 10% sucrose, 0.5 mM TCEP. In this buffer the protein can be stored at -80°C. Light-scattering was used to confirm monodispersity of the refolded purified sample.

4.5.2 NMR experiments

NMR samples were rebuffered into 20 mM deuterated Tris pH 8.0, 100 mM KCl, 10 mM DTT. Procaspase-8 that was used to monitor the time-course of cleavage and active caspase-8 were both ^{2}H, ^{15}N-labeled. The irreversible tetrapeptidic AC-DEVD-cmk inhibitor was added in five-fold excess to ^{2}H, ^{15}N-labelled active caspase-8. All NMR experiments were recorded at

305 K on a Bruker Avance 700 MHz spectrometer, equipped with a triple-resonance cryoprobe. [^{15}N, ^{1}H]-HSQC and [^{15}N, ^{1}H]-TROSY experiments were recorded during cleavage for monomeric proteins and of dimeric caspase-8 using, respectively. The spectra were processed in Topspin2.1 (Bruker) and transferred to CARA for spectral analysis [134]. Complete processing at both cleavage sites was confirmed by MALDI mass spectroscopy.

4.5.3 Analytical ultracentrifugation

Analytical ultracentrifugation was performed with an Optima XL-1 centrifuge (Beckman Coulter) and a TI50 rotor using epoxy centerpieces (12 mm) with sapphire windows. Samples were run at 20°C and 42000 rpm. Absorption was measured between 280 and 315 nm, depending on protein concentration. Results were analyzed using Sedfit [143].

4.5.4 CD Spectroscopy

Thermal denaturation was performed on a Jasco J-715 spectropolarimeter equipped with a temperature control unit. The concentrations of the samples were 100 μM using a quartz cuvette with a 1 mm path length. Data points were taken at 222 nm while increasing the temperature by 1°C/min from 5°C to 95°C. The band-width was set to 1 nm and the response time to 4 s.

4.5.5 In vitro cleavage experiments

All proteins were dialyzed against phosphorylation buffer (50 mM Tris pH 8.0, 150 mM NaCl, 0.5 mM TCEP, 20 mM MgCl2, 12.5 mM MnCl2, 12.5 mM β-glycrolphosphate). Phosphorylation of procaspase-8 was accomplished by incubation with Src kinase (SignalChem) with 25-fold excess of procaspase and 5 fold excess of ATP at 37°C for 3 hrs. Small amounts of precipitated protein were removed by centrifugation. The final sample volume for monitoring the cleavage reaction was 200 μlcontaining 250 μMprocaspase-8 mutants. The reaction was started by addition of 250 nM caspase-8. Small aliquots were removed at indicated time points, immediately suspended in hot 5x SDS loading buffer and incubated for 5 min at 95°C. The cleavage educts and products were separated by SDS PAGE. The gels were scanned

in a Fuji LAS 3000 image reader (FujiFilm) and the bands corresponding to full-length caspase-8 analyzed by densitometry using the AIDA image analyzer software. The obtained values were normalized by setting the concentration of full-length protein at the beginning of the reaction to 100% and by appropriate scaling of all subsequent data. Measurements were performed in triplicate and the standard deviations were calculated. Initially we tried to fit the kinetic data against single-exponentially decaying functions but discovered that data could not be fit well due to inactivation of caspase-8. Inactivation of caspase-8 in the absence and presence of PC8 DDAA was determined by addition of the Ac-DEVD-AMC substrate at a final concentration of 100 μM. The concentrations of the proteins and the buffer were the same as used in the cleavage reactions described above. Measurements were performed in triplicate in black 96-well Nuncion microtiter plates using the Magellan6 software on a GENios plate reader (Tecan). AMC release was monitored by its fluorescence at 465 nm following excitation at 360 nm.

4.6 Acknowledgments

This work was supported by the Swiss National Science Foundation (grant 31-1022181 to M.G. Grütter) and the European Commission (CAMP Project LSHG-2006-018830). We thank Prof. A. Baici for valuable discussions of the cleavage data. Nadine Keller is a member of the PhD Program in Molecular Life Sciences, University of Zurich and ETH Zurich, Switzerland.

Bibliography

[1] J. C. Ameisen, T. Idziorek, O. Billaut-Mulot, M. Loyens, J. P. Tissier, A. Potentier, and A. Ouaissi. Apoptosis in a unicellular eukaryote (Trypanosoma cruzi): Implications for the evolutionary origin and role of programmed cell death in the control of cell proliferation, differentiation and survival. *Cell Death Differ.*, 2(4):285–300, 1995.

[2] J. F. Kerr, A. H. Wyllie, and A. R. Currie. Apoptosis: A basic biological phenomenon with wide-ranging implications in tissue kinetics. *Br. J. Cancer*, 26(4):239–57, 1972.

[3] N. Andre. Hippocrates of Cos and apoptosis. *Lancet*, 361(9365):1306, 2003.

[4] A. Diamantis, E. Magiorkinis, G. H. Sakorafas, and G. Androutsos. A brief history of apoptosis: From ancient to modern times. *Onkologie*, 31(12):702–6, 2008.

[5] K. Vogt. Untersuchungen über die Entwicklungsgeschichte der Geburtshelferkröte (Alytes obstretricians). Technical report, 1842.

[6] R. Virchow. Cellular pathology as based upon physiological and pathological histology, 1860.

[7] W. Flemming. Über die Bildung von Richtungsfiguren in Säugetieren beim Untergang Graaf'scher Follikel. *Arch. Anat. Physiol*, pages 221–244, 1885.

[8] A. Glucksmann. Cell deaths in normal vertebrate ontogeny. *Biol. Rev. Camb. Phil. Soc.*, 26:59–86, 1951.

[9] W. Zoli, P. Ulivi, A. Tesei, F. Fabbri, M. Rosetti, R. Maltoni, D. C. Giunchi, L. Ricotti, G. Brigliadori, I. Vannini, and D. Amadori. Addition of 5-fluorouracil to doxorubicin-paclitaxel sequence increases caspase-dependent apoptosis in breast cancer cell lines. *Breast Cancer Res*, 7(5):R681–9, 2005.

[10] G. Hacker. The morphology of apoptosis. *Cell Tissue Res.*, 301(1):5–17, 2000.

[11] A. H. Wyllie, J. F. Kerr, and A. R. Currie. Cell death: The significance of apoptosis. *Int. Rev. Cytol.*, 68:251–306, 1980.

[12] J. E. Sulston and H. R. Horvitz. Post-embryonic cell lineages of the nematode, Caenorhabditis elegans. *Dev. Biol.*, 56(1):110–56, 1977.

[13] H.R. Horvitz, H.M. Ellis, and P.W Sternberg. Programmed cell death in nematode development. *Neurosci. Comment*, 1:56–65, 1982.

[14] E. Finkel. The mitochondrion: Is it central to apoptosis? *Science*, 292(5517):624–6, 2001.

[15] J. E. Chipuk and D. R. Green. How do BCL-2 proteins induce mitochondrial outer membrane permeabilization? *Trends Cell. Biol.*, 18(4):157–64, 2008.

[16] D. Acehan, X. Jiang, D. G. Morgan, J. E. Heuser, X. Wang, and C. W. Akey. Three-dimensional structure of the apoptosome: Implications for assembly, procaspase-9 binding, and activation. *Mol. Cell*, 9(2):423–32, 2002.

[17] J. M. Adams and S. Cory. Apoptosomes: Engines for caspase activation. *Current Opinion in Cell Biology*, 14(6):715–720, 2002.

[18] E. A. Slee, M. T. Harte, R. M. Kluck, B. B. Wolf, C. A. Casiano, D. D. Newmeyer, H. G. Wang, J. C. Reed, D. W. Nicholson, E. S. Alnemri, D. R. Green, and S. J. Martin. Ordering the cytochrome c-initiated caspase cascade: Hierarchical activation of caspases-2, -3, -6, -7, -8, and -10 in a caspase-9-dependent manner. *J. Cell. Biol.*, 144(2):281–92, 1999.

[19] S. J. Korsmeyer, M. C. Wei, M. Saito, S. Weiler, K. J. Oh, and P. H. Schlesinger. Pro-apoptotic cascade activates BID, which oligomerizes BAK or BAX into pores that result in the release of cytochrome c. *Cell Death Differ.*, 7(12):1166–73, 2000.

[20] H. Li, H. Zhu, C. J. Xu, and J. Yuan. Cleavage of BID by caspase-8 mediates the mitochondrial damage in the Fas pathway of apoptosis. *Cell*, 94(4):491–501, 1998.

[21] X. Luo, I. Budihardjo, H. Zou, C. Slaughter, and X. Wang. Bid, a Bcl2 interacting protein, mediates cytochrome c release from mitochondria in response to activation of cell surface death receptors. *Cell*, 94(4):481–90, 1998.

[22] Y. Guo, S. M. Srinivasula, A. Druilhe, T. Fernandes-Alnemri, and E. S. Alnemri. Caspase-2 induces apoptosis by releasing proapoptotic proteins from mitochondria. *J. Biol. Chem.*, 277(16):13430–7, 2002.

[23] J. D. Robertson, M. Enoksson, M. Suomela, B. Zhivotovsky, and S. Orrenius. Caspase-2 acts upstream of mitochondria to promote cytochrome c release during etoposide-induced apoptosis. *J. Biol. Chem.*, 277(33):29803–9, 2002.

[24] Z. Danilevicius. Apoptosis: A factor in neoplastic growth? *Jama*, 223(4):434–5, 1973.

[25] H. J. Chun, L. Zheng, M. Ahmad, J. Wang, C. K. Speirs, R. M. Siegel, J. K. Dale, J. Puck, J. Davis, C. G. Hall, S. Skoda-Smith, T. P. Atkinson, S. E. Straus, and M. J. Lenardo. Pleiotropic defects in lymphocyte activation caused by caspase-8 mutations lead to human immunodeficiency. *Nature*, 419(6905):395–9, 2002.

[26] L. Salmena, B. Lemmers, A. Hakem, E. Matysiak-Zablocki, K. Murakami, P. Y. Au, D. M. Berry, L. Tamblyn, A. Shehabeldin, E. Migon, A. Wakeham, D. Bouchard, W. C. Yeh, J. C. McGlade, P. S. Ohashi, and R. Hakem. Essential role for caspase-8 in T cell homeostasis and T cell-mediated immunity. *Genes Dev.*, 17(7):883–95, 2003.

[27] A. Philchenkov, M. Zavelevich, TJ. Kroczak, and M. Los. Caspases and cancer: Mechanisms of inactivation and new treatment modalities. *Eksp. Onkol.*, 26(2):82–97, 2004.

[28] R. Gerl and D. L. Vaux. Apoptosis in the development and treatment of cancer. *Carcinogenesis*, 26(2):263–70, 2005.

[29] J. T. Opferman. Apoptosis in the development of the immune system. *Cell Death Differ.*, 15(2):234–242, 2007.

[30] O. Ekshyyan and T. Y. Aw. Apoptosis in acute and chronic neurological disorders. *Frontiers in Bioscience*, 1(9):1567–76, 2004.

[31] D. Limonta, V. Capo, G. Torres, A. B. Perez, and M. G. Guzman. Apoptosis in tissues from fatal dengue shock syndrome. *J. Clin. Virol.*, 40(1):50–4, 2007.

[32] R. A. Black, S. R. Kronheim, and P. R. Sleath. Activation of interleukin-1 beta by a co-induced protease. *FEBS Letters*, 247(2):386–90, 1989.

[33] M. J. Kostura, M. J. Tocci, G. Limjuco, J. Chin, P. Cameron, A. G. Hillman, N. A. Chartrain, and J. A. Schmidt. Identification of a monocyte specific pre-interleukin 1 beta convertase activity. *Proc Natl Acad Sci U S A*, 86(14):5227–31, 1989.

[34] A. U. Luthi and S. J. Martin. The CASBAH: A searchable database of caspase substrates. *Cell Death Differ.*, 14(4):641–50, 2007.

[35] Y. Shi. Caspase activation, inhibition, and reactivation: A mechanistic view. *Protein Sci.*, 13(8):1979–87, 2004.

[36] C. Pop, P. Fitzgerald, D. R. Green, and G. S. Salvesen. Role of proteolysis in caspase-8 activation and stabilization. *Biochemistry*, 46(14):4398–407, 2007.

[37] M. Muzio, B. R. Stockwell, H. R. Stennicke, G. S. Salvesen, and V. M. Dixit. An induced proximity model for caspase-8 activation. *J. Biol. Chem.*, 273(5):2926–2930, 1998.

[38] K. M. Boatright, M. Renatus, F. L. Scott, S. Sperandio, H. Shin, I. M. Pedersen, J.-E. Ricci, W. A. Edris, D. P. Sutherlin, D. R. Green, and G. S. Salvesen. A unified model for apical caspase activation. *Mol. Cell*, 11(2):529–541, 2003.

[39] A. Roy, J. H. Hong, J. H. Lee, Y. T. Lee, B. J. Lee, and K. S. Kim. In vitro activation of procaspase-8 by forming the cytoplasmic component of the death-inducing signaling complex (cDISC). *Mol. Cells*, 26(2):165–70, 2008.

[40] S. J. Riedl and G. S. Salvesen. The apoptosome: Signalling platform of cell death. *Nat. Rev. Mol. Cell Biol*, 8(5):405–413, 2007.

[41] V. Petrilli, C. Dostert, D. A. Muruve, and J. Tschopp. The inflammasome: A danger sensing complex triggering innate immunity. *Curr. Opin. Immunol.*, 19(6):615–22, 2007.

[42] H. B. Yu and B. B. Finlay. The caspase-1 inflammasome: A pilot of innate immune responses. *Cell Host Microbe*, 4(3):198–208, 2008.

[43] H. H. Park, E. Logette, S. Raunser, S. Cuenin, T. Walz, J. Tschopp, and H. Wu. Death domain assembly mechanism revealed by crystal structure of the oligomeric PIDDosome core complex. *Cell*, 128(3):533–46, 2007.

[44] A. Kohl and M. G. Grütter. Fire and death: The pyrin domain joins the death-domain superfamily. *C. R. Biol.*, 327(12):1077–86, 2004.

[45] J. C. Reed, K. S. Doctor, and A. Godzik. The domains of apoptosis: A genomics perspective. *Sci. STKE*, 2004(239):re9, 2004.

[46] S. Hiller, A. Kohl, F. Fiorito, T. Herrmann, G. Wider, J. Tschopp, M. G. Grütter, and K. Wüthrich. NMR structure of the apoptosis- and inflammation-related NALP1 pyrin domain. *Structure*, 11(10):1199–1205, 2003.

[47] B. Huang, M. Eberstadt, E. T. Olejniczak, R. P. Meadows, and S. W. Fesik. NMR structure and mutagenesis of the Fas (APO-1/CD95) death domain. *Nature*, 384(6610):638–41, 1996.

[48] E. J. Jeong, S. Bang, T. H. Lee, Y. I. Park, W. S. Sim, and K. S. Kim. The solution structure of FADD death domain. Structural basis of death domain interactions of Fas and FADD. *J. Biol. Chem.*, 274(23):16337–42, 1999.

[49] F. L. Scott, B. Stec, C. Pop, M. K. Dobaczewska, J. J. Lee, E. Monosov, H. Robinson, G. S. Salvesen, R. Schwarzenbacher, and S. J. Riedl. The Fas-FADD death domain complex structure unravels signalling by receptor clustering. *Nature*, 2008.

[50] X. Yu, D. Acehan, J. F. Menetret, C. R. Booth, S. J. Ludtke, S. J. Riedl, Y. Shi, X. Wang, and C. W. Akey. A structure of the human apoptosome at 12.8 Å resolution provides insights into this cell death platform. *Structure*, 13(11):1725–35, 2005.

[51] P. Li, D. Nijhawan, I. Budihardjo, S. M. Srinivasula, M. Ahmad, E. S. Alnemri, and X. Wang. Cytochrome c and dATP-dependent formation of Apaf-1/caspase-9 complex initiates an apoptotic protease cascade. *Cell*, 91(4):479–89, 1997.

[52] S. J. Riedl, W. Li, Y. Chao, R. Schwarzenbacher, and Y. Shi. Structure of the apoptotic protease-activating factor 1 bound to ADP. *Nature*, 434(7035):926–933, 2005.

[53] H. Qin, S. M. Srinivasula, G. Wu, T. Fernandes-Alnemri, E. S. Alnemri, and Y. Shi. Structural basis of procaspase-9 recruitment by the apoptotic protease-activating factor 1. *Nature*, 399(6736):549–57, 1999.

[54] S. M. Srinivasula, M. Ahmad, T. Fernandes-Alnemri, and E. S. Alnemri. Autoactivation of procaspase-9 by Apaf-1-mediated oligomerization. *Mol. Cell*, 1(7):949–57, 1998.

[55] H. R. Stennicke, Q. L. Deveraux, E. W. Humke, J. C. Reed, V. M. Dixit, and G. S. Salvesen. Caspase-9 can be activated without proteolytic processing. *J. Biol. Chem.*, 274(13):8359–62, 1999.

[56] P. Lassus, X. Opitz-Araya, and Y. Lazebnik. Requirement for caspase-2 in stress-induced apoptosis before mitochondrial permeabilization. *Science*, 297(5585):1352–4, 2002.

[57] A. Tinel and J. Tschopp. The PIDDosome, a protein complex implicated in activation of caspase-2 in response to genotoxic stress. *Science*, 304(5672):843–6, 2004.

[58] S. Janssens, A. Tinel, S. Lippens, and J. Tschopp. PIDD mediates NF-kappaB activation in response to DNA damage. *Cell*, 123(6):1079–92, 2005.

[59] A. Tinel, S. Janssens, S. Lippens, S. Cuenin, E. Logette, B. Jaccard, M. Quadroni, and J. Tschopp. Autoproteolysis of PIDD marks the bifurcation between pro-death caspase-2 and pro-survival NF-kappaB pathway. *EMBO J.*, 26(1):197–208, 2007.

[60] F. Martinon and J. Tschopp. NLRs join TLRs as innate sensors of pathogens. *Trends Immunol.*, 26(8):447–54, 2005.

[61] J. L. Poyet, S. M. Srinivasula, M. Tnani, M. Razmara, T. Fernandes-Alnemri, and E. S. Alnemri. Identification of Ipaf, a human caspase-1-activating protein related to Apaf-1. *J. Biol. Chem.*, 276(30):28309–13, 2001.

[62] F. Martinon, K. Burns, and J. Tschopp. The inflammasome: A molecular platform triggering activation of inflammatory caspases and processing of proIL-beta. *Mol. Cell*, 10(2):417–26, 2002.

[63] M. Chen, A. Orozco, D. M. Spencer, and J. Wang. Activation of initiator caspases through a stable dimeric intermediate. *J. Biol. Chem.*, 277(52):50761–50767, 2002.

[64] D. W. Chang, Z. Xing, V. L. Capacio, M. E. Peter, and X. Yang. Interdimer processing mechanism of procaspase-8 activation. *EMBO J.*, 22(16):4132–42, 2003.

[65] H. Blanchard, L. Kodandapani, P. R. Mittl, S. D. Marco, J. F. Krebs, J. C. Wu, K. J. Tomaselli, and M. G. Grütter. The three-dimensional

structure of caspase-8: An initiator enzyme in apoptosis. *Structure Fold. Des.*, 7(9):1125–33, 1999.

[66] W. Watt, K. A. Koeplinger, A. M. Mildner, R. L. Heinrikson, A. G. Tomasselli, and K. D. Watenpaugh. The atomic-resolution structure of human caspase-8, a key activator of apoptosis. *Structure Fold. Des.*, 7(9):1135–43, 1999.

[67] M. Donepudi, A. Mac Sweeney, C. Briand, and M. G. Grütter. Insights into the regulatory mechanism for caspase-8 activation. *Mol. Cell*, 11(2):543–549, 2003.

[68] H. Blanchard, M. Donepudi, M. Tschopp, L. Kodandapani, J. C. Wu, and M. G. Grütter. Caspase-8 specificity probed at subsite S4: Crystal structure of the caspase-8-Z-DEVD-cho complex. *J. Mol. Biol.*, 302(1):9–16, 2000.

[69] G. Xu, M. Cirilli, Y. Huang, R. L. Rich, D. G. Myszka, and H. Wu. Covalent inhibition revealed by the crystal structure of the caspase-8/p35 complex. *Nature*, 410(6827):494–7, 2001.

[70] O. D. Ekici, Z. Z. Li, A. J. Campbell, K. E. James, J. L. Asgian, J. Mikolajczyk, G. S. Salvesen, R. Ganesan, S. Jelakovic, M. G. Grütter, and J. C. Powers. Design, synthesis, and evaluation of aza-peptide Michael acceptors as selective and potent inhibitors of caspases-2, -3, -6, -7, -8, -9, and -10. *J. Med. Chem.*, 49(19):5728–49, 2006.

[71] M. Lu, T. Min, D. Eliezer, and H. Wu. Native chemical ligation in covalent caspase inhibition by p35. *Chem. Biol.*, 13(2):117–22, 2006.

[72] J. K. Yang, L. Wang, L. Zheng, F. Wan, M. Ahmed, M. J. Lenardo, and H. Wu. Crystal structure of MC159 reveals molecular mechanism of DISC assembly and FLIP inhibition. *Mol. Cell*, 20(6):939–49, 2005.

[73] P. E. Carrington, C. Sandu, Y. Wei, J. M. Hill, G. Morisawa, T. Huang, E. Gavathiotis, Y. Wei, and M. H. Werner. The structure of FADD and its mode of interaction with procaspase-8. *Mol. Cell*, 22(5):599–610, 2006.

[74] M. Irmler, M. Thome, M. Hahne, P. Schneider, K. Hofmann, V. Steiner, J. L. Bodmer, M. Schroter, K. Burns, C. Mattmann, D. Rimoldi, L. E. French, and J. Tschopp. Inhibition of death receptor signals by cellular FLIP. *Nature*, 388(6638):190–5, 1997.

[75] D. W. Chang, Z. Xing, Y. Pan, A. Algeciras-Schimnich, B. C. Barnhart, S. Yaish-Ohad, M. E. Peter, and X. Yang. c-FLIP$_L$ is a dual function regulator for caspase-8 activation and CD95-mediated apoptosis. *EMBO J.*, 21(14):3704–14, 2002.

[76] A. Krueger, S. Baumann, P. H. Krammer, and S. Kirchhoff. FLICE-inhibitory proteins: Regulators of death receptor-mediated apoptosis. *Mol. Cell Biol.*, 21(24):8247–54, 2001.

[77] A. Golks, D. Brenner, C. Fritsch, P. H. Krammer, and I. N. Lavrik. c-FLIP$_R$, a new regulator of death receptor-induced apoptosis. *J. Biol. Chem.*, 280(15):14507–13, 2005.

[78] O. Micheau, M. Thome, P. Schneider, N. Holler, J. Tschopp, D. W. Nicholson, C. Briand, and M. G. Grütter. The long form of FLIP is an activator of caspase-8 at the Fas death-inducing signaling complex. *J. Biol. Chem.*, 277(47):45162–45171, 2002.

[79] Jeffrey P. D. Shi Y. Yu, J. W.

[80] M. H. Cardone, N. Roy, H. R. Stennicke, G. S. Salvesen, T. F. Franke, E. Stanbridge, S. Frisch, and J. C. Reed. Regulation of cell death protease caspase-9 by phosphorylation. *Science*, 282(5392):1318–21, 1998.

[81] L. A. Allan and P. R. Clarke. Phosphorylation of caspase-9 by CDK1/cyclin B1 protects mitotic cells against apoptosis. *Mol. Cell*, 26(2):301–10, 2007.

[82] S. C. Brady, L. A. Allan, and P. R. Clarke. Regulation of caspase-9 through phosphorylation by protein kinase C zeta in response to hyperosmotic stress. *Mol. Cell. Biol.*, 25(23):10543–55, 2005.

[83] S. Cursi, A. Rufini, V. Stagni, I. Condo, V. Matafora, A. Bachi, A. P. Bonifazi, L. Coppola, G. Superti-Furga, R. Testi, and D. Barila. Src kinase phosphorylates Caspase-8 on Tyr380: A novel mechanism of apoptosis suppression. *EMBO J.*, 25(9):1895–905, 2006.

[84] M. C. Frame. Src in cancer: Deregulation and consequences for cell behaviour. *Biochim. Biophys. Acta*, 1602(2):114–30, 2002.

[85] J. Maelfait and R. Beyaert. Non-apoptotic functions of caspase-8. *Biochem. Pharmacol.*, 76(11):1365–73, 2008.

[86] T.-B. Kang, T. Ben-Moshe, E. E. Varfolomeev, Y. Pewzner-Jung, N. Yogev, A. Jurewicz, A. Waisman, O. Brenner, R. Haffner, E. Gustafsson, P. Ramakrishnan, T. Lapidot, and D. Wallach. Caspase-8 serves both apoptotic and nonapoptotic roles. *J. Immunol.*, 173(5):2976–2984, 2004.

[87] C. Rebe, S. Cathelin, S. Launay, R. Filomenko, L. Prevotat, C. L'Ollivier, E. Gyan, O. Micheau, S. Grant, A. Dubart-Kupperschmitt, M. Fontenay, and E. Solary. Caspase-8 prevents sustained activation of NF-kappaB in monocytes undergoing macrophagic differentiation. *Blood*, 109(4):1442–50, 2007.

[88] O. Sordet, C. Rebe, S. Plenchette, Y. Zermati, O. Hermine, W. Vainchenker, C. Garrido, E. Solary, and L. Dubrez-Daloz. Specific involvement of caspases in the differentiation of monocytes into macrophages. *Blood*, 100(13):4446–53, 2002.

[89] K. Ruckdeschel, G. Pfaffinger, R. Haase, A. Sing, H. Weighardt, G. Hacker, B. Holzmann, and J. Heesemann. Signaling of apoptosis through TLRs critically involves toll/IL-1 receptor domain-containing adapter inducing IFN-beta, but not MyD88, in bacteria-infected murine macrophages. *J. Immunol.*, 173(5):3320–8, 2004.

[90] C. De Trez, B. Pajak, M. Brait, N. Glaichenhaus, J. Urbain, M. Moser, G. Lauvau, and E. Muraille. TLR4 and Toll-IL-1 receptor domain-containing adapter-inducing IFN-beta, but not MyD88, regulate Es-

cherichia coli-induced dendritic cell maturation and apoptosis in vivo. *J. Immunol.*, 175(2):839–46, 2005.

[91] H. Su, N. Bidere, L. Zheng, A. Cubre, K. Sakai, J. Dale, L. Salmena, R. Hakem, S. Straus, and M. Lenardo. Requirement for caspase-8 in NF-kappaB activation by antigen receptor. *Science*, 307(5714):1465–8, 2005.

[92] R. S. Misra, J. Q. Russell, A. Koenig, J. A. Hinshaw-Makepeace, R. Wen, D. Wang, H. Huo, D. R. Littman, U. Ferch, J. Ruland, M. Thome, and R. C. Budd. Caspase-8 and c-FLIP$_L$ associate in lipid rafts with NF-kappaB adaptors during T cell activation. *J. Biol. Chem.*, 282(27):19365–74, 2007.

[93] J. W. Yu and Y. Shi. FLIP and the death effector domain family. *Oncogene*, 27(48):6216–27, 2008.

[94] N. Bidere, A. L. Snow, K. Sakai, L. Zheng, and M. J. Lenardo. Caspase-8 regulation by direct interaction with TRAF6 in T cell receptor-induced NF-kappaB activation. *Curr. Biol.*, 16(16):1666–71, 2006.

[95] T. Xiao, T. Towb, S.A. Wasserman, and Sprang S.R. Three-dimensional structure of a complex between the death domains of Pelle and Tube. *Cell*, 99:545–555, 1999.

[96] C. H. Weber and C. Vincenz. A docking model of key components of the DISC complex: Death domain superfamily interactions redefined. *FEBS Letters*, 492(3):171–6, 2001.

[97] M. Kaufmann, D. Bozic, C. Briand, J.-L. Bodmer, O. Zerbe, A. Kohl, J. Tschopp, and M. G. Grütter. Identification of a basic surface area of the FADD death effector domain critical for apoptotic signaling. *FEBS Letters*, 527(1-3):250–254, 2002.

[98] H. Wajant. The Fas signaling pathway: More than a paradigm. *Science*, 296(5573):1635–1636, 2002.

[99] C. Ghisleni. Molecular interactions of death effector domains in apoptotic signaling, 2003.

[100] T. Ducat, N. Declerck, T. Gostan, M. Kochoyan, and H. Demene. Rapid determination of protein solubility and stability conditions for NMR studies using incomplete factorial design. *J. Biomol. NMR*, 34(3):137–51, 2006.

[101] P. M. Domingos and H. Steller. Pathways regulating apoptosis during patterning and development. *Current Opinion in Genetics and Development*, 17(4):294–299, 2007.

[102] C. Fumarola and G. G. Guidotti. Stress-induced apoptosis: Toward a symmetry with receptor-mediated cell death. *Apoptosis*, 9(1):77–82, 2004.

[103] C. J. Norbury and B. Zhivotovsky. DNA damage-induced apoptosis. *Oncogene*, 23(16):2797–808, 2004.

[104] N. Droin, S. Cathelin, A. Jacquel, L. Guery, C. Garrido, M. Fontenay, O. Hermine, and E. Solary. A role for caspases in the differentiation of erythroid cells and macrophages. *Biochimie*, 90(2):416–22, 2008.

[105] R. C. Taylor, S. P. Cullen, and S. J. Martin. Apoptosis: Controlled demolition at the cellular level. *Nat. Rev. Mol. Cell Biol*, 9(3):231–41, 2008.

[106] S. K. Rupinder, A. K. Gurpreet, and S. Manjeet. Cell suicide and caspases. *Vascul. Pharmacol.*, 46(6):383–93, 2007.

[107] H. Y. Chang and X. Yang. Proteases for cell suicide: Functions and regulation of caspases. *Microbiol. Mol. Biol. Rev.*, 64(4):821–46, 2000.

[108] K. M. Boatright and G. S. Salvesen. Mechanisms of caspase activation. *Current Opinion in Cell Biology*, 15(6):725–731, 2003.

[109] R. Koradi, M. Billeter, and K. Wüthrich. MOLMOL: A program for display and analysis of macromolecular structures. *J. Mol. Graphics*, 14:51–55, 1996.

[110] N. Keller, J. Mares, O. Zerbe, and M. G. Grütter. Structural and biochemical studies on procaspase-8: New insights on initiator caspase activation. *Structure*, 17(3):438–448, 2009.

[111] R. Bhattacharyya and P. Chakrabarti. Stereospecific interactions of proline residues in protein structures and complexes. *J. Mol. Biol.*, 331(4):925–40, 2003.

[112] S. H. Gellman and D. N. Woolfson. Mini-proteins Trp the light fantastic. *Nat. Struct. Biol.*, 9(6):408–10, 2002.

[113] A. Neumoin, J. Mares, M. Lerch-Bader, R. Bader, and O. Zerbe. Probing the formation of stable tertiary structure in a model miniprotein at atomic resolution: Determinants of stability of a helical hairpin. *J. Am. Chem. Soc.*, 129(28):8811–7, 2007.

[114] J. Chai, Q. Wu, E. Shiozaki, S. M. Srinivasula, E. S. Alnemri, and Y. Shi. Crystal structure of a procaspase-7 zymogen: Mechanisms of activation and substrate binding. *Cell*, 107(3):399–407, 2001.

[115] Y. Shi. Caspase activation: Revisiting the induced proximity model. *Cell*, 117(7):855–8, 2004.

[116] A. Fernandez-Flores, B. Aguilera, P. Yau, and H. Oliva. An old meaning of the word apoptosis. *Lancet*, 359(9311):1072, 2002.

[117] C. Pop, J. Timmer, S. Sperandio, and G. S. Salvesen. The Apoptosome activates caspase-9 by dimerization. *Mol. Cell*, 22(2):269–275, 2006.

[118] M. Renatus, H. R. Stennicke, F. L. Scott, R. C. Liddington, and G. S. Salvesen. Dimer formation drives the activation of the cell death protease caspase-9. *Proc. Natl. Acad. Sci. U S A*, 98(25):14250–5, 2001.

[119] Y. Chao, E. N. Shiozaki, S. M. Srinivasula, D. J. Rigotti, R. Fairman, and Y. Shi. Engineering a dimeric caspase-9: A re-evaluation of the induced proximity model for caspase activation. *PLoS Biol.*, 3(6):e183, 2005.

[120] G. S. Salvesen. Caspase-8: Igniting the death machine. *Structure Fold. Des.*, 7(10):R225–9, 1999.

[121] Q. Bao and Y. Shi. Apoptosome: A platform for the activation of initiator caspases. *Cell Death Differ.*, 14(1):56–65, 2006.

[122] A. Schweizer, C. Briand, and M. G. Grütter. Crystal structure of caspase-2, apical initiator of the intrinsic apoptotic pathway. *J. Biol. Chem.*, 278(43):42441–42447, 2003.

[123] M. Garcia-Calvo, E. P. Peterson, D. M. Rasper, J. P. Vaillancourt, R. Zamboni, D. W. Nicholson, and N. A. Thornberry. Purification and catalytic properties of human caspase family members. *Cell Death Differ.*, 6(4):362–9, 1999.

[124] X. Shan, K. H. Gardner, D. R. Muhandiram, N. S. Rao, C. H. Arrowsmith, and L. E. Kay. Assignment of N-15, C-13(alpha), C-13(beta), and HN resonances in an N-15, C-13, H-2 labeled 64 kDa trp repressor-operator complex using triple-resonance NMR spectroscopy and H-2-decoupling. *J. Am. Chem. Soc.*, 118(28):6570–6579, 1996.

[125] S. A. McCallum, T. K. Hitchens, and G. S. Rule. Unambiguous correlations of backbone amide and aliphatic gamma resonances in deuterated proteins. *J. Magn. Reson.*, 134(2):350–354, 1998.

[126] T. Yamazaki, W. Lee, C. H. Arrowsmith, D. R. Muhandiram, and L. E. Kay. A suite of triple-resonance NMR experiments for the backbone assignment of N-15, C-13, H-2 labeled proteins with high sensitivity. *J. Am. Chem. Soc.*, 116(26):11655–11666, 1994.

[127] R. Weisemann, H. Rüterjans, and W. Bermel. 3D triple-resonance NMR techniques for the sequential assignment of NH and ^{15}N resonances in ^{15}N- and ^{13}C-labelled proteins. *J. Biomol. NMR*, 3(1):113–20, 1993.

[128] J.H. Noggle and R.E. Schirmer. *The nuclear Overhauser effect - Chemical applications.* Academic Press, New York, 1971.

[129] A. Bax, G. M. Clore, P. C. Driscoll, A. M. Gronenborn, M. Ikura, and L. E. Kay. Practical aspects of proton-carbon-carbon-proton three-dimensional correlation spectroscopy of ^{13}C labelled proteins. *J. Magn. Reson.*, 87:620–627, 1990.

[130] E. T. Olejniczak, R. X. Xu, and S. W. Fesik. A 4D HCCH-TOCSY experiment for assigning the side chain ^{1}H and ^{13}C resonances of proteins. *J. Biomol. NMR*, 2(6):655–9, 1992.

[131] R. A. Venters, 2nd Farmer, B. T., C. A. Fierke, and L. D. Spicer. Characterizing the use of perdeuteration in NMR studies of large proteins: ^{13}C, ^{15}N and ^{1}H assignments of human carbonic anhydrase II. *J. Mol. Biol.*, 264(5):1101–16, 1996.

[132] T. Yamazaki, J. D. Forman-Kay, and L. E. Kay. 2-Dimensional NMR experiments for correlating C-13-beta and H-1-delta/epsilon chemical-shifts of aromatic residues in C-13-labeled proteins via scalar couplings. *J. Am. Chem. Soc.*, 115(23):11054–11055, 1993.

[133] O. Zerbe, T. Szyperski, M. Ottiger, and K. Wüthrich. Three-dimensional 1H-TOCSY-relayed ct-[^{13}C,^{1}H]-HMQC for aromatic spin system identification in uniformly ^{13}C-labeled proteins. *J. Biomol. NMR*, 7(2):99–106, 1996.

[134] R. Keller. *The computer aided resonance assignment.* CANTINA Verlag, 2004.

[135] T. Herrmann, P. Güntert, and K. Wüthrich. Protein NMR structure determination with automated NOE-identification in the NOESY spectra using the new software ATNOS. *J. Biomol. NMR*, 24:171–189, 2002.

[136] G. Cornilescu, F. Delaglio, and A. Bax. Protein backbone angle restraints from searching a database for chemical shift and sequence homology. *J. Biomol. NMR*, 13(3):289–302, 1999.

[137] C. Bartels, T.-H. Xia, M. Billeter, P. Güntert, and K. Wüthrich. The program XEASY for computer-supported spectral analysis of biological macromolecules. *J. Biomol. NMR*, 6:1–10, 1995.

[138] P. Güntert. Automated NMR structure calculation with CYANA. *Methods Mol. Biol.*, 278:353–78, 2004.

[139] T. Herrmann, P. Güntert, and K. Wüthrich. Protein NMR structure determination with automated NOE assignment using the new software CANDID and the torsion angle dynamics algorithm DYANA. *J. Mol. Biol.*, 319(1):209–227, 2002.

[140] E. Ab, D. J. Pugh, R. Kaptein, R. Boelens, and A. M. Bonvin. Direct use of unassigned resonances in NMR structure calculations with proxy residues. *J. Am. Chem. Soc.*, 128(23):7566–71, 2006.

[141] D.A. Case, D.A. Pearlman, J.W. Caldwell, T.E. Cheatham III, W.S. Ross, C.L. Simmerling, T.A. Darden, K.M. Merz, R.V. Stanton, A.L. Cheng, J.J. Vincent, M. Crowley, V. Tsui, V.J. Radmer, Y. Duan, J. Pitera, I. Massova, G.L. Seibel, U.C. Singh, P.K. Weiner, and P.A. Kollman. AMBER 6. 1999.

[142] D.A. Pearlman, D.A. Case, J.W. Caldwell, W.S. Ross, T.E. Cheatham, S. DeBolt, D. Ferguson, G.L. Seibel, and P.A. Kollman. AMBER, a package of computer programs for applying molecular mechanics, normal mode analysis, molecular dynamics and free energy calculations to simulate the structural and energectic properties of molecules. *Comp. Phys. Commun.*, 91:1–41, 1995.

[143] P. Schuck, M. A. Perugini, N. R. Gonzales, G. J. Howlett, and D. Schubert. Size-distribution analysis of proteins by analytical ultracentrifugation: Strategies and application to model systems. *Biophys. J.*, 82(2):1096–111, 2002.

[144] G. W. Vuister and A. Bax. Resolution enhancement and spectral editing of uniformly ^{13}C-enriched proteins by homonuclear broadband 13C decoupling. *J. Magn. Reson.*, 98:428, 1992.

[145] G. S. Salvesen and S. J. Riedl. Caspase mechanisms. *Adv. Exp. Med. Biol.*, 615:13–23, 2008.

[146] J. B. Denault and G. S. Salvesen. Apoptotic caspase activation and activity. *Methods Mol. Biol.*, 414:191–220, 2008.

[147] S. Kumar. Caspase function in programmed cell death. *Cell Death Differ.*, 14(1):32–43, 2007.

[148] H. Liu, D. W. Chang, and X. Yang. Interdimer processing and linearity of procaspase-3 activation: A unifying mechanism for the activation of initiator and effector caspases. *J. Biol. Chem.*

[149] I. Chowdhury, B. Tharakan, and G.K. Bhat. Caspases - An update. *Comp. Biochem. Physiol. B Biochem. Mol. Biol.*, 151(1):10–27, 2008.

[150] M. J. Romanowski, J. M. Scheer, T. O'Brien, and R. S. McDowell. Crystal structures of a ligand-free and malonate-bound human caspase-1: Implications for the mechanism of substrate binding. *Structure*, 12(8):1361–71, 2004.

[151] N. Yan, J. R. Huh, V. Schirf, B. Demeler, B. A. Hay, and Y. Shi. Structure and activation mechanism of the Drosophila initiator caspase Dronc.

[152] J.M. Elliott, L. Rouge, C. Wiesmann, and J.M. Scheer. Crystal structure of procaspase-1 zymogen domain reveals insight into inflammatory caspase autoactivation. *J. Biol. Chem.*, 284(10):6546–53, 2009.

[153]

[154] C.Z. Ni, C. Li, J.C. Wu, A.P. Spada, and K.R. Ely. Conformational restrictions in the active site of unliganded human caspase-3. *J. Mol. Recognit.*, 16(3):121–124, 2003.

[155] L. Mannocci, Y. Zhang, J. Scheuermann, M. Leimbacher, G. De Bellis, E. Rizzi, C. Dumelin, S. Melkko, and D. Neri. High-throughput sequencing allows the identification of binding molecules isolated from DNA-encoded chemical libraries. *Proc. Natl. Acad. Sci. U S A*, 105(46):17670–75, 2008.

[156] M. K. Manion, J. W. O'Neill, C. D. Giedt, Kim K. M., K. Y. Z. Zhang, and D. M. Hockenbery. Bcl-XL Mutations Suppress Cellular Sensitivity to Antimycin A. *J. Biol. Chem.*, 279(9):2159–65, 2004.

[157] W. Kabsch. Automatic processing of rotation diffraction data from crystals of initially unknown symmetry and cell constants. *J. Appl. Cryst.*, 26:795–800, 1993.

[158] A. J. McCoy, R. W. Grosse-Kunstleve, P. D. Adams, M. D. Winn, L. C. Storoni, and R. J. Read. Phaser crystallographic software. *J. Appl. Cryst.*, 40(4):658–74, 2007.

[159] P. H. Zwart, P. V. Afonine, R. W. Grosse-Kunstleve, L. W. Hung, T. R. Ioerger, A. J. McCoy, E. McKee, N. W. Moriarty, R. J. Read, J. C. Sacchettini, N. K. Sauter, L. C. Storoni, T. C. Terwilliger, and P. D. Adams. Automated structure solution with the PHENIX suite. *Methods Mol. Biol.*, 426:419–35, 2008.

[160] P. Emsley and K. Cowtan. Coot: Model-building tools for molecular graphics. *Acta Cryst. D Biol. Cryst.*, 60(12):2126–32, 2004.

Appendix A

Protein sequences

A.1 Caspase-8 mutants

A.1.1 Full-length caspase-8

The following constructs were cloned into pCR3-vectors for mammalian cell expression. Point mutations for C130S and C163S were generated by Quikchange mutagenesis. All constructs contain an C-terminal myc-tag (underlined) for detection purposes. The cysteine to alanine mutations and the active site cysteine are indicated by boxes. In the corresponding PC8 constructs the active site cysteine was mutated to alanine

C8-myc - MW = 56834.6 Da, ϵ_{280} = 33070
PC8-myc - MW = 56802.5 Da, ϵ_{280} = 33070

MDFSRNLYDIGEQLDSEDLASLKFLSLDYIPQRKQEPIKDALMLFQRLQEKRMLEESNLSFLK
ELLFRINRLDLLITYLNTRKEEMERELQTPGRAQISAYRVMLYQISEEVSRSELRSFKFLLQE
EISKCKLDDDMNLLDIFIEMEKRVILGEGKLDILKRVCAQINKSLLKIINDYEEFSKERSSSL
EGSPDEFSNGEELCGVMTISDSPREQDSESQTLDKVYQMKSKPRGYCLIINNHNFAKAREKVP
KLHSIRDRNGTHLDAGALTTTFEELHFEIKPHDDCTVEQIYEILKIYQLMDHSNMDCFICCIL
SHGDKGIIYGTDGQEAPIYELTSQFTGLKCPSLAGKPKVFFIQA C QGDNYQKGIPVETDSEE
QPYLEMDLSSPQTRYIPDEADFLLGMATVNNCVSYRNPAEGTWYIQSLCQSLRERCPRGDDIL
TILTEVNYEVSNKDDKKNMGKQMPQPTFTLRKKLVFPSDSGEQKLISEEDLN

C8 C130S-myc - MW = 56790.4 Da, ϵ_{280} = 33070
PC8 C130S-myc - MW = 56758.3 Da, ϵ_{280} = 32945

MDFSRNLYDIGEQLDSEDLASLKFLSLDYIPQRKQEPIKDALMLFQRLQEKRMLEESNLSFLK
ELLFRINRLDLLITYLNTRKEEMERELQTPGRAQISAYRVMLYQISEEVSRSELRSFKFLLQE
EIS NSN LDDDMNLLDIFIEMEKRVILGEGKLDILKRVCAQINKSLLKIINDYEEFSKERSSS
LEGSPDEFSNGEELCGVMTISDSPREQDSESQTLDKVYQMKSKPRGYCLIINNHNFAKAREKV
PKLHSIRDRNGTHLDAGALTTTFEELHFEIKPHDDCTVEQIYEILKIYQLMDHSNMDCFICCI
LSHGDKGIIYGTDGQEAPIYELTSQFTGLKCPSLAGKPKVFFIQA C QGDNYQKGIPVETDSE
EQPYLEMDLSSPQTRYIPDEADFLLGMATVNNCVSYRNPAEGTWYIQSLCQSLRERCPRGDDI
LTILTEVNYEVSNKDDKKNMGKQMPQPTFTLRKKLVFPSDSGEQKLISEEDLN

C8 C163S-myc - MW = 56818.5 Da, ϵ_{280} = 33070
PC8 C163S-myc - MW = 56786.5 Da, ϵ_{280} = 32945

MDFSRNLYDIGEQLDSEDLASLKFLSLDYIPQRKQEPIKDALMLFQRLQEKRMLEESNLSFLK
ELLFRINRLDLLITYLNTRKEEMERELQTPGRAQISAYRVMLYQISEEVSRSELRSFKFLLQE
EISKCKLDDDMNLLDIFIEMEKRVILGEGKLDILKRV S AQINKSLLKIINDYEEFSKERSSS
LEGSPDEFSNGEELCGVMTISDSPREQDSESQTLDKVYQMKSKPRGYCLIINNHNFAKAREKV
PKLHSIRDRNGTHLDAGALTTTFEELHFEIKPHDDCTVEQIYEILKIYQLMDHSNMDCFICCI
LSHGDKGIIYGTDGQEAPIYELTSQFTGLKCPSLAGKPKVFFIQA C QGDNYQKGIPVETDSE
EQPYLEMDLSSPQTRYIPDEADFLLGMATVNNCVSYRNPAEGTWYIQSLCQSLRERCPRGDDI
LTILTEVNYEVSNKDDKKNMGKQMPQPTFTLRKKLVFPSDSGEQKLISEEDLN

A.1.2 Prodomain of caspase-8

The following constructs were cloned into pET-20b(+) vectors (Invitrogen) [99]. Point mutations for C130S and C163S were generated by Quikchange mutagenesis. The TEV cleavage site (underlined) was cloned into a *BamH*I located directly in front of the DED sequence. Mutations are indicated by boxes. All constructs contain an N-terminal GB1-tag for enhanced solubility and a C-terminal His-tag for purification and detection purposes. Purification was performed as described on page 127.

Single domains

GB1-DED1-His - MW = 17569.8 Da, ϵ_{280} = 14440

MQYKLILNGKTLKGETTTEAVDAATAEKVFKQYANDNGVDGEWTYDDATKTFTVTEGSMDFSR
NLYDIGEQLDSEDLASLKFLSLDYIPQRKQEPIKDALMLFQRLQEKRMLEESNLSFLKELLFR
INRLDLLITYLNTRKELEHHHHHH

GB1-DED2-His - MW = 17870.3 Da, ϵ_{280} = 14565

MQYKLILNGKTLKGETTTEAVDAATAEKVFKQYANDNGVDGEWTYDDATKTFTVTEGSMPGRA
QISAYRVMLYQISEEVSRSELRSFKFLLQEEISKCKLDDDMNLLDIFIEMEKRVILGEGKLDI
LKRVCAQINKSLLKIINDYEELEHHHHHH

GB1-DED2 C130S-His - MW = 17826.1 Da, ϵ_{280} = 14440

MQYKLILNGKTLKGETTTEAVDAATAEKVFKQYANDNGVDGEWTYDDATKTFTVTEGSMPGRA
QISAYRVMLYQISEEVSRSELRSFKFLLQEEIS NSN LDDDMNLLDIFIEMEKRVILGEGKLD
ILKRVCAQINKSLLKIINDYEELEHHHHHH

GB1-DED2 C163S-His - MW = 17854.2 Da, ϵ_{280} = 14440

MQYKLILNGKTLKGETTTEAVDAATAEKVFKQYANDNGVDGEWTYDDATKTFTVTEGSMPGRA
QISAYRVMLYQISEEVSRSELRSFKFLLQEEISKCKLDDDMNLLDIFIEMEKRVILGEGKLDI
LKRV S AQINKSLLKIINDYEELEHHHHHH

Double domains

His-GB1-TEV-DED12 - MW = 29758.8 Da, ϵ_{280} = 20400

MQYKLILNGKTLKGETTTEAVDAATAEKVFKQYANDNGVDGEWTYDDATKTFTVTEGSENLYF
Q - GGSDFSRNLYDIGEQLDSEDLASLKFLSLDYIPQRKQEPIKDALMLFQRLQEKRMLEES
NLSFLKELLFRINRLDLLITYLNTRKEEMERELQTPGRAQISAYRVMLYQISEEVSRSELRSF
KFLLQEEISKCKLDDDMNLLDIFIEMEKRVILGEGKLDILKRVCAQINKSLLKIINDYEELEH
HHHHH

His-GB1-TEV-DED12 C130S - MW = 29714.6 Da, ϵ_{280} = 20400

MQYKLILNGKTLKGETTTEAVDAATAEKVFKQYANDNGVDGEWTYDDATKTFTVTEGSENLYF
Q - GGSDFSRNLYDIGEQLDSEDLASLKFLSLDYIPQRKQEPIKDALMLFQRLQEKRMLEES
NLSFLKELLFRINRLDLLITYLNTRKEEMERELQTPGRAQISAYRVMLYQISEEVSRSELRSF
KFLLQEEIS NSN LDDDMNLLDIFIEMEKRVILGEGKLDILKRVCAQINKSLLKIINDYEELE
HHHHHH

His-GB1-TEV-DED12 C163S - MW = 29742.8 Da, ϵ_{280} = 20400

MQYKLILNGKTLKGETTTEAVDAATAEKVFKQYANDNGVDGEWTYDDATKTFTVTEGSENLYF
Q - GGSDFSRNLYDIGEQLDSEDLASLKFLSLDYIPQRKQEPIKDALMLFQRLQEKRMLEES
NLSFLKELLFRINRLDLLITYLNTRKEEMERELQTPGRAQISAYRVMLYQISEEVSRSELRSF
KFLLQEEISKCKLDDDMNLLDIFIEMEKRVILGEGKLDILKRV S AQINKSLLKIINDYEELE
HHHHHH

A.1.3 Catalytic domain of caspase-8 – single-chain constructs

The following single-chain constructs were cloned into pQE-50 vectors (Qiagen). Single amino acid mutations are indicated by boxes. Purification was performed as described on page 129. ' - ' indicate the cleavage sites at which the constructs are autocatalytically processed during the purification procedure.

Unprocessed caspase-8 – MW = 30340.4 Da, ϵ_{280} = 24005

MRGSESQTLDKVYQMKSKPRGYCLIINNHNFAKAREKVPKLHSIRDRNGTHLDAGALTTTFEE
LHFEIKPHDDCTVEQIYEILKIYQLMDHSNMDCFICCILSHGDKGIIYGTDGQEAPIYELTSQ
FTGLKCPSLAGKPKVFFIQACQGDNYQKGIPVETD - SEEQPYLEMD - LSSPQTRYIPDE
ADFLLGMATVNNCVSYRNPAEGTWYIQSLCQSLRERCPRGDDILTILTEVNYEVSNKDDKKNM
GKQMPQPTFTLRKKLVFPSD

Processed caspase-8 - C8 – MW = 29118.1 Da, ϵ_{280} = 22515

MRGSESQTLDKVYQMKSKPRGYCLIINNHNFAKAREKVPKLHSIRDRNGTHLDAGALTTTFEE
LHFEIKPHDDCTVEQIYEILKIYQLMDHSNMDCFICCILSHGDKGIIYGTDGQEAPIYELTSQ
FTGLKCPSLAGKPKVFFIQACQGDNYQKGIPVETD - LSSPQTRYIPDEADFLLGMATVNNC
VSYRNPAEGTWYIQSLCQSLRERCPRGDDILTILTEVNYEVSNKDDKKNMGKQMPQPTFTLRK
KLVFPSD

Procaspase-8 - PC8 – MW = 30308.4 Da, ϵ_{280} = 23880

MRGSESQTLDKVYQMKSKPRGYCLIINNHNFAKAREKVPKLHSIRDRNGTHLDAGALTTTFEE
LHFEIKPHDDCTVEQIYEILKIYQLMDHSNMDCFICCILSHGDKGIIYGTDGQEAPIYELTSQ
FTGLKCPSLAGKPKVFFIQA[A]QGDNYQKGIPVETD - SEEQPYLEMD - LSSPQTRYIPD
EADFLLGMATVNNCVSYRNPAEGTWYIQSLCQSLRERCPRGDDILTILTEVNYEVSNKDDKKN
MGKQMPQPTFTLRKKLVFPSD

DDAA – MW = 30252.4 Da, ϵ_{280} = 24005

MRGSESQTLDKVYQMKSKPRGYCLIINNHNFAKAREKVPKLHSIRDRNGTHLDAGALTTTFEE
LHFEIKPHDDCTVEQIYEILKIYQLMDHSNMDCFICCILSHGDKGIIYGTDGQEAPIYELTSQ
FTGLKCPSLAGKPKVFFIQACQGDNYQKGIPVET[A]SEEQPYLEM[A]LSSPQTRYIPDEADFL
LGMATVNNCVSYRNPAEGTWYIQSLCQSLRERCPRGDDILTILTEVNYEVSNKDDKKNMGKQM
PQPTFTLRKKLVFPSD

D374A – MW = 30296.4 Da, ϵ_{280} = 24005

MRGSESQTLDKVYQMKSKPRGYCLIINNHNFAKAREKVPKLHSIRDRNGTHLDAGALTTTFEE
LHFEIKPHDDCTVEQIYEILKIYQLMDHSNMDCFICCILSHGDKGIIYGTDGQEAPIYELTSQ
FTGLKCPSLAGKPKVFFIQACQGDNYQKGIPVET[A]SEEQPYLEMD - LSSPQTRYIPDEAD
FLLGMATVNNCVSYRNPAEGTWYIQSLCQSLRERCPRGDDILTILTEVNYEVSNKDDKKNMGK
QMPQPTFTLRKKLVFPSD

D384A – MW = 30296.4 Da, ϵ_{280} = 24005

MRGSESQTLDKVYQMKSKPRGYCLIINNHNFAKAREKVPKLHSIRDRNGTHLDAGALTTTFEE
LHFEIKPHDDCTVEQIYEILKIYQLMDHSNMDCFICCILSHGDKGIIYGTDGQEAPIYELTSQ
FTGLKCPSLAGKPKVFFIQACQGDNYQKGIPVETD - SEEQPYLEM[A]LSSPQTRYIPDEAD
FLLGMATVNNCVSYRNPAEGTWYIQSLCQSLRERCPRGDDILTILTEVNYEVSNKDDKKNMGK
QMPQPTFTLRKKLVFPSD

F468A – MW = 30264.3 Da, ϵ_{280} = 24005

MRGSESQTLDKVYQMKSKPRGYCLIINNHNFAKAREKVPKLHSIRDRNGTHLDAGALTTTFEE
LHFEIKPHDDCTVEQIYEILKIYQLMDHSNMDCFICCILSHGDKGIIYGTDGQEAPIYELTSQ
FTGLKCPSLAGKPKVFFIQACQGDNYQKGIPVETDSEEQPYLEMDLSSPQTRYIPDEADFLLG
MATVNNCVSYRNPAEGTWYIQSLCQSLRERCPRGDDILTILTEVNYEVSNKDDKKNMGKQMPQ
PT[A]TLRKKLVFPSD

A.1.4 Catalytic domain of caspase-8 – two-chain constructs

The following two-chain constructs were cloned separately in pET-11d vectors (Invitrogen). Single amino acid mutations are indicated by boxes. Purification was performed as described on page 131.

$\alpha\beta$ F468A – MW = 29042.0 Da, ϵ_{280} = 22515

MRGSESQTLDKVYQMKSKPRGYCLIINNHNFAKAREKVPKLHSIRDRNGTHLDAGALTTTFEE
LHFEIKPHDDCTVEQIYEILKIYQLMDHSNMDCFICCILSHGDKGIIYGTDGQEAPIYELTSQ
FTGLKCPSLAGKPKVFFIQACQGDNYQKGIPVETD - LSSPQTRYIPDEADFLLGMATVNNC
VSYRNPAEGTWYIQSLCQSLRERCPRGDDILTILTEVNYEVSNKDDKKNMGKQMPQPT A TLR
KKLVFPSD

β-trunc – MW = 28278.2 Da, ϵ_{280} = 22515

MRGSESQTLDKVYQMKSKPRGYCLIINNHNFAKAREKVPKLHSIRDRNGTHLDAGALTTTFEE
LHFEIKPHDDCTVEQIYEILKIYQLMDHSNMDCFICCILSHGDKGIIYGTDGQEAPIYELTSQ
FTGLKCPSLAGKPKVFFIQACQGDNYQ - LSSPQTRYIPDEADFLLGMATVNNCVSYRNPAE
GTWYIQSLCQSLRERCPRGDDILTILTEVNYEVSNKDDKKNMGKQMPQPTFTLRKKLVFPSD

α-trunc – MW = 27859.7 Da, ϵ_{280} = 21025

MRGSESQTLDKVYQMKSKPRGYCLIINNHNFAKAREKVPKLHSIRDRNGTHLDAGALTTTFEE
LHFEIKPHDDCTVEQIYEILKIYQLMDHSNMDCFICCILSHGDKGIIYGTDGQEAPIYELTSQ
FTGLKCPSLAGKPKVFFIQACQGDNYQKGIPVETD - EADFLLGMATVNNCVSYRNPAEGTW
YIQSLCQSLRERCPRGDDILTILTEVNYEVSNKDDKKNMGKQMPQPTFTLRKKLVFPSD

A.2 FADD

The TEV cleavage recognition site is underlined. The protein is processed at '. Purification was performed as described on page 133.

FADD – MW = 50822.2 Da, ϵ_{280} = 62840

MSPILGYWKIKGLVQPTRLLLEYLEEKYEEHLYERDEGDKWRNKKFELGLEFPNLPYYIDGDV
KLTQSMAIIRYIADKHNMLGGCPKERAEISMLEGAVLDIRYGVSRIAYSKDFETLKVDFLSKL
PEMLKMFEDRLCHKTYLNGDHVTHPDFMLYDALDVVLYMDPMCLDAFPKLVCFKKRIEAIPQI
DKYLKSSKYIAWPLQGWQATFGGGDHPPKSDLVPRENLYFQG - GSPEFRDPFLVLLHSVSS
SLSSSELTELKFLCLGRVGKRKLERVQSGLDLFSMLLEQNDLEPGHTELLRELLASLRRHDLL
RRVDDFEAGAAAGAAPGEEDLCAAFNVICDNVGKDWRRLARQLKVSDTKIDSIEDRYPRNLTE
RVRESLRIWKNTEKENATVAHLVGALRSCQMNLVADLVQEVQQARDLQNRSGAMSPMSWNSDA
STSEAS

Appendix B

Purification protocols

B.1 Caspase-8 prodomain

The protocol was adapted from Ghisleni et al. [99].

Day -4:

- Transform pET plasmids (Amp) into BL21(DE3) cells

Day -3:

- Set up 10 ml ON culture (Amp)

Day -2:

- Inoculate 2 x 500 ml LB (Amp) with 5 ml ON culture each
- Grow at 37°C until $OD_{600}\bar{0}.5$
- Induce with 1 mM IPTG
- Express at 37°C for 4 hours

Day -1:

- Harvest at 5 K for 20 min
- Resuspend cells in 25 ml Ni-buffer A
- Freeze at -20 or proceed with Day 1

Day 1:

- Thaw cells
- Add DNaseI

- French press
- Centrifuge at 24,000 x g for 30 min
- Load soluble protein onto Ni column equilibrated with Ni-buffer A
- Wash out unbound protein with wash buffer
- Elute with Ni-buffer B

Buffers (adjusted for a 1000 ml prep):

Ni-buffer A
50 mM Tris 8.0
100 mM NH_4Cl
0.5 mM TCEP

Wash buffer
50 mM Tris 8.0
100 mM NH_4Cl
0.5 mM TCEP
20 mM Imidazole

Ni-buffer B
50 mM Tris 8.0
100 mM NH_4Cl
0.5 mM TCEP
200 mM Imidazole

B.2 Caspase-8 catalytic domain – single chain constructs

The protocol was adapted from Watt et al. and adjusted for a prep starting from 1000 ml cell culture [66].

Day -4:

- Transform pQE plasmid (Amp) into M15 cells (Kan)

Day -3:

- Set up 10 ml ON culture (Amp/Kan)

Day -2:

- Inoculate 2 x 500 ml LB (Amp/Kan) with 5 ml ON culture each
- Grow at 37°C until $OD_{600}\bar{0}$.8-1.0
- Induce with 1 mM IPTG
- Express at 37°C ON

Day -1:

- Harvest at 5 K for 20 min
- Resuspend cells in 25 ml PBS
- Freeze at -20 or proceed with Day 1

Day 1:

- Thaw cells
- Add DNaseI
- French press
- Pellet IB at 8,000 x g for 20 min
- Wash 4 x 25 ml with wash buffer or until clear
- Solubilize in 5 ml solubilization buffer (store at -70)
- Add 5 ml 100% AcOH
- Dialyze against 50% AcOH for 4 hrs (with buffer exchanges)
- Add to 90 ml H2O
- Refold at RT ON in 900 ml refolding buffer

Day 2:

- Remove precipitation by centrifugation
- Concentrate in 400 ml Amicon

Day 3:

- Purify on S200 column

Buffers (adjusted for a 1000 ml prep):

Wash buffer (100 ml)

20 mM Tris 8.0

0.1% LDAO

1 mM EDTA

Solubilization buffer (5 ml)

6 M GdHCl

20 mM Tris pH 8.0

2 mM EDTA

100 mM DTT

Refolding buffer (900 ml)

1 M Tris

10 mM DTT

1 Protease inhibitor tablet (Roche)

Size exclusion buffer (1000 ml)

20 mM Tris 8.0

100 mM NaCl

0.5 mM TCEP

B.3 Caspase-8 catalytic domain – two-chain constructs

The protocol was adapted from Garcia-Calvo et al. adjusted to a prep starting from 500 ml cell culture [123].

Day -4:

- Transform pAT22-PC2 + BirA into BL-21(DE3)
- Plate on LB Amp/Cam
- Incubate at 37°C ON

Day -3:

- Pick colony for ON culture

Day -2:

- Inoculate 500 ml LB Amp/Cam with 5 ml ON culture
- Grow until OD_{600} = 0.5 • Induce with 1 mM IPTG
- Express at 37°C ON

Day -1:

- Harvest at 5 K for 20 min
- Resuspend cells in 25 ml PBS
- Freeze at -20 or proceed with Day 1

Day 1:

- Thaw cells
- Add DNaseI
- French press
- Pellet IB at 8,000 x g for 20 min
- Wash 4 times 25 ml with wash buffer or until clear
- Solubilize in 2.5 ml solubilization buffer
- Store at -70 or proceed with Day 2

Day 2:

- Refold into 200 ml Refolding buffer
- Incubate ON at RT

Day 3:

- Remove precipitation by centrifugation
- Concentrate in Amicon filtration cell
- Dialyze against ResQ buffer A

Day 4:

- Load onto ResQ
- Elute with gradient of 0 - 300 mM NaCl over 30 CV
- Concentrate positive fractions
- Purify on S200 column

Buffers (adjusted for two 500 ml preps or one 1000 ml prep):

Wash buffer (100 ml)
20 mM 1M Tris 8.0
0.1% LDAO
1 mM EDTA

Solubilization buffer (5 ml)
6 M GdHCl
20 mM Tris pH 8.0
2 mM EDTA
100 mM 1M DTT

Refolding buffer (900 ml)
100 mM HEPES 7.5
10 mM NaCl

Size exclusion buffer (150 ml)
20 mM Tris 8.0
100 mM NaCl
0.5 mM TCEP

B.4 FADD

The protocol was adapted from Ghisleni et al. [99].

Day -4:

- Transform pGEX plasmid (Amp) into BL21(DE3) cells

Day -3:

- Set up 10 ml ON culture (Amp)

Day -2:

- Inoculate 2 x 500 ml LB (Amp) with 5 ml ON culture each
- Grow at 37°C until $OD_{600}\bar{0}.5$
- Induce with 1 mM IPTG
- Express at 18°C over night

Day -1:

- Harvest at 5 K for 20 min
- Resuspend cells in 25 ml Buffer A
- Freeze at -20 or proceed with Day 1

Day 1:

- Thaw cells
- Add DNaseI
- French press
- Centrifuge at 24,000 x g for 30 min
- Load soluble protein onto GST trap column equilibrated with Buffer A
- Wash out unbound proteins with buffer A
- Elute with Buffer B

Buffers (adjusted for a 1000 ml prep):

Ni-buffer A

50 mM Tris 8.0

150 mM NaCl

Ni-buffer B

50 mM Tris 8.0

10 mM reduced glutathione

Appendix C

Crystallization of Bcl-xl

The goal of this project was to crystallize the anti-apoptotic protein Bcl-xl with a small molecule inhibitor that was selected from a DNA-encoded chemical library [155]. Several specific binders were selected for Bcl-xl with the compound 19/93 binding with the hightest affinity (0.93 μM; Melkko, S. unpublished results). Competition assays using an excess of Bak-derived BH3 peptide suggest binding of the inhibitor to the same peptide binding cleft that is occupied by the natural BH3 peptide.

C.1 Protein purification, crystallization and data collection

The protein Bcl-xl was expressed and purified by Alessandra Villa from the group of Dario Neri at the Institute of Pharmaceutical Science at the ETH Zurich. Purification included Ni-NTA affinity purification, dialysis against Mes buffer pH 6.0 and size exclusion chromatography using an S200 column and resulted in pure and homogeneous material (Figure C.1).
The protein was concentrated to 1 mM and crystallization was set up using a Phoenix liquid handler (Art Robbins Instruments). The crystallization buffer contained Mes and ammonium sulfate and was adapted from published conditions [156]. The pH of the Mes buffer varied from 5.5 to 6.5 and ammonium sulfate was used in concentrations from 1.6 to 2.2 M. First crystals at both, 4°C and 20°C appeared after one week of incubation and were fully grown after 2-3 weeks (Figure C.2). Nucleation of crystal growth was higher at 4°C resulting in more but smaller crystals than compared to

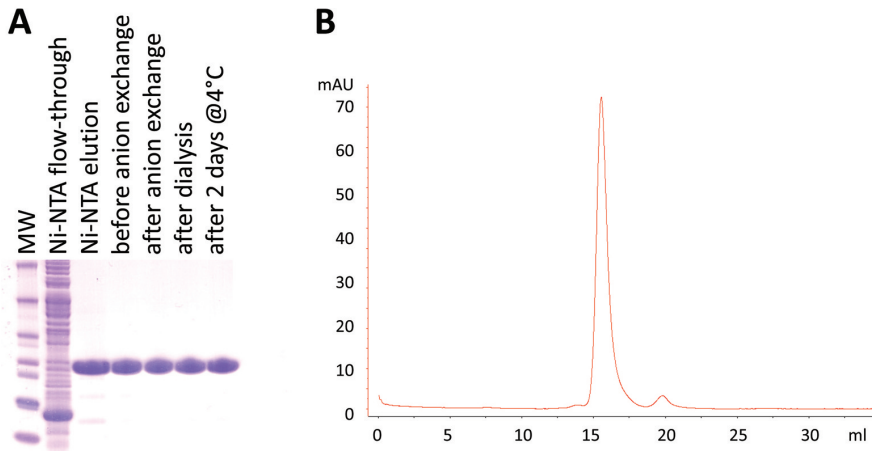

Figure C.1: Purification of Bcl-xl.
A) SDS PAGE showing different steps of the Bcl-xl purification. The individual steps are indicated above the lanes.
B) Analytical size exclusion chromatogram of Bcl-xl to verify protein purity and homogeneity.

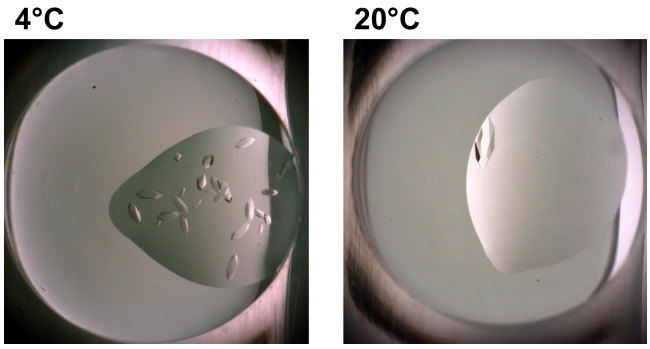

Figure C.2: Crystal growth at 4°C and 20°C.

20°C where usually one to three crystals were observed.
The crystals were isolated from the drops and soaked for half a minute to five minutes in cryo buffer (50 mM Mes pH 5.5, 2.0 mM ammonium sulfate, 10% ethylen glycol) containing a final concentration of 10 mM of in DMSO dissolved 19/93 inhibotor. Addition of the inhibitor to the cryo buffer resulted in precipitation of it but this precipitation mostly dissolved after several hours of incubation, indicating that the inhibitor was still present in excess to the protein. After soaking the crystals were flash frozen in liquid nitrogen. Various crystals from 4°C and 20°C with different soaking conditions were

Data collection	
Beamline	PXI, Swiss Light Source, PSI
λ (Å)	1.0
Spacegroup	$P4_12_12$
Cell parameters	a = b = 63.7 Å, c = 109.9Å, $\alpha = \beta = \gamma = 90°$
Reflections	
unique	272333 (90089)
observed	21679 (7059)
Redundancy	12.6 (12.8)
Resolution limit (Å)	40 - 1.8 (2.06 - 1.8)
Completeness (%)*	100 (100)
Average I/σ	37.6 (6.3)
R_{sym}	3.6 (49.4)
Refinement	
Resolution (Å)	
R_{cryst}/R_{free} (%)	20.7 / 23.3
Number of	
molecules in assymetric unit	1
protein atoms	1185
water molecules	120
inhibitor molecules	0
Ramachandran plot (Procheck)	
Most vafored (%)	95.3
Allowed (%)	4.7
Generously allowed (%)	0
Disallowed (%)	0
Root mean square deviations	
bond length (Å)	0.004
Bond angles (degrees)	0.795

Table C.1: X-ray data collection and refinement statistics.
The data of the highest resolution shell are displayed in parentheses. R_{free} represents the R factor calculated using 6% of the data that were excluded from the refinement.

tested at the Swiss Light Source Synchroton at the Paul Scherer Institute in Villingen and data sets were recorded for diffracting crystals.

C.2 Structure determination

The data were processed and scaled in XDS and XSCALE, respectively [157]. The processing statistics are summarized in Table C.1. The determined space group, $P4_12_12$ corresponds to a previously published Bcl-xl structure (PDB code 1R2D). Both structure also have very similar unit cell parame-

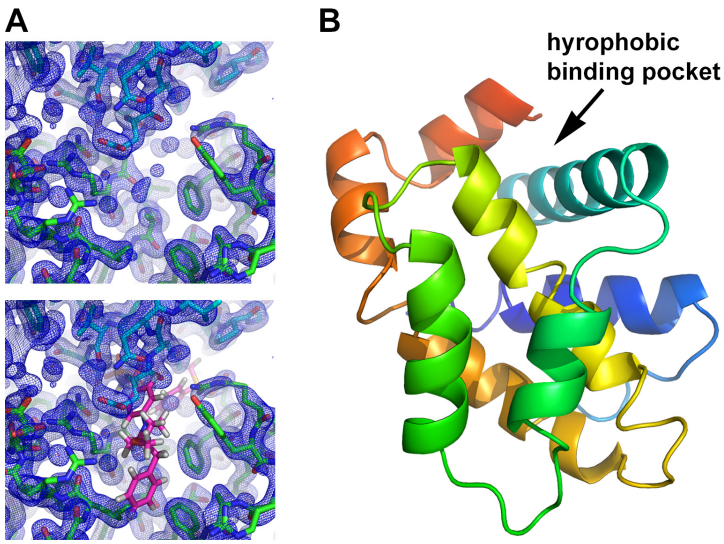

Figure C.3: Bcl-xl structure
A) Electron density maps contoured at 1.5 σ. Presented is a hydrophobic pocket which was previously found to be involved in inhibitor binding. One Bcl-xl molecule is depicted in green. A second molecule is represented in blue. Due to crystal packing a loop of the cyan molecule protrudes into the hydrophobic binding pocket.
B) Structure of Bcl-xl. The helices are colored in rainbow from blue at the N-terminus to red at the C-terminus. A) and B) are displayed in the same orientation.

ters. Therefore, this structure was used as a searched model for molecular replacement using the programm Phaser [158]. The model was refined in Phenix [159] and was build using Coot [160].

Due to time constraints the structure could not yet be fully refined. The current refinement statistics are listed in Table C.1 and the corresponding structure is diplayed in Figure C.3 B. Unfortunately, no electron density for the inhibitor was detected. Figure C.3 A depticts the electron density map of the region where inhibitor binding was expected. Interestingly, this region is involved in crystal contacts with a neighboring molecule with a loop of the second molecule protruding into the substrate binding pocket, partially occupying it. This indicates that the current approach of soaking wild-type crystals with the inhibitor is impossible. Therefore, co-crystallization experiments were set up to screen for new crystallization conditions.

Appendix D

Curriculum vitae

Personal Data

Name:	Nadine Keller
Date of birth:	22nd of July 1978
Place of birth:	Berlin, Germany
Nationality:	German

Publications

Hipfner D.R., Keller N., Cohen S.M., Slik Sterile-20 kinase regulates Moesin activity to promote epithelial integrity during tissue growth. *Genes Development*, **18**(18):2243-8, 2004.

Keller N., Mares J., Zerbe O., Grütter M.G., Structural and biochemical studies on procaspase-8: New insights on initiator caspase activation. *Structure*, **7** (3):438-448, 2209

Keller, N. Grütter, M.G., Zerbe, O, From Procaspase-8 to Caspase-8: Characterization of the Processing Mechanism and Inhibitor Binding by solution NMR. *submitted Manuscript*

Education

09/95 - 06/98 **Lise-Meitner-Oberstufenzentrum, Berlin, Germany**
Degree: Abitur - 11th of June 1998

10/98 - 07/00 **Technical University Berlin, Germany**
Undergraduate studies in Chemistry
Degree: Vordiploma - 25th of July 2000

08/00 - 09/01 **University of Oklahoma, USA**
Graduate studies in Biochemistry
Thesis titel: The Function of the "EF"-Linker Region in the Phosphorelay Protein YPD1
Degree: Master of Science - 11th of May 2002

10/01 - 10/03 **Technical University Berlin, Germany**
Graduate studies in Chemistry

03/03 - 12/03 **European Molecular Biology Laboratory, Heidelberg, Germany**
Diploma thesis
Thesis titel: Functional Analysis of the Different Domains of the Drosophila melanogaster Survival Kinase Slik
Degree: Diploma - 31st of October 2003

01/04 - 04/04 **European Molecular Biology Laboratory, Heidelberg, Germany**
Internship in Structural Biology
Project titel: Purification and Crystallization of the Drosophila melanogaster Proteins Fringe and OFUT1

Since 06/04 **University of Zurich, Switzerland**
PhD in Biochemistry
Thesis titel: Functional and Structural Analysis of the Activation Mechanism of Caspase-8
Defense: 10th of July 2009

Courses and Conferences

09/08 Meeting of the Swiss Chemical Society, Zurich, Switzerland
Poster: Structure and Activation Studies of the Initiator Procaspase-8

10/07 15th Euroconference on Apoptosis, Portoroz, Slovenia
Poster: NMR structure of the initiator procaspase-8 - New insights in its activation mechanism

09/07 4th Annual Retreat of the Moleclular Life Science Programme, Fiescheralp, Switzerland
Poster: Structure of an initiator caspase

10/06 NCCR Practical Course on Advanced NMR methods, Zurich, Switzerland
Presentation: Structure determination of procaspase-8

10/06 3rd Annual Retreat of the Moleclular Life Science Programme, Chandolin, Switzerland

10/05 2nd Annual Retreat of the Moleclular Life Science Programme, Lenk, Switzerland
Poster: Determination of the structure of an initiator procaspase

09/05 19th Regio Meeting on Biocrystallography, La Bresse, France

09/04 3rd Swiss Apoptosis Meeting, Bern, Switzerland

Stipends and Fellowships

10/06	Travel grant and conference fee waiver for 15th Eurocon- ference on Apoptosis, Portoroz, Slovenia European Cell Death Organisation (ECDO)
2003	Klaus Koch Stipend for extraordinary studies Technical University Berlin, Germany
08/00 - 05/01	Stipend for studying abroad Technical University Berlin, Germany
08/00 - 09/01	Tuition waiver University of Oklahoma, USA